A Novel Robotic Platform to Assist, Train, and Study Head-Neck Movements

Haohan Zhang

Submitted in partial fulfillment of the
requirements for the degree of
Doctor of Philosophy
in the Graduate School of Arts and Sciences
COLUMBIA UNIVERSITY
2019

ABSTRACT

A Novel Robotic Platform to Assist, Train, and Study Head-Neck Movements

Haohan Zhang

Moving the head-neck freely is an everyday task that a healthy person takes for granted. Such a simple movement, however, may be very challenging for individuals with neurological disorders such as amyotrophic lateral sclerosis. These individuals often do not have enough neck muscle strength to stabilize the head at the upright neutral or to move it in a controlled manner. Static braces are commonly prescribed to these patients. However, these braces often fix the head at a single configuration, which makes them uncomfortable to wear for an extended period of time.

In this thesis, a robotic neck brace is developed. It accommodates three rotations and covers roughly 70% range of motion of the head-neck of a typical able-bodied adult. The hardware is lightweight (1.5 kilogram) and wearable, with a pair of pads and a soft band attached to the shoulders and the forehead, respectively. A parallel mechanism connecting the shoulder pads and the headband was designed to meet the empirical human movement data. This design choice is novel where the parasitic motion (translation of the head) was parameterized and optimized to address misalignment between the robot and the user's head.

A user can control this neck brace to assist intended head-neck movement through input devices, including hand-held joysticks, keyboards, and eye-trackers. This provides a potential solution to remediate head drop. Additionally, this robotic brace is developed into a versatile platform to train and study head-neck movements. The robot was designed to be highly transparent to the user and features different force controllers. Therefore, it can be used to assess the free movement of the head-neck and mimic different interactions between a therapist and a patient. The modalities of this neck brace have been validated with different users. To the best of our knowledge, this robotic neck brace is the first in the literature to assist, train, and study head-neck movements.

Contents

List of Figures

List of Tables

Acknowledgments

This research cannot be accomplished without help from others. I want to express my great appreciation towards my family for their unconditional support. I want to thank my advisor, Dr. Sunil Agrawal, for his guidance during my Ph.D. career. It is his excellent teaching that makes me grow into not just a tinker but a true thinker. I want to thank our clinical collaborators, Dr. Jinsy Andrews, Dr. Hiroshi Mitsumoto, and Dr. Neil Shneider for patient subject recruitment without which this project would have not succeeded. I want to thank my defense committee, Dr. Matei Ciocarlie, Dr. Gerard Ateshian, and Dr. Andrew Gordon for their time and efforts to be the judges and their invaluable feedback to my dissertation. Last but certainly not least, I would like to thank everyone from the ROAR lab for their critical suggestions and enormous help to this dissertation. Of these great lab mates, I want to particularly thank Biing-Chwen Chang, Keenan Albee, and Youngjae Ryu, for their respective contributions to this research.

To

My Late Grandmother

Whose Caring Love Will Forever Be In My Memory,

This Dissertation Is Dedicated.

Introduction

The goal of rehabilitation is to restore functional movements of patients with movement irregularities through supervised training and/or assistive technologies. Traditional therapy often demands one or more physicians to treat a single patient at the same time. For example, gait training of an individual with incomplete spinal cord injury usually requires three physical therapists [1]. These therapists need to synchronize their movements to move the patient's legs during training. Such a training usually leads to inevitable fatigue for the therapists, compromising their consistency of hand maneuvers and the motivation from patients.

Assistive devices allow an individual to perform daily tasks or maintain a good posture. For example, walkers and crutches help a person lacking in strength to ambulate, and an ankle-foot orthosis stabilizes the foot of someone with foot drop. However, these passive strategies require the patients to input effort, causing fatigue, discomfort, and secondary complications such as muscle atrophy due to disuse during long-term use [2–4].

Robotic technologies have helped retool the field of rehabilitation in the past two decades, thanks to the advances in sensors, actuators, and computation power. From motorized limb exoskeletons [5–7] and orthoses [8–10] to neurologically controlled prostheses [11–13], roboticists have developed intelligent machines that interact with humans to enhance the quality of life of individuals and reduce the labor demands of physical therapy. These robotic devices quantify movements in real-time, provide assistance during complex functional tasks, and help users relearn motor skills through challenging and repetitive training. Due to the importance of limb functions in activities of daily life, improving gait and arm movements has been the primary research focus.

Restoring functional head-neck movements using a wearable robot has not yet been explored

in the literature. This is partially due to research community's perception towards the role of head-neck movements. From an evolutionary point of view, head-neck movements play a role to supplement vision and enlarge the field of view (FOV). In addition to this, head-neck movements are also used in social interactions. The neck helps a person make eye contact with others to continue a respectful and engaging conversation. People may also nod or shake their head to express their point of view. The movement of the head and neck are effortless and an able-bodied person often takes it for granted.

It is difficult, however, for some individuals with neurological disorders to perform simple head movements. In severe cases, these individuals may not be able to support the head upright, resulting in head drop. This symptom creates various challenges and impairs their quality of life. For example, prolonged head drop may cause spine deformity, chronic pain, and speech and respiratory difficulties. Lack of strength of muscles that control head movements also hinders the effectiveness and ease of interactions with others. This could lead to social embarrassment or even psychological decline [14, 15]. Head drop can be caused by neck extensor weakness or increased tone of flexor muscles [16]. It is commonly seen in neuromuscular diseases, such as amyotrophic lateral sclerosis (ALS), Parkinson's disease, and cerebral palsy, among others [16–18].

In current clinical practices, neck braces are prescribed to the patients [19, 20]. These braces are typically made of foam and plastic, forming an enclosure around the neck while supporting the chin. For wheelchair users, reclining the chair or installing a head support to the chair are also options [21]. These solutions stabilize the head in a static configuration, eliminating the effort from the individuals to hold their head up on their own. However, these devices restrict all movements of the head. Static braces are typically uncomfortable to wear, limiting their usage over extended periods of time. This may lead to a patient losing their range of motion or developing muscle atrophy. In addition, these static devices fail to provide a solution for social interaction. An individual needs to turn their entire body or their wheelchair to make eye contact with others.

There have been engineering attempts to improve the comfort of these neck braces. Sheffield Support Snood was designed to provide a flexible support around the patient's neck so that the

head can be held upright, while maintaining freedom of small local movements [22, 23]. Another passive head support system was designed and evaluated with ALS patients with head drop [24]. This system uses linkages to bypass the neck and attach to the forehead so that the device does not restrict lung expansion of a user. These passive systems improve comfort while supporting the head; however, they do not restore the dynamic movements of the head and neck.

A robotic device, outfitted with sensors, powered actuators, a control system, and an easy-to use interface could provide such dynamic movements of the head-neck externally. However, such a robotic system would come with an additional weight and complexity. Designing a machine that fits between the head and shoulders is very challenging given the limited space and relatively large range of motion of the head. To carry this additional machine weight, a wheelchair-mounted motorized headrest [25] was prototyped to help move the head of ALS patients. It allowed two degrees-of-freedom (DOF), flexion/extension and axial rotation, of the head. However, mounting on an inertial frame (wheelchair) could limit the usage of the device. In addition, the head of the user needs to be aligned properly with the machine, which constrains the natural movements of the person. The prototype was evaluated by healthy individuals although no data was published to show its efficacy. Another neck robot, albeit not for rehabilitation, was designed for pilot training [26]. The architecture of the robot used a Stewart platform with the base fixed to an inertial frame. This robot design complies with all six DOFs of the head. It is very bulky, however, and also requires a proper alignment between the robot end-effector and the user's head.

A wearable robotic neck brace is designed in this thesis. It provides dynamic head-neck movements to a patient with head drop. The robot uses a parallel architecture which attaches to the shoulders and forehead of the user. The system is fully portable, with the actuators, controllers, and batteries onboard. It provides about 70% of the head-neck's range of rotation during daily activities. The motion of the brace can be commanded by a user through various input devices, including a hand-held joystick, a keyboard, and a wearable eye-tracker.

This robotic brace is developed into a versatile robotic platform which aims to meet a variety of needs in the research and clinical communities. For example, the robotic brace can be used to

study head-neck movements in multiple populations. The position and current sensors embedded in the brace allow it to quantify the kinematics and forces of the head. Additionally, it can be integrated with external sensor systems such as surface electromyogrphy (sEMG) and eye-trackers, which allow researchers to study topics like the movement of the head-neck on the neuromuscular scale or behaviors in head-eye coordination. Additionally, the neck brace can be used to mimic different patient-therapist interaction through multiple force controllers. The brace, therefore, can potentially train an individual to improve functional strength of neck muscles and learn new head-neck movements.

The modalities of the robotic brace have been validated through a series of human studies. The results have shown the efficacy of this robotic brace in movement characterization, assistance, and training [27–32]. These experiments produced meaningful datasets that could potentially be used as baseline for future studies. These human evaluations also provided valuable feedback to the iterations of this robotic brace.

Following this introduction, Chapter 1 proposes the design concept and underlying model used in the robotic neck brace. Kinematics of the mechanism are formally derived. Chapter 2 details the realization process of the robotic neck brace and introduces its versatile modalities. It is followed by a series of validation studies with healthy subjects in Chapter 3. These three chapters document the design process of the robotic neck brace whereas the following two chapters include two studies to demonstrate the use of this robotic brace in scientific and clinical research. Chapter 4 presents a study where the performance of using the head-neck to orient virtual objects was investigated. The robotic neck brace was used to measure the head-neck movement of the subjects. Chapter 5 presents a clinical study where the neck brace was used to characterize and assist the head-neck movements of individuals with ALS. The thesis is concluded with a summary of the contributions and recommendation for envisioned researches.

Chapter 1

Neck Brace Design (Part I): Mathematical Model

This chapter details the design aspects of the robotic neck brace which was based on the understanding of human kinematics during head-neck motion. A parallel mechanism is proposed to satisfy the empirical human data and allow for the large range of rotation of the head-neck. The kinematics of this mechanism are defined and derived.

1.1 Movement of the Head-Neck

The head is connected to the trunk through the cervical spine. The cervical spine is composed of a series of vertebrae, articulated by zygapophysial joints and intervertebral discs. To design a machine that complies with the head-neck motion, the kinematics of the natural movement of the head-neck needs to be studied. Empirical data were collected from a healthy person using a motion capture (MoCap) system with ten cameras (VICON Bonita, Vicon Motion Systems, Oxford, UK).

Infrared markers were placed on the individual's head and shoulders to record the relative motion between them (Figure 1.1). In this data collection, the subject was asked to first perform self-paced head motions in each of the three anatomical planes (sagittal, coronal, and transverse) and then a general head motion in space (rolling). Each of these motions was repeated three times continuously. The rotation and translation of the head with respect to the shoulders were computed by reconstructing the marker trajectories.

The result of this computation revealed that the head motion is predominantly rotations with small translations. Additionally, head follows the same pattern during different repetitions. As evidenced in Figure 1.2, the translation of the head (e.g., x component) repeated itself as a function of the bending angle (i.e., β) in different repetitions. This means that the translation of the head

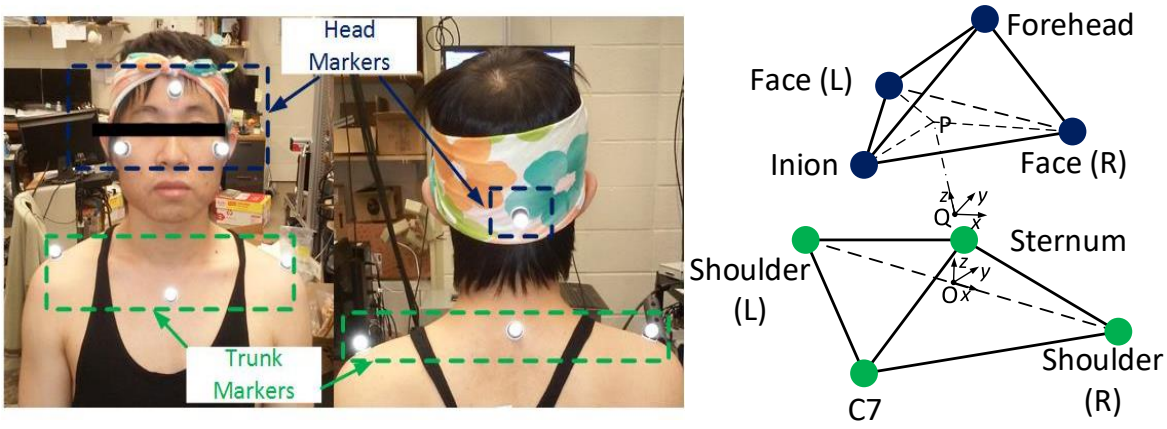

Figure 1.1: Marker placement for head-neck motion characterization. The markers represent two rigid bodies, trunk $\{O\}$ and head $\{Q\}$, each composed of four markers[1,2]. The origin of the trunk, O, is located midway between the two shoulder markers. The origin of the head, Q, is set to be along the line PQ which is perpendicular to the plane formed by three head markers with point P being the geometric center of the triangle. The length of $\overrightarrow{PQ}$ is the estimated length of the neck.

may highly depend on the its orientation when performing a natural movement.

1.2 Underlying Mechanism

Designing a neck exoskeletal device requires a mechanical structure to accommodate the head-neck motion. If one wants the robot to fully comply with the natural motion of the head-neck, a six-degree-of-freedom (DOF) mechanism that allows both translation and rotation may be an obvious choice. However, with limited space between the head and shoulders, actuating all six DOFs with actuators may not be realistic. On the other hand, due to predominantly rotation, one may propose to use a pure spherical mechanism to emulate the head-neck rotations. However, such a spherical mechanism would fail to accommodate small, yet critical, translations of the head during a dynamic motion. Moreover, common spherical mechanisms require additional kinematic constraints that may not be easy to construct physically [33, 34].

[1]Technically, only three markers are needed to construct a coordinate frame. In practice, a fourth marker is used to ensure the body reconstruction when one marker is blocked during dynamic motions.

[2]To eliminate the misplacement of the markers to the subject, a static trial was performed when the subject was seated with the head at upright neutral. At this configuration, the true trunk and head frames were assumed to be aligned to the global frame, i.e., no rotation between frames. With this static trial, the misalignment of the markers can be minimized from the true frames of interest.

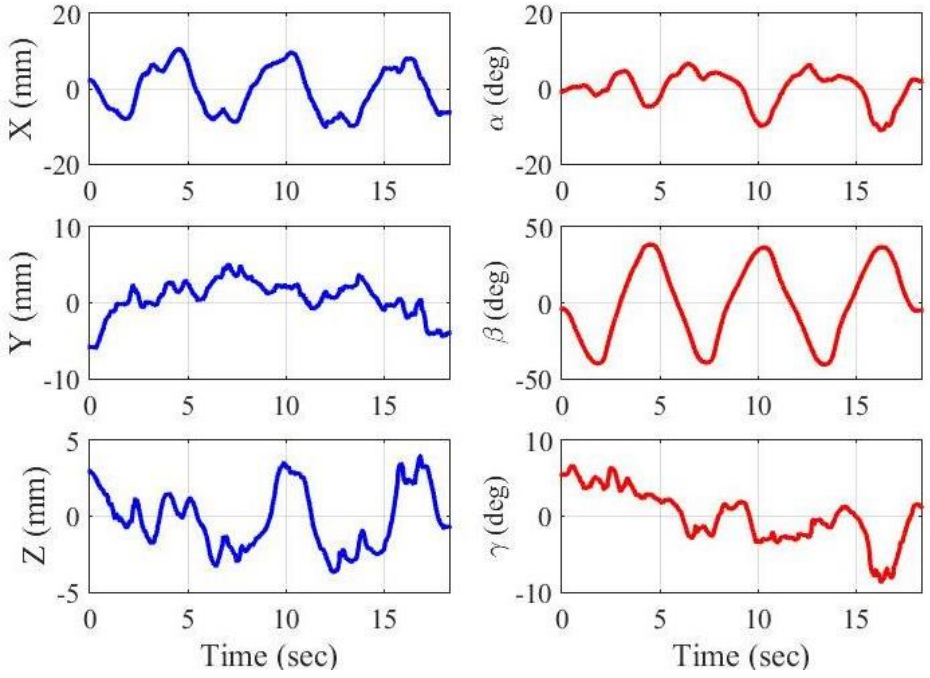

Figure 1.2: Movement trajectory of the head relative to the shoulders of a healthy subject during lateral bending: (left) translation of a reference point in the head and (right) rotation of the head expressed in Body Two 3-2-3 sequence. The coordinate system is based on Figure 1.1:

A three-DOF general structure, derived from a spherical mechanism [34] (Figure 1.3 top left), is proposed with coupled rotation and translation. In this chosen spherical mechanism, all six revolute axes must intersect at a common point to ensure a pure rotation of the end-effector about this point. The proposed mechanism, on the other hand, splits this common point into three different points, with each the intersecting point of the two revolute axes within a chain (Figure 1.3 top right). In this way, the end-effector no longer purely rotates but translates along with its rotations. Additionally, this motion coupling is determined by the locations of these intersecting points. Using the collected human data, the structure of the robot can be optimized to best represent the human head-neck movement, while minimizing the ergonomic footprint.

Because it does not require revolute axes from different chains to intersect which is typically difficult to construct, the proposed mechanism is easy to be realized into a physical model. With additional kinematic chains, actuators can all be placed on the proximal joints at the base, which

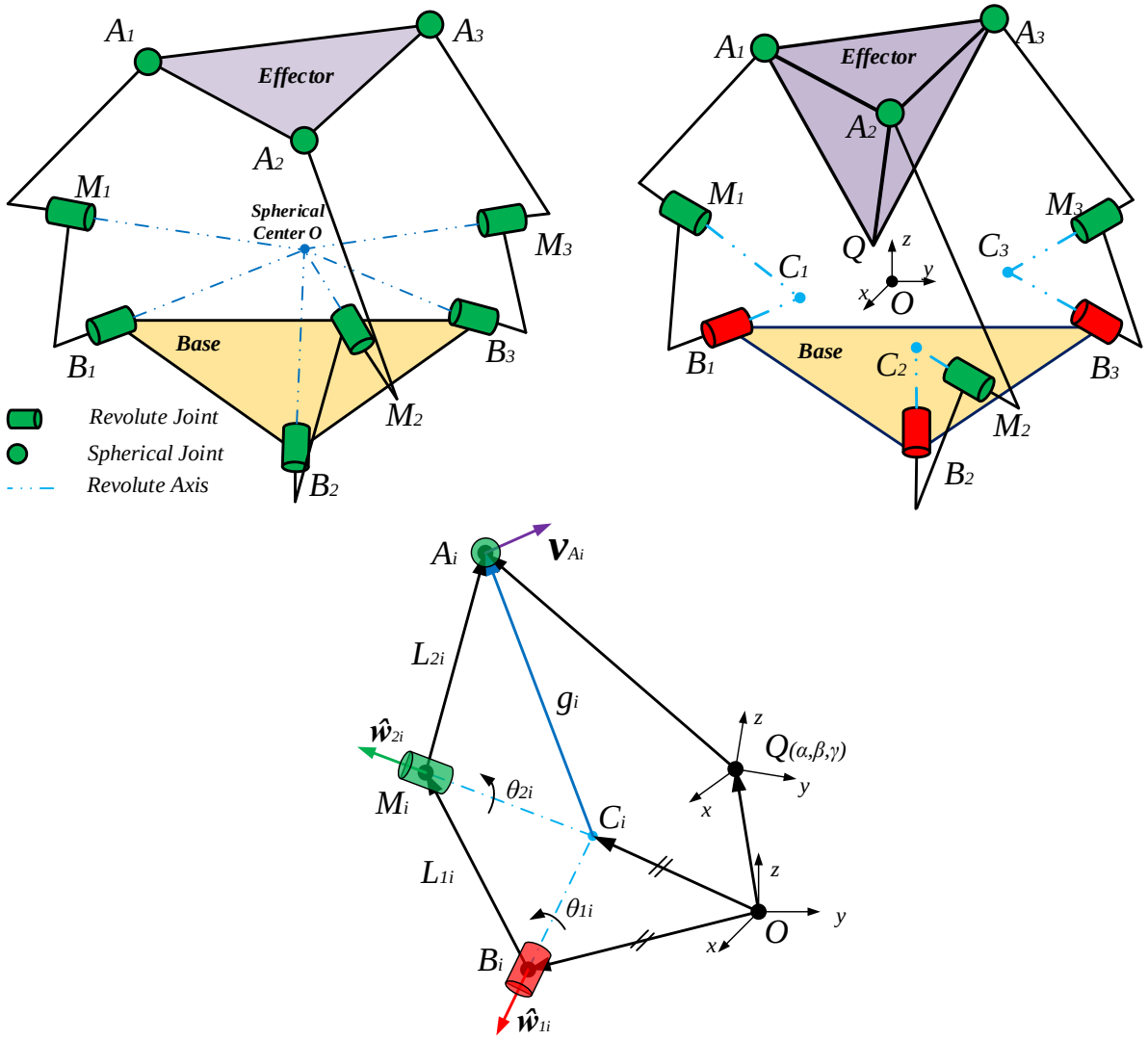

Figure 1.3: Underlying kinematic model of the robotic neck brace: (top left) the schematics of a 3-RRS wrist from which the proposed mechanism was derived, (top right) the kinematic model of the 3-RRS mechanism of the robotic neck brace, and (bottom) the loop closure of one kinematic chain. The proximal joints, labeled in red, are designated to be actuated. B_1, B_2, and B_3 form the stationary base in the inertial frame $\{O\}$. A_1, A_2, A_3, and Q form the end-effector. Three RRS chains whose joints are centered at B_i, M_i, and A_i, where $i = 1, 2, 3$, connect the end-effector to the base. B_iC_i and M_iC_i are the revolute axes which intersect at stationary point C_i. The lengths of the two links in a chain are L_{1i} and L_{2i}, respectively. $\hat{\mathbf{w}}_{1i}$ and $\hat{\mathbf{w}}_{2i}$ are unit vectors indicating the orientations of the two revolute axes and the joint angles are represented by θ_{1i} and θ_{2i}, respectively. End-effector frame is centered at a reference point Q. The orientation of frame $\{Q\}$ is represented by (α, β, γ) in Body Two 3-2-3 sequence. $\boldsymbol{v}_{A_i}$ is the velocity of point A_i and g_i is the distance between points A_i and C_i.

reduces the inertial load of the actuators during a dynamic motion[3]. As a trade-off, such a parallel architecture may sacrifice the volume of its workspace that would be saved by a serial structure.

In each chain, the center of the ball joint, A_i, moves on a spherical surface centered at the intersecting point, C_i, of the two revolute axes, $\hat{\mathbf{w}}_{1i}$ and $\hat{\mathbf{w}}_{2i}$, where $i = 1, 2, 3$. Therefore, A_i's move on three spherical surfaces centered at different origin C_i's, causing the movement of the end-effector to have coupled rotation and translation. Manipulating the locations of C_i's results in different rotation-translation coupling of the end-effector.

The two revolute axes in each chain are required to intersect. However, the locations of the centers of these revolute joints, i.e., M_i and B_i, can be anywhere along the axes. This provides flexibility in choosing design parameters in a physical model. For the simplicity of computation, the revolute joint centers, M_i and B_i, are chosen, as shown in Figure 1.3, such that the linkage vectors, $\overrightarrow{B_iM_i}$ and $\overrightarrow{M_iA_i}$, are perpendicular to respective revolute axes, $\hat{\mathbf{w}}_{1i}$ and $\hat{\mathbf{w}}_{2i}$.

1.3 Position Analysis

The kinematics of this 3-RRS mechanism is governed by three vectorial equations. Referring to Figure 1.3, each RRS chain forms a loop closure equation,

$$\mathbf{r}_{OQ} + \mathbf{r}_{QA_i} = \mathbf{r}_{OC_i} + \mathbf{r}_{C_iB_i} + \mathbf{r}_{B_iM_i} + \mathbf{r}_{M_iA_i} \tag{1.1}$$

where $\mathbf{r}_{XY}$ represents a vector from point X to Y (Figure 1.3) expressed in the inertial frame $\{O\}$. On the left hand side of Equation 1.1, the translation, $\{x_Q, y_Q, z_Q\}$, and rotation, $\{\alpha, \beta, \gamma\}$, of the end-effector are embedded while the angles of the revolute joints, θ_{1i} and θ_{2i}, are included on the right hand side of this equation. Therefore, there are a total of twelve variables and nine scalar equations in this system. Given the values of three variables, the rest can be determined.

Since the neck brace is designed to achieve head-neck rotations with torques provided by motors fixed on the base, the rotation of the end-effector, $\{\alpha, \beta, \gamma\}$, and the angles of the three proximal

[3]This choice also impacts the force controller design (Chapter 2). Because of the low inertia of the moving components, along with other simplifications, the force applied on the end-effector was considered quasi-statically balanced by the torques output by the actuators.

revolute joints, θ_{1i}, are of the most interest. The position analysis is, therefore, to provide a mapping from the proximal joint angles, θ_{1i}, to the rotation of the end-effector, $\{\alpha, \beta, \gamma\}$ (forward problem), and vice versa (inverse problem).

Analytical solutions to the forward and inverse problems are always desired because they take less time to compute in real-time. An analytical solution to the inverse problem is firstly derived. Solving the forward kinematics analytically, however, turns out to be very difficult for the proposed mechanism. A numerical approach of integrating angular rates is used to obtain the orientation of the end-effector. This approach relies on a first order mapping (velocity kinematics) between the angular rates of the end-effector, $\{\dot{\alpha}, \dot{\beta}, \dot{\gamma}\}$, and the proximal joint rates, $\dot{\theta_{1i}}$, where $i = 1, 2, 3$. This velocity kinematics is also used in the static analysis when computing the torques required at the proximal revolute joints to balance a force applied at the end-effector.

Inverse Kinematics

The inverse kinematics problem is defined as solving the angles of three proximal revolute joints, θ_{1i}, where $i = 1, 2, 3$, provided the rotation of the end-effector, $\{\alpha, \beta, \gamma\}$. The center of each spherical joint, A_i, moves on a sphere centered at the stationary point C_i in each chain with a known radius of g_i. Therefore,

$$||\mathbf{r}_{A_iC_i}||^2 = g_i^2 \,. \tag{1.2}$$

The positions of C_i's are known quantities from the model and the positions of A_i's can be expressed as $\mathbf{r}_{OA_i} = \mathbf{r}_{OQ} + \mathbf{r}_{QA_i}$. Using Equation 1.2, one can therefore obtain three quadratic equations involving the position of Q in the inertial frame $\{O\}$,

$$(a_{i1} + x_Q)^2 + (a_{i2} + y_Q)^2 + (a_{i3} + z_Q)^2 = g_i^2 \tag{1.3}$$

where x_Q, y_Q, and z_Q are components of the position of Q and a_{ij} are components of vector $\vec{a_i} = \mathbf{r}_{QA_i} - \mathbf{r}_{OC_i}$ which is a known quantity given the orientation of the end-effector. On manipulating

Equation 1.3, one can find two sets of $\{x_Q, y_Q, z_Q\}$.

Once both the position and orientation of the end-effector are solved, the coordinate of A_i in the inertial frame $\{O\}$ can be expressed. On the other hand, the position of M_i can be formulated using proximal joint angle θ_{1i}'s. Because the lengths of each distal link, L_{2i}, are constants, the following equation holds true,

$$||\mathbf{r}_{M_iA_i}||^2 = L_{2i}^2 \tag{1.4}$$

where $i = 1, 2, 3$. Each θ_{1i} can be solved independently using one of the component equations which can be simplified into a quadratic polynomial. Therefore, up to two solutions can be found for each θ_{1i} and Equation 1.4 admits at most a total of eight sets of θ_{1i} given one set of $\{x_Q, y_Q, z_Q\}$. Hence, there are up to sixteen solutions to the inverse kinematics problem.

Velocity Kinematics

Velocity kinematics provides a first order approximation when mapping the proximal joint rates, $\dot{\boldsymbol{\theta}}_1 = \begin{bmatrix} \dot{\theta_{11}} & \dot{\theta_{12}} & \dot{\theta_{13}} \end{bmatrix}^T$, to the linear and angular velocities, $\boldsymbol{v}_Q$ and $\boldsymbol{\omega}^Q$, of the end-effector through a configuration dependent matrix (Jacobian).

The velocity of A_i can be expressed using the linear and angular velocities of the end-effector,

$$\boldsymbol{v}_{A_i} = \boldsymbol{v}_Q + \boldsymbol{\omega}^Q \times \mathbf{r}_{QA_i}. \tag{1.5}$$

Because point A_i moves on a spherical surface centered at point C_i, the following holds true,

$$\boldsymbol{v}_{A_i} \cdot \mathbf{r}_{C_iA_i} = 0 \tag{1.6}$$

for $i = 1, 2, 3$. Substituting Equation 1.5 into Equation 1.6, one can obtain

$$\mathbf{r}_{CiAi} \cdot \boldsymbol{v}_Q + (\boldsymbol{\omega}_Q \times \mathbf{r}_{QAi}) \cdot \mathbf{r}_{CiAi} = 0.$$

Rewriting this equation, one can express $\boldsymbol{v}_Q$ in terms of $\boldsymbol{\omega}_Q$,

$$\boldsymbol{v}_Q = -\mathbf{M}_1^{-1}\mathbf{M}_2\boldsymbol{\omega}_Q$$

where

$$\mathbf{M}_1 = \begin{bmatrix} \mathbf{r}_{C_1A_1} & \mathbf{r}_{C_2A_2} & \mathbf{r}_{C_3A_3} \end{bmatrix}^T_{3\times3}$$

and

$$\mathbf{M}_2 = \begin{bmatrix} \mathbf{r}_{QA_1} \times \mathbf{r}_{C_1A_1} & \mathbf{r}_{QA_2} \times \mathbf{r}_{C_2A_2} & \mathbf{r}_{QA_3} \times \mathbf{r}_{C_3A_3} \end{bmatrix}^T_{3\times3}.$$

Defining a matrix $\mathbf{M} = -\mathbf{M}_1^{-1}\mathbf{M}_2$, gives

$$\boldsymbol{v}_Q = \mathbf{M}\,\boldsymbol{\omega}_Q. \tag{1.7}$$

The velocity of A_i can also be expressed as

$$\boldsymbol{v}_{A_i} = \boldsymbol{v}_{M_i} + \boldsymbol{\omega}^{M_iA_i} \times \mathbf{r}_{M_iA_i}$$

where $\boldsymbol{v}_{M_i}$ and $\omega^{M_iA_i}$ are the linear and angular velocities of the distal link M_iA_i, respectively. On manipulating this equation, one can obtain

$$\boldsymbol{v}_{A_i} = \dot{\theta_{1i}}\hat{\mathbf{w}}_{1i} \times \mathbf{r}_{B_iA_i} + \dot{\theta_{2i}}\hat{\mathbf{w}}_{2i} \times \mathbf{r}_{M_iAi}. \tag{1.8}$$

Equating Equations 1.5 and 1.8 and canceling the unknown quantity $\dot{\theta_{2i}}$, one can obtain

$$(\mathbf{r}_{B_iA_i} \times \hat{\mathbf{w}}_{2i}) \cdot \hat{\mathbf{w}}_{1i}\,\dot{\theta_{1i}} = (\mathbf{M}^T\hat{\mathbf{w}}_{2i} + \mathbf{r}_{QA_i} \times \hat{\mathbf{w}}_{2i}) \cdot \boldsymbol{v}_Q\,.$$

Defining Matrices, **H** and **N**, leads to

$$\mathbf{H}\,\dot{\boldsymbol{\theta}}_1 = \mathbf{N}\,\boldsymbol{\omega}^Q \tag{1.9}$$

where

$$\mathbf{H} = \begin{bmatrix} (\mathbf{r}_{B_1A_1} \times \hat{\mathbf{w}}_{21}) \cdot \hat{\mathbf{w}}_{11} & 0 & 0 \\ 0 & (\mathbf{r}_{B_2A_2} \times \hat{\mathbf{w}}_{22}) \cdot \hat{\mathbf{w}}_{12} & 0 \\ 0 & 0 & (\mathbf{r}_{B_3A_3} \times \hat{\mathbf{w}}_{23}) \cdot \hat{\mathbf{w}}_{13} \end{bmatrix}_{3\times3}$$

and

$$\mathbf{N} = \begin{bmatrix} (\mathbf{M}^T\hat{\mathbf{w}}_{21} + \mathbf{r}_{QA_1} \times \hat{\mathbf{w}}_{21}) & (\mathbf{M}^T\hat{\mathbf{w}}_{22} + \mathbf{r}_{QA_2} \times \hat{\mathbf{w}}_{22}) & (\mathbf{M}^T\hat{\mathbf{w}}_{23} + \mathbf{r}_{QA_3} \times \hat{\mathbf{w}}_{23}) \end{bmatrix}^T_{3\times3}.$$

Therefore,

$$\dot{\boldsymbol{\theta}}_1 = \mathbf{J}_\omega\,\boldsymbol{\omega}^Q \tag{1.10}$$

where

$$\mathbf{J}_\omega = \mathbf{H}^{-1}\,\mathbf{N}\,.$$

Equation 1.10 provides a velocity mapping between the joint rates, $\dot{\boldsymbol{\theta}}_1$, and the angular velocity of the end-effector, $\boldsymbol{\omega}^Q$.

Forward Kinematics

Forward kinematics is defined as solving the orientation of the end-effector, $\{\alpha, \beta, \gamma\}$, expressed in Body Two 3-2-3 (i.e., Body Z-Y-Z) of the end-effector frame given the angles, θ_{1i}, where $i = 1,\ 2,\ 3$, in the proximal revolute joints.

Analytically solving the forward kinematics problem using the loop closure equations (Equa-

tion 1.1) turns out to be very difficult [27]. On the other hand, the orientation of the end-effector can be achieved through integrating the angular rates of the end-effector, $\dot{\boldsymbol{\psi}} = \{\dot{\alpha}, \dot{\beta}, \dot{\gamma}\}$, with respect to time, giving

$$\boldsymbol{\psi} = \int_t \dot{\boldsymbol{\psi}}\, dt\,. \tag{1.11}$$

Because the angular velocity of the end-effector, $\boldsymbol{\omega}^Q$, is mapped to the rates of the proximal revolute joints, $\dot{\theta}_{1i}$, through the Jacobian matrix (Equation 1.10), Equation 1.11 can be expressed in terms of $\dot{\boldsymbol{\theta}}_1$ as,

$$\boldsymbol{\psi} = \int_t \mathbf{B}\,(\mathbf{J}_\omega{}^{-1}\,\dot{\boldsymbol{\theta}}_1)\, dt \tag{1.12}$$

where matrix $\mathbf{B}$ relates the angular velocity, $\boldsymbol{\omega}^Q$, to the angular rates, $\dot{\boldsymbol{\psi}}$,

$$\mathbf{B} = \begin{bmatrix} -\cos\gamma/\sin\beta & \sin\gamma/\sin\beta & 0 \\ \sin\gamma & \cos\gamma & 0 \\ \cos\gamma/\tan\beta & -\sin\gamma/\tan\beta & 1 \end{bmatrix}.$$

In practice, this integration is obtained numerically with a first order approximation,

$$\boldsymbol{\psi}^{(t+1)} = \boldsymbol{\psi}^{(t)} + \dot{\boldsymbol{\psi}}^{(t)} \cdot \delta t$$

where $\dot{\boldsymbol{\psi}}^{(t)}$ is the angular rate of the end-effector at time t, $\boldsymbol{\psi}^{(t)}$ and $\boldsymbol{\psi}^{(t+1)}$ are the orientations of the end-effector at time t and $t+1$, and δt is the sampling period of a controller. Equation 1.12 then becomes,

$$\boldsymbol{\psi}^{(t+1)} = \boldsymbol{\psi}^{(t)} + \mathbf{B}^{(t)}\,(\mathbf{J}_\omega{}^{(t)})^{-1}\ \dot{\boldsymbol{\theta}}_1{}^{(t)} \cdot \delta t\,.$$

Similarly, the joint rates, $\dot{\boldsymbol{\theta}}_1{}^{(t)}$, can also be approximated as,

$$\dot{\boldsymbol{\theta}}_1{}^{(t)} = (\boldsymbol{\theta}_1^{(t)} - \boldsymbol{\theta}_1^{(t-1)})/\delta t\,.$$

Therefore, the orientation of the end-effector at time $t+1$, $\boldsymbol{\psi}^{(t+1)}$, can be formulated as,

$$\boldsymbol{\psi}^{(t+1)} = \boldsymbol{\psi}^{(t)} + \mathbf{B}^{(t)}\,(\mathbf{J}_\omega{}^{(t)})^{-1}\;(\boldsymbol{\theta}_1^{(t)} - \boldsymbol{\theta}_1^{(t-1)})\,. \tag{1.13}$$

1.4 Force Balance

Not only does the Jacobian matrix (Equation 1.10) provide a velocity mapping between the joint and Cartesian spaces, but it also relates the wrench on the end-effector to the torques applied at the proximal joints. Using the principle of virtual work, when the end-effector is balanced by the joint torques, the total work in the system should equal zero,

$$W_f + W_\tau = 0 \tag{1.14}$$

where W_f and W_τ are the virtual works achieved by a force applied on the end-effector and by torques applied on the proximal joints, respectively. W_f can be then expressed as

$$W_f = \boldsymbol{f}_P \cdot \delta\boldsymbol{x}_P$$

where $\boldsymbol{f}_P$ is the force applied at a reference point P on the end-effector and $\delta\boldsymbol{x}_P$ is a resultant infinitesimal displacement by $\boldsymbol{f}_P$.

Similarly, W_τ can be expressed as

$$W_\tau = \boldsymbol{\tau} \cdot \delta\boldsymbol{\theta}_1$$

where $\boldsymbol{\tau} = \begin{bmatrix}\tau_1 & \tau_2 & \tau_3\end{bmatrix}^T$ are the torques applied at the proximal joints and $\delta\boldsymbol{\theta}_1$ are the angular

displacements resulting from these torques. As $\delta \boldsymbol{x}_P$ and $\delta \boldsymbol{\theta}_1$ are both arbitrarily small with a first order approximation, they can be replaced by the velocity of point P, $\boldsymbol{v}_P$, and the rates of proximal joints, $\dot{\boldsymbol{\theta}}_1$, respectively.

Substituting these two equations along with Equation 1.10 into Equation 1.14, one can obtain,

$$\boldsymbol{\tau} \cdot (\mathbf{J}_\omega \, \boldsymbol{\omega}^Q) = -\boldsymbol{f}_P \cdot \boldsymbol{v}_P \, . \tag{1.15}$$

Because P is a fixed point on the end-effector, $\boldsymbol{v}_P$ can be expressed in terms of the linear and angular velocity of the end-effector,

$$\boldsymbol{v}_P = \boldsymbol{v}_Q + \boldsymbol{\omega}^Q \times \mathbf{r}_{QP} \, .$$

Then, Equation 1.15 becomes

$$({\mathbf{J}_\omega}^T \, \boldsymbol{\tau}) \cdot \, \boldsymbol{\omega}^Q = -\boldsymbol{f}_P \cdot \boldsymbol{v}_Q - (\mathbf{r}_{QP} \times \boldsymbol{f}_P) \cdot \boldsymbol{\omega}^Q \, .$$

Recalling Equation 1.7 that the linear velocity of the end-effector is related to its angular velocity through matrix $\mathbf{M}$, therefore,

$$({\mathbf{J}_\omega}^T \, \boldsymbol{\tau}) \cdot \boldsymbol{\omega}^Q = -(\mathbf{M}^T \, \boldsymbol{f}_P + \mathbf{r}_{QP} \times \boldsymbol{f}_P) \cdot \boldsymbol{\omega}^Q \, .$$

This equation holds true for all $\boldsymbol{\omega}^Q$. Hence,

$$\boldsymbol{\tau} = -({\mathbf{J}_\omega}^T)^{-1} \, (\mathbf{M}^T \, \boldsymbol{f}_P + \mathbf{r}_{QP} \times \boldsymbol{f}_P) \, . \tag{1.16}$$

With Equation 1.16, the torques required at the proximal joints to balance a specific force applied at a known point on the end-effector can be computed.

Chapter 2

Neck Brace Design (Part II): Physical Model

In this chapter, geometric optimization and physical realization of the robotic neck brace are presented. Additionally, a collection of modalities are introduced to demonstrate the versatility of this robotic platform through an array of designs in actuation, interfaces, and controllers.

The brace was intended to be a versatile robotic platform that goes beyond fulfilling a specific task. It was engineered to be used in a wide variety of applications, from movement assessment to assisting user-controlled head motion and from physically training head-neck movement to providing affordable home-use head supports.

2.1 Optimization

As mentioned in Chapter 1.2, the brace geometry is intended to best fit the empirical data collected from the head-neck motion of a healthy individual. Additionally, an optimal design should maximize the range of motion from the home configuration[1].

Parameter Space

The parameters to be optimized are the ones that govern the kinematics of the proposed mechanism (Equation 1.1)[2]. Therefore, the parameter space includes the location of the intersecting point, C_i, the position of the proximal revolute joint, B_i, the lower and upper link lengths, L_{1i} and L_{2i}, and the position of the spherical joint in the end-effector frame, A_i, for each of the three chains.

[1] The home configuration of this neck brace is defined as when the orientation of the end-effector is aligned with the robot base. At this configuration, the robot also aligns with its user at the upright neutral posture of the head relative to the shoulders.

[2] Vectors $\overrightarrow{B_iM_i}$ and $\overrightarrow{M_iA_i}$ are perpendicular to respective revolute axes, $\hat{\mathbf{w}}_{1i}$ and $\hat{\mathbf{w}}_{2i}$, where $i = 1,\ 2,\ 3$, referring to Figure 1.3.

To reduce the amount of parameters and ensure an aesthetic design, a symmetry constraint is imposed: an optimal design should be symmetric about the sagittal plane when the brace is at its home configuration. This means two chains, namely chain 1 and chain 2, are mirrored about the sagittal plane, and critical points in chain 3, i.e., C_3, B_3, and A_3, are all located on the sagittal plane.

Objectives

The objectives of the optimization are to: (1) minimize the translational error of the end-effector as compared to the human data and (2) maximize the range of rotation of the end-effector from the home configuration of the robot.

According to Equations 1.2 and 1.3, given an end-effector orientation, its translation is determined by the coordinates of three pairs of A_i's and C_i's, which are fixed points in the moving and inertial frames, respectively. Additionally, the distance between each pair of A_i and C_i is a constant regardless of the orientation of the end-effector. Therefore, to minimize the translational error, it is equivalent to searching for three non-colinear pairs of such points in the end-effector and base frame, respectively, to have **constant distances** among all instances in the human data.

Because the underlying mechanism allows fewer DOFs, it is very difficult to analytically find three pairs of A_i's and C_i's with constant distances from the unconstrained human data. Instead, the optimal A_i and C_i in each chain are searched to have **minimally deviated distances**. That is,

$$\begin{aligned} &\min\ \mathbb{E}[\mathrm{g}_i^2] - \mathbb{E}[\mathrm{g}_i]^2 \\ s.t.\ \ &\mathbf{r}_{A_i}^Q \in [lb,\, ub],\ i = 1,\, 2,\, 3\,. \end{aligned} \tag{2.1}$$

where $\mathbb{E}[\cdot]$ represents the mean of an independent variable, g_i is the distance between a pair of A_i and C_i, i.e., $\mathrm{g}_i = ||\mathbf{r}_{A_iC_i}||$, and lb and ub are the lower and upper bounds of the search range of A_i in end-effector frame.

Once the optimal pairs of A_i's and C_i's are found, other parameters can be optimized to maximize the **continuous** range of rotation of the end-effector from its home configuration in each of the anatomical planes, i.e., the sagittal, coronal, and transverse planes.

Algorithm

A two-phase hierarchical random search was used to find an optimal set of parameters. In phase I, three pairs of A_i's and C_i's with minimally deviated distances were found[3]. In phase II, optimal values of other parameters, i.e., the locations of base joints, B_i's, and link lengths, L_{1i}'s and L_{2i}'s, were found.

Result

Phase I ran for $10,000$ cases and phase II ran for $3,000$ cases. These simulations were completed in Matlab (MathWorks Inc. Natick, MA, USA) on a lab-based desktop (Intel CPU @ 3.40 GHz and 16 GB RAM). The final result is shown in Figure 2.1. This model optimizes the parameters that govern the kinematics of the mechanism which does not infer the physical design of the brace.

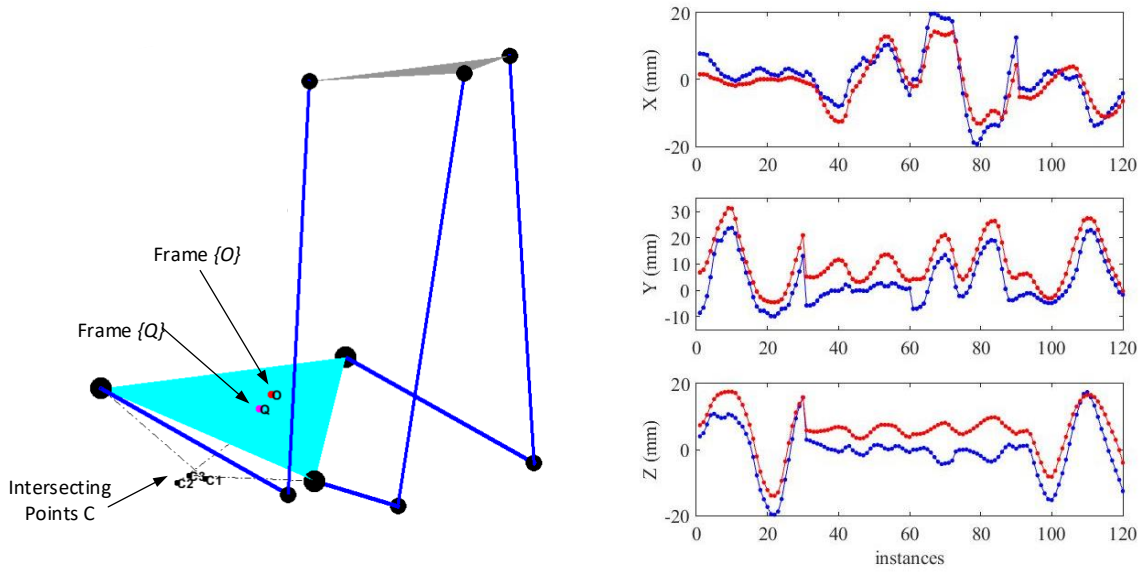

Figure 2.1: Optimization results of the robotic brace in simulation: (left) the geometry of the optimal model and (right) the comparison of the head translation between the actual human data (red) and the predicted values using the optimal model (blue). The overall translational errors for all four motions of the optimal design are: $x = 1.3 \pm 3.5\,mm$, $y = 6.0 \pm 2.9\,mm$ and $z = -5.8 \pm 2.7\,mm$. The optimal design maintains the ranges of rotation of $+25/-45°$ in sagittal plane, $\pm 35°$ in frontal plane and $\pm 65°$ in horizontal plane. All values are based on the coordinate system in Figure 1.1.

[3]Two pairs were symmetric about the sagittal plane, and the third pair was located on the sagittal plane.

2.2 Realization

The optimal geometry was then realized into a physical brace using computer-aided design (CAD), as shown in Figure 2.2. This physical model attaches to the shoulders and the forehead of a user through a pair of pads and a soft headband, respectively. Three mechanical chains are articulated between these two attachments using RRS connections. The locations of the revolute joints in each chain were manually selected along the optimal axes such that the range of motion of the robot from the simulation result is preserved. The brace structure is 3D-printed using ABS plastic, and the joints are realized by inexpensive off-the-shelf parts. The brace weighs 1.2 kg. The majority of this weight is carried by the shoulders of the user.

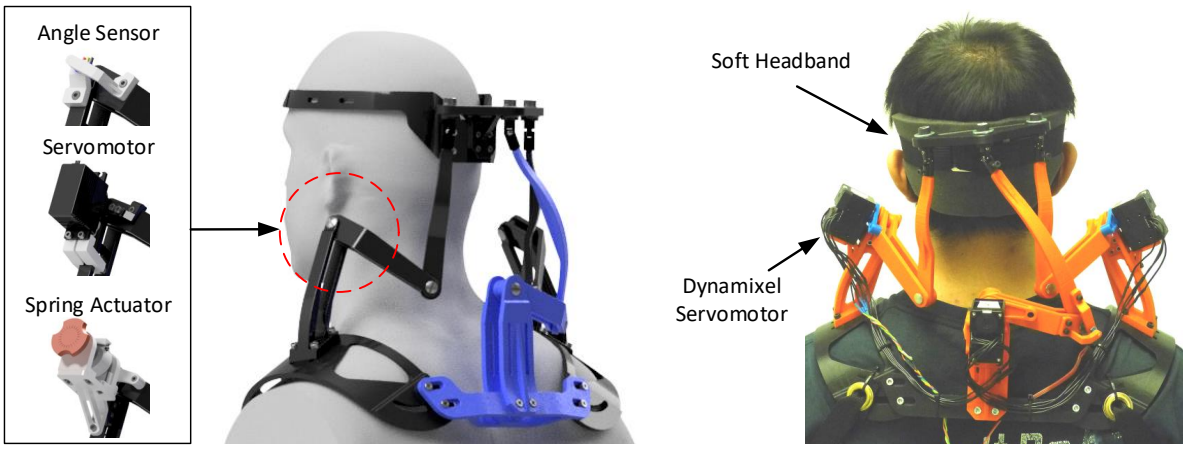

Figure 2.2: Physical model iterations of the robotic neck brace: (left) the first iteration of the robotic brace where three joint modules share a same brace structure and are designed to achieve measurement, assistance, and flexible passive support and (right) the second iteration of the neck brace where three Dynamixel servomotors are used as joint units and a soft headband is implemented to improve comfort.

The design of joint modules to measure and actuate the brace has been transformed through two major iterations (Figure 2.2). In the beginning, the design philosophy was to provide multiple specialized joint modules for different applications. These joint modules needed to be interchangeable so that they can be installed on the same brace structure and easily swapped between applications. This approach, however, has some practical limitations. For example, it requires a second person

to change the modules for a potential user, possibly an individual with head drop. Frequent changes may also increase wear and tear to the plastic structure over time.

To address these drawbacks, the philosophy has been morphed to using only one joint module design for all applications. Three dynamixel servomotors (XM430-W350-R, ROBOTIS Inc., Seoul, South Korea) are therefore used in the second generation of the brace. Encoders and current sensors are housed in these motors to measure the position of the motor shaft and the current generated due to the back electromotive force (back emf). Within its calibrated range, this current is linearly related to the external torque exerted on the output shaft[4]. In this way, these current sensors can be used to estimate the joint torques and consequently allow the brace to control the forces applied to its user. Additionally, these motors are backdrivable, which in conjunction with the specific lengths of the linkages allows this robotic brace to achieve a desired 'transparency'[5] when the output torques of the motors are switched off in software. This enables the brace to measure free head-neck motion of the user.

Compared to its predecessor (Table 2.1), the second version of the neck brace also improves its wearability by using a soft headband to attach to the forehead of the user. Batteries, a microcontroller (NI myRIO-1900, National Instruments, Austin, TX, USA), and a custom-made communication circuit[6] are all embedded in a small pouch which can be worn around the waist of the user. This improves the portability of the brace.

2.3 Modalities

Motion Measurement and Visual Displays

The motor encoders measure the proximal joint angles of the brace. The orientation of the end-effector can then be computed through forward kinematics. This information can be used in real-

[4]Although each motor allows a torque up to 4.1 Nm, the current generated by each motor is limited to a value that is sufficient to move the head against gravity to ensure safety.

[5]Transparency means there is zero force applied from the robot to its user.

[6]The serial communication between the servomotors and the microcontroller is converted from RS-485 (half-duplex) to UART (universal asynchronous receiver/transmitter) with a baud rate of $115,200$ bit-per-second (bps).

Table 2.1: Comparison between the two iterations of the robotic neck brace

	1st Iteration	2nd Iteration
# of Joint Modules	3	1
Portability	Low	High
Weight of Brace	0.5 ~1.2 kg	1.2 kg
Head Attachment	Rigid	Soft
Transparent Mode	✓	✓
Position Control	✓	✓
Force Control	×	✓

time controllers to apply specific forces to the head based on its posture. It can also be used to provide visual feedback to a user through, for example, a screen display.

Figure 2.3 demonstrates two visual interfaces developed for the brace system to date. The first is an avatar interface. It is designed to provide visual feedback to a user during a targeted head-neck trajectory. Two 3D humanoid avatars are superimposed on one another. Of the two, the avatar with solid colors (target avatar, TA) demonstrates the target motion and the translucent avatar (user avatar, UA) displays the movements of the user[7]. A bar indicator is placed on the top of each avatar's head to help the user track the target motion, aligning the 3D facial geometry of the avatars. The color of the bars indicates the tracking accuracy of the subject. The users can also switch the camera view to see the avatars from different angles. In a default setting, users see the front view of the avatars with their facial features. The motion of the avatars are mirrored to the actual motion of the user.

The second interface visualizes a pick-and-place task on a 2D plane. The idea is that the user can use the head as an end-effector to displace a virtual object (red dot) to a target (blue circle). The 2D task is a projection on the transverse plane where the flexion/extension and lateral bending of the head move the object anterior/posteriorly and mediolaterally, respectively. Counters and timers are also included in this interface to facilitate the subject to complete the tasks.

Measuring free motion of the head assesses a baseline performance of a user. This requires the

[7]Usually this movement is executed by the head of a user and measured by the neck brace. There are exceptions, however. An example is introduced in Chapter 4 where the movement of the phantom avatar is commanded by the wrist of the user through a hand-held joystick.

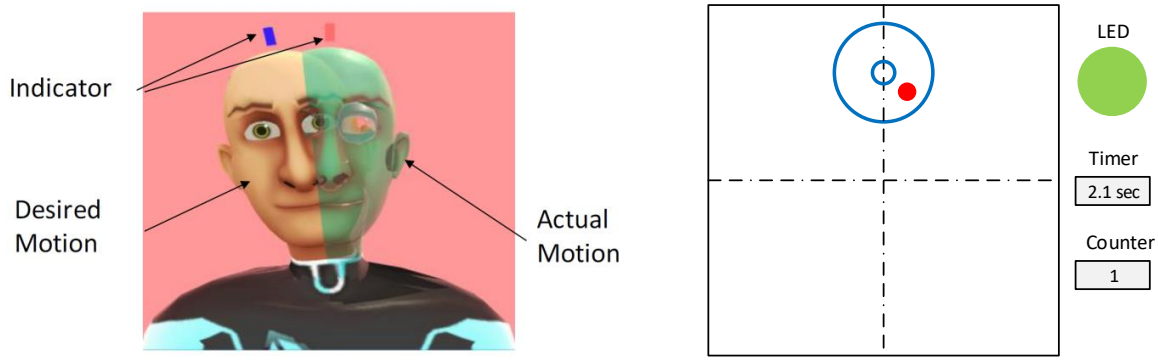

Figure 2.3: Visual interfaces designed for the robotic neck brace system: (left) the 'Avatar' interface and (right) the 'pick-and-place' interface.

brace to be 'transparent' to the user, purely measuring the head angles without applying any force. The use of the dynamixel servomotors, in conjunction with the specific brace geometry, allow the robot to achieve this 'transparency'.

Assisting Head Motions

The robotic brace is built to apply sufficient forces to counterbalance the weight of the head, which is about 5 kg for an adult [35, 36]. The main control strategy for assisting the movement of the head is through a position controller. As shown in Figure 2.4, when a desired head orientation is sampled based on a input command by the user, the motor angles are computed through inverse kinematics. Internal PID controllers then deliver the movement to the head by regulating the motor positions based on these position commands and the encoder values.

Another important aspect of this application is the effective acquisition of the user intention. Currently, it can be achieved through an array of input devices, including hand-held joysticks, keyboards, and eye-trackers. For each of these devices, a corresponding interface is designed.

In the joystick interface, the angle of the stick is mapped to the angle of the brace in each direction. This mapping is scaled to account for the different ranges of rotation for each direction of the joystick and the brace. When a user moves the stick with an angle, the brace would respond to it and move the head with a scaled angle (Table 2.2). In this way, the joystick control allows

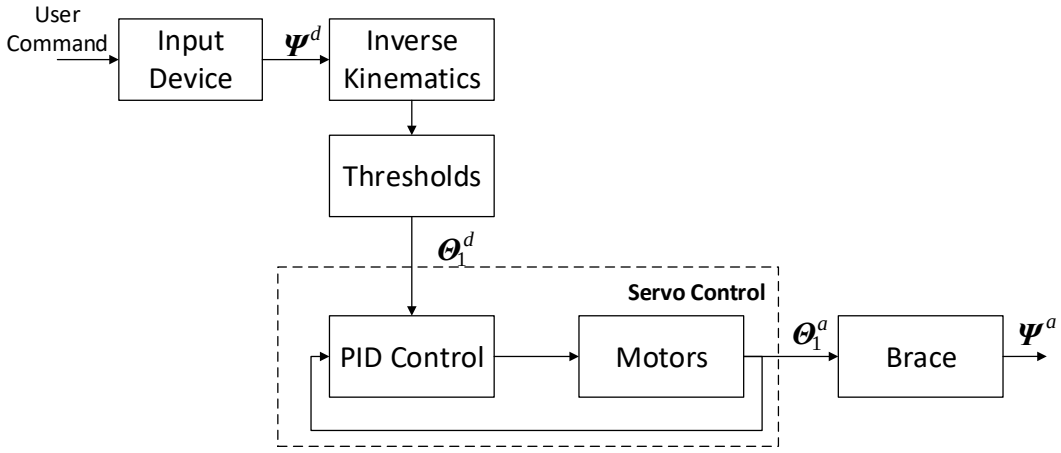

Figure 2.4: Position control of the robotic neck brace. ψ^d, ψ^a are desired and actual orientation of the end-effector. $\boldsymbol{\theta}_1^d$ and $\boldsymbol{\theta}_1^d$ are desired and actual angles of the proximal revolute joints.

fast movement of the head using one hand. However, because of the existence of the springs in the joystick, the brace would return suddenly to its home configuration if the hand of the user slips off the joystick. This may create a jarring movement for the user. This hazard is mitigated by setting velocity and acceleration limits in the servomotors. Additionally, the raw signal from the joystick is low-pass filtered before being sent to the main controller to prevent such a sudden change. The trade-off, however, is that this creates a small time delay with the head movement being behind the hand operation.

Table 2.2: Angle mapping in different directions between the joystick and the neck brace in the 'Joystick' control

	Joystick Range	ROM of Brace
Flexion/Extension	$-32767/32767$	$40°/10°$
Left/Right Bending	$-32767/32767$	$30°/30°$
Left/Right Rotation	$-32767/32767$	$45°/45°$

*Note - When each angle component of the joystick is 0, the brace is at its home configuration.

Instead of using the absolute angular mapping of the joystick, the keyboard interface exploits an incremental approach to command the orientation of the brace. A user can press certain keys to position the head with a speed (increment per sample) in three dimensions. In this approach, the head can be stopped at a posture when no key is pressed by the user. However, it is challenging

for the user to correlate the finger presses to a spatial head orientation. Additionally, although the speed can be modulated by keys, it may be difficult to adjust it during a motion. Therefore, in order to use this approach proficiently, the user may need extensive practices to adapt to it.

Whether using a joystick or a keyboard, one major flaw of the control methods is that they require full or partial function in the upper limb of the user. This may not be available for those with severe weakness in the upper limbs, which is commonly seen in patients with ALS. To address this issue, an interface using a wearable eye-tracker is developed. This eye-tracker, similar to the frame of a pair of glasses, can be worn along with the neck brace. It consists of a video camera (world camera) which takes real-time images and behaves as the field of view (FOV) of the user, and two infrared cameras (eye camera) which focus on the pupils of the eyes. The gaze point in the FOV is then estimated by an internal model of the tracker based on these camera images.

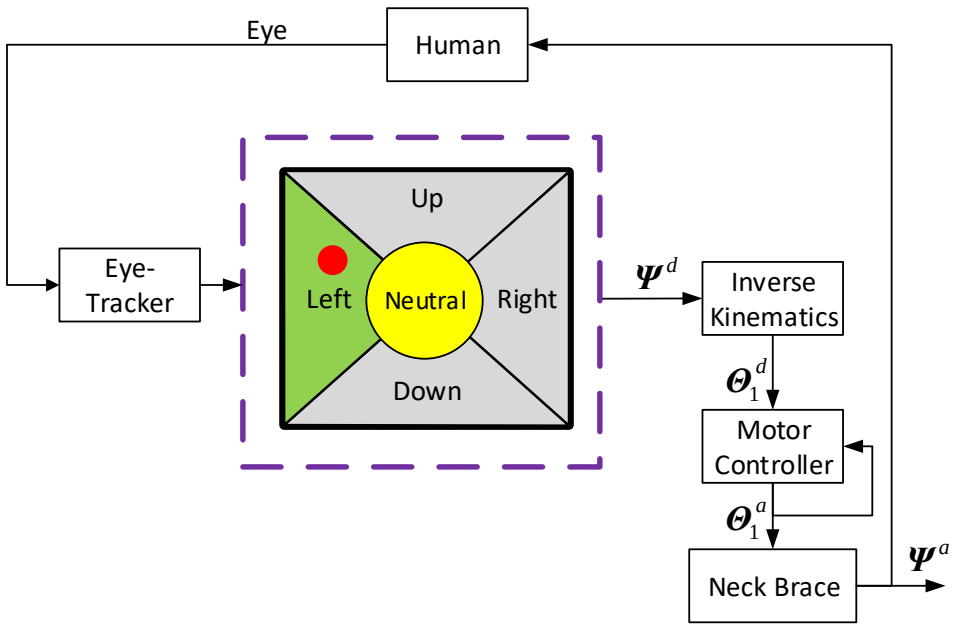

Figure 2.5: The eye-control scheme of the robotic neck brace with human in the loop. The normalized world image is updated by the actual head movement of the user, ψ^a. Given a gaze location in the image, the desired orientation, ψ^d, updates incrementally towards the selected direction. As shown in this example, the gaze point (red dot) is located in the 'Left' region of the world image, indicating an intended left rotation of the head from its current orientation. The desired joint angles, $\boldsymbol{\theta}_1^d$, are then computed using inverse kinematics, and the actual joint angles, $\boldsymbol{\theta}_1^a$, are regulated by a PID controller of the servomotors.

The design of this eye-controlled interface is inspired by one of the behaviors in eye-head coordination: fixation-saccade-fixation. When a visual stimuli occurs in the FOV, the eyes respond to it first due to their relatively low moving inertia compared to the head. The head then follows and the eyes move back to the center of the FOV. Based on this behavior, the world image is divided into five regions (Figure 2.5). When the gaze point of a user is located in one of the directional regions, the brace makes a move in that direction with a constant step size. When the head reaches the target, the eyes would move back to the center of the FOV. As a result, the gaze point falls back to the neutral zone (Figure 2.5) and the brace stops at that position. In this design, the user can command head orientation in two directions: longitudinal and latitudinal rotations. The bending motion of the head is not allowed by this interface and is restricted to 0 constantly. In its current form, the step size of the increment and the size of the neutral zone are predefined constants.

Force Control

The forces applied to the head from the brace can be rendered through a force controller. Considering the light weight of the moving components and the low operating speed of the robot, the complex dynamics of the system is simplified into a quasi-static problem. This means that the desired torques supplied by the motors can be computed using Equation 1.16 based on a desired force between the end-effector and the head.

A simple force controller, as illustrated in Figure 2.6, can be designed to track a desired force profile. Such a controller can be used in applications such as perturbation training, where the brace applies a sudden force impulse to the user. Similar paradigms have been successfully used, for example, to improve dynamic stability in patients with cerebellar ataxia during walking [37].

A tabletop testing was conducted to validate the brace to follow a desired force (Figure 2.6). The brace was fixed to a static frame at its home configuration. A six-axis F/T sensor was mounted between the end-effector and the frame. A series of sinusoidal and impulse forces were sent to the controller to follow. The results indicated that this robotic brace is able to produce the desired

[8] The current caused by back emf is actually sensed and controlled but because the motor torque is proportional to this current within the motor operating range, torque τ is loosely used in the schematics.

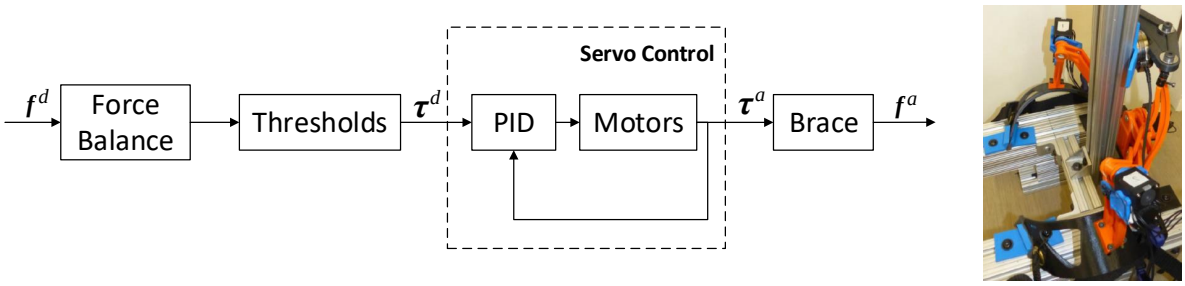

Figure 2.6: Table-top testing of the robotic neck brace controlling Cartesian forces: (left) the schematics of the force control and (right) the physical setup of the testing. $\boldsymbol{f}^d$ and $\boldsymbol{f}^a$ are desired and actual forces applied at the end-effector, respectively, and $\boldsymbol{\tau}^d$ and $\boldsymbol{\tau}^a$ are desired and actual torques applied by servomotors, respectively[8].

forces with small ($< 10\%$) errors due to deflections of the mechanical components [30].

If the desired force in Figure 2.6 is dependent on the posture of the head, then it becomes a position-based force controller. Such a controller can be used to mimic the interaction between a therapist and a patient during movement training. As shown in Figure 2.7, an example of such a position-based controller is designed to confine the head of the user to a cone-shaped region. This approach generates a desired force based on the difference between the desired and actual positions of a reference point in the end-effector frame[9]. In order to achieve a smooth transition between zero-force and the force field, the magnitude of the desired force, $||\boldsymbol{f}^d||$, is generated using

$$||\boldsymbol{f}^d|| = \begin{cases} 0 & d \leq r_c \\ K_n(1 - e^{(-(\frac{2d}{r_n})^2)}) & d > r_c \end{cases} \tag{2.2}$$

where K_n and r_n are controller gains, d is the distance between the desired and actual positions of the reference point in the end-effector, and r_c is the radius of the cone.

In addition to this approach that applies a Cartesian force, another controller is designed to render the interactive force in the joint space, as shown in Figure 2.8. When there is a difference between the desired and actual orientation of the end-effector, it will be reflected in the joint angles.

[9]The actual position of the reference point can be obtained through solving forward kinematics using encoder data measured by the base revolute joints.

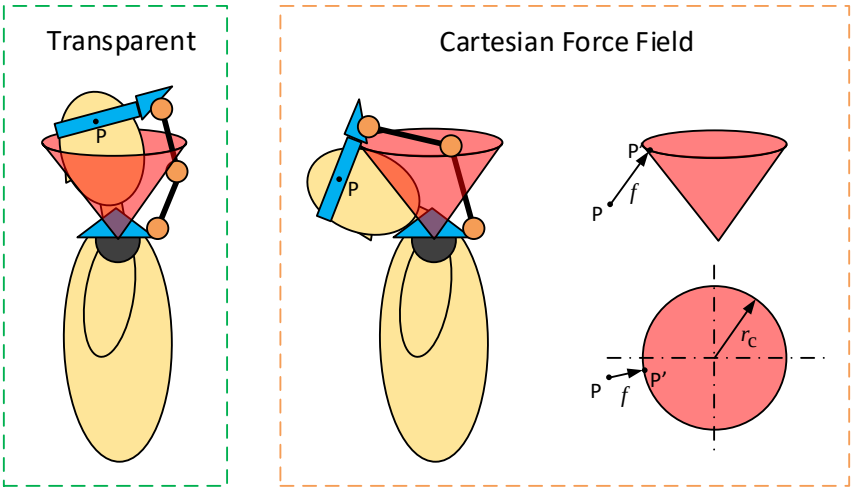

Figure 2.7: Schematics of a cone-shaped Cartesian force controller of the robotic neck brace: (left) no force is applied to the head when a reference point of the head, P, is within the cone and (right) a Cartesian force, f, is applied to push the reference point towards the boundary when the head moves outside the cone. The location of the boundary point, P', is found on the transverse plane projection. r_c represents the radius of the cone.

The torque applied by each joint can then be modeled as a spring-damper to correct such an angle difference. Therefore, the control law in Figure 2.8 can be formulated as

$$\tau_i^d = k_p^i \left(\theta_{1i}^d - \theta_{1i}^a\right) + k_d^i \left(\dot{\theta}_{1i}^d - \dot{\theta}_{1i}^a\right), \; i = 1, \, 2, \, 3 \tag{2.3}$$

where k_p^i and k_d^i are controller gains, θ_{1i}^d and θ_{1i}^a are desired and actual joint angles, and $\dot{\theta}_{1i}^d$ and $\dot{\theta}_{1i}^a$ are desired and actual angular rates of the base joints, respectively.

Passive Head Support with Adjustment

The control methods reviewed thus far all feature active configurations, however, a design without expensive motors and electronics could be beneficial for home usage. This passive design would also improve comfort where current rigid head support systems only keep the head at a single configuration without any movement. The key design concept was to use springs instead of externally powered actuators to balance the head at a selected posture. Because of the flexibility of the springs, the user can potentially deviate from the equilibrium configuration. As a matter of fact,

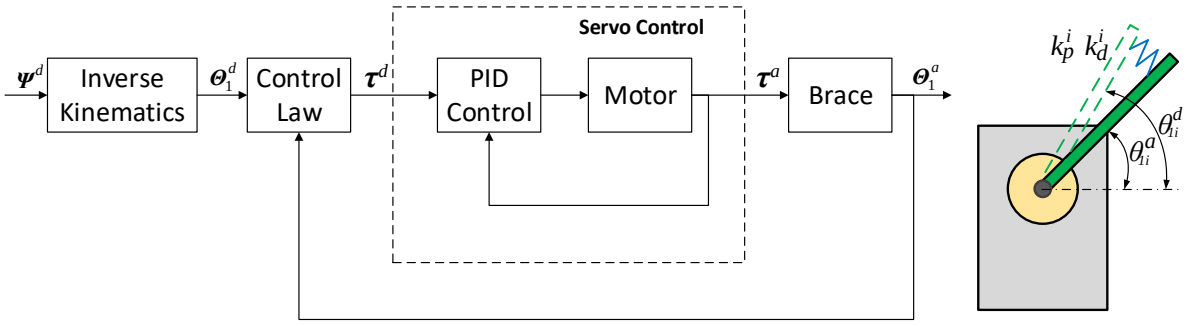

Figure 2.8: Schematics of a joint torque controller used in the robotic neck brace: ψ^d, $\boldsymbol{\theta}_1^d$, and $\boldsymbol{\tau}^d$ are desired head trajectory, desired base joint angles, and desired joint torques, respectively. $\boldsymbol{\theta}_1^a$ and $\boldsymbol{\tau}^a$ are the actual angles of the proximal joints and actual torque applied by the motors, respectively. k_p^i and k_d^i are the controller gains for each joint, where $i = 1,\ 2,\ 3$.

such a design can balance the head at many configurations, as long as the target configuration is within the workspace of the neck brace.

A spring actuator is therefore designed (Figure 2.9) to replace each servomotor at the proximal revolute joints. To provide dual-directional torques, two identical right-handed torsional springs are used in one actuator. A clutch is designed to engage/disengage the springs to the shaft of an actuator. This clutch is assembled to the shaft with a slit above its inner hole. The diameter of the inner hole is slightly larger than the shaft's diameter. In this way, tightening a screw to close the slit would deform the clutch and consequently engage the springs to the shaft.

Since the springs are attached to the shaft, they can be deformed and produce torques to counterbalance the weight of the head at a selected posture, $\{\alpha,\ \beta,\ \gamma\}$. The torque needed at each joint can be computed using Equation 1.16 given the force applied at the end-effector. Knowing the spring constant, the torque, τ_i, provided by a spring unit can be modeled as

$$\tau_i = k_i(\theta_{1i} - \theta_{1i}^0),\ \ i = 1,\ 2,\ 3 \tag{2.4}$$

where k_i is the spring constant of a unit, and θ_{1i} and θ_{1i}^0 are the final and free angle of the spring,

respectively. Then, the free angle, θ_{1i}^0, of each unit can be solved by

$$\theta_{1i}^0 = \theta_{1i} - \frac{\tau_i}{k_i} \ , \tag{2.5}$$

for $i = 1, 2, 3$. The final angles of the springs are the same as the joint angles at the proximal revolute joints. Therefore, they can be solved using the inverse kinematics with the desired end-effector orientation, $\{\alpha, \beta, \gamma\}$, as the input.

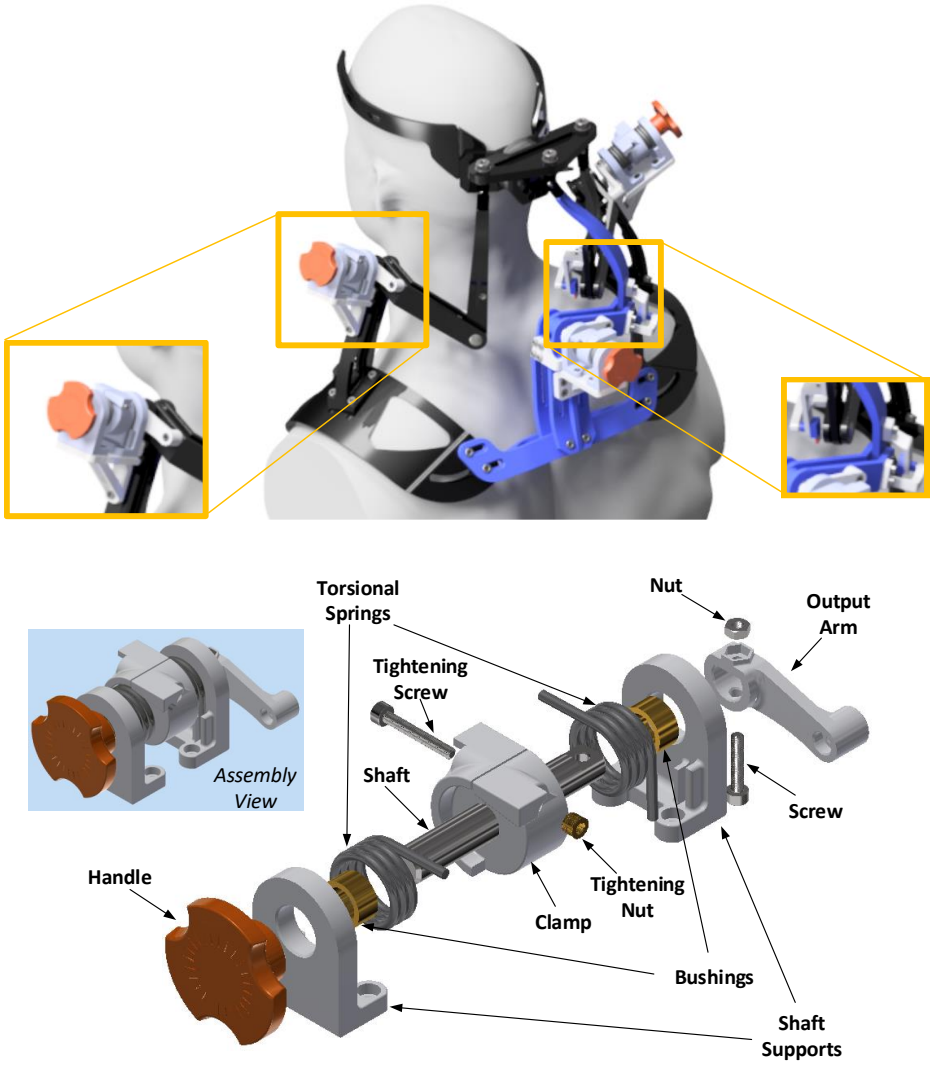

Figure 2.9: The model of the spring-loaded neck brace: (top) CAD assembly and (bottom) exploded-view of the spring actuator.

The procedure of adjusting the springs is as follows: (1) Compute the proximal joint angles, θ_{1i}'s, of the final (desired) posture of the head, (2) use Equation 2.5 to solve the free angles of the springs, (3) loosen the clutches and disengage the springs from the shafts so that the brace can be freely rotated, (4) manually place the brace at the initial configuration and tighten the screws to engage the spring actuators to the proximal joints, and (5) gently move the head towards the final configuration and balance it around the final posture. Step (4) requires a precise placement of the brace at its computed initial configuration. Therefore, angle measurements need to be added to the brace. To reduce the size of this brace module, three potentiometers are installed on the distal revolute joints instead of the proximal ones to provide these measurements. This design slightly changes the computation procedure as a numerical solver is used with an initial guess to compute the head angles through the loop closure equation (Equation 1.1).

There is a limitation of this procedure: the force needs to be provided at the end-effector of the brace at its final pose. For an application where the brace supports the weight of the head, the gravitational force is the only external force to be balanced by the spring torques. Therefore, with precise estimations of the center of gravity and weight of the head based on biomechanical models, this procedure can balance the head at a selected posture. The most useful posture to be balanced, however, is probably the upright neutral which happens to be an unstable equilibrium. In this configuration, The free angles of the springs can be set at its home configuration. In this way, the brace supports the head at upright neutral but allows it to move locally, thereby improving the comfort.

Chapter 3

Neck Brace Design (Part III): Validation Studies

In this chapter, validation studies are presented for different modalities introduced in Chapter 2. Healthy young subjects were recruited to evaluate the performance of the robotic brace. These human studies were approved by the Institutional Review Board (IRB) at Columbia University. The measurement, assistance, and training aspects were respectively evaluated in a setting of interacting with human subjects. The results showed that this robotic neck brace was able to accurately measure, assist as intended, and train movements of the head-neck. Additionally, some of these experiments also created baseline datasets for future studies with which the performance from patient population could be compared.

3.1 Measuring Head-Neck Motion

An experiment with ten healthy subjects (gender: 2 females and 8 males, age: 26.6 ± 4.4 yr, height: 177.2 ± 6.3 cm, and weight: 73.7 ± 15.6 kg) was carried out to evaluate the measurement accuracy and the range of motion of the neck brace[1]. Each subject sat on a stationary stool within the workspace of a MoCap system consisted of ten Vicon cameras which served as the measurement ground truth. The experiment had two parts: first, the subjects performed natural head-neck motions without the neck brace, and then they repeated these movements with the neck brace attached[2]. In this way, the range of motion of the head when wearing the brace can be compared with its natural range. Each part of the experiment started with a static trial where a subject holding an upright position for five seconds to capture the relative positions among the markers. This was then

[1] In this experiment, an earlier version of the neck brace was used where the joint angles were measured by rotary low-profile potentiometers.

[2] Performing the head-neck motions without the neck brace first to eliminate any potential effect from experiencing the neck brace to the natural movements of the head.

followed by the subject moving the head in three anatomical planes for ten consecutive cycles[3]. Lastly, each subject performed a general rolling motion[4] for another ten times.

The ranges of rotation of the head in each trial was quantified by the maximum/minimum value differential. The range in each motion reduced when the subjects moved the head with the neck brace (Figure 3.1). The medians of the remaining range of rotation, the ratio between with the neck brace and the free head-neck motion, in each direction among all subjects were: 77.9% (SD[5]: 16%) in flexion, 53.1% (SD: 12%) in extension, 88.1% (SD: 8%) in left bending, 79.2% (SD: 13%) in right bending, 69.7% (SD: 8%)in left rotation, and 60.8% (SD: 11%) in right rotation. Overall, the brace allows about 70% ranges of rotations of the head. The results in lateral bending and axial rotation show slight asymmetry which is due to the specific linkage design of the brace.

The experiment also evaluated the accuracy of the brace measurement with respect to the head rotations measured by the MoCap system. The absolute mean and root mean square errors were computed for each participant in each motion and the average and standard deviation among all subjects are summarized in Table 3.1. The measurement becomes less accurate when a subject reaches the extreme positions allowed by the brace. This is because the collisions among mechanical components made of plastic cause certain deflections which slightly changes the model parameters used for computing the head angles through forward kinematics. Additionally, such a collision may also cause the brace to slide slightly on the subject, resulting in measurement errors at the extremes.

Table 3.1: Average of absolute mean and root mean square errors of brace measurement

	Flexion/Extension	Bending	Rotation	Rolling
Absolute Mean	$1.1° \pm 2.5°$	$2.5° \pm 2.5°$	$2.5° \pm 2.9°$	$3.6° \pm 2.3°$
Root Mean Square	$1.8° \pm 2.9°$	$3.1° \pm 2.8°$	$3.0° \pm 3.0°$	$4.9° \pm 2.7°$

When the head moves within the workspace of the neck brace, the measurement is more accu-

[3]A movement cycle is defined as: starting from neutral and move to one extreme posture, moving back and passing the neutral to reach another extreme, and finally returning back to neutral.

[4]This motion starts with the head flexed forward about $30°$, followed by a full rotation about the vertical axis.

[5]This is abbreviated for standard deviation.

rate. Figure 3.1 shows the accurate workspace of the neck brace using a threshold value of $\pm 3^\circ$ against the ground truth, i.e., computed head angles using marker trajectories recorded by the Mo-Cap system. It shows that the brace has a larger measurable range in flexion/extension and lateral bending, while this measurable range becomes smaller in axial rotation.

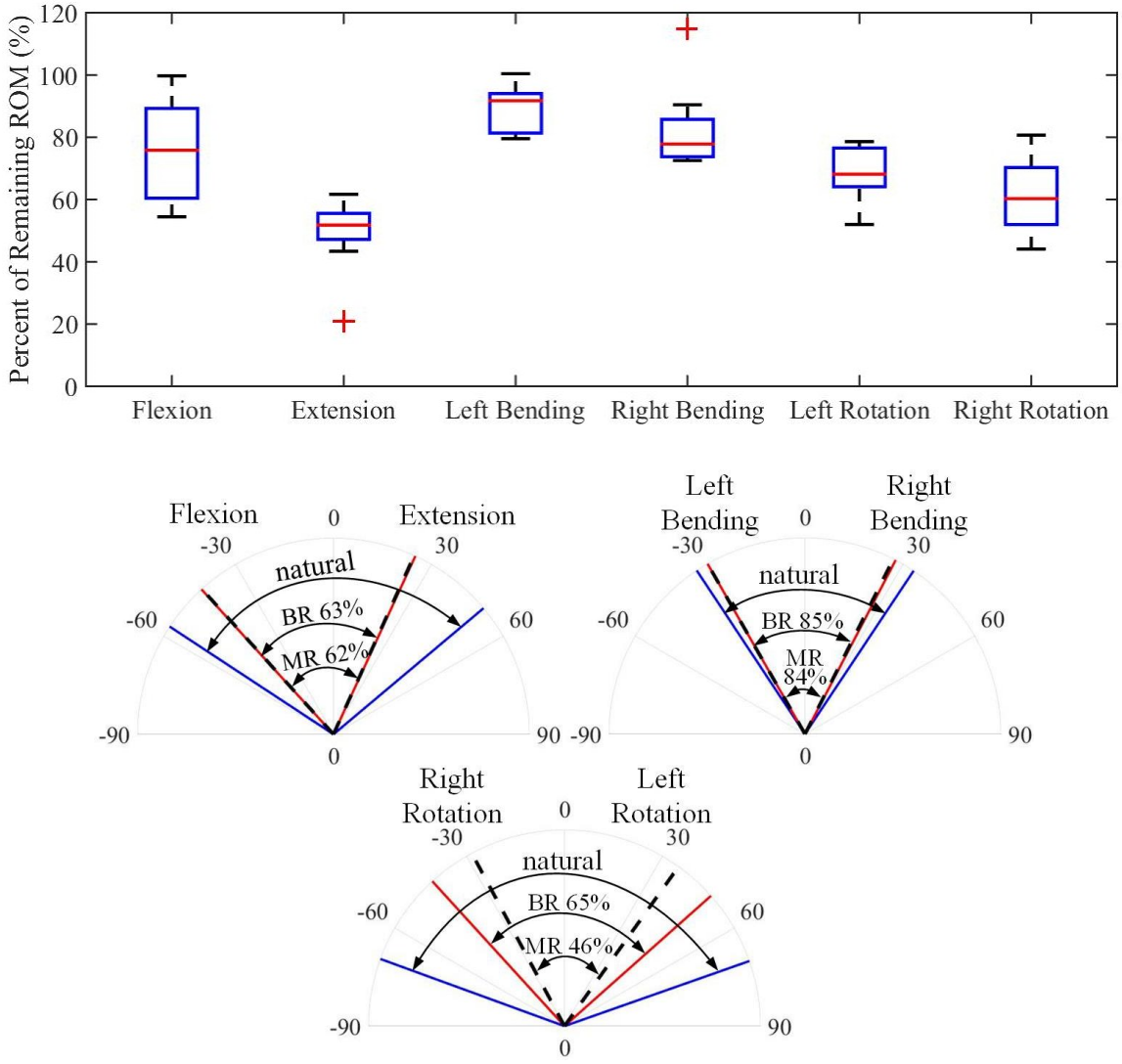

Figure 3.1: Validating the measurement accuracy of the neck brace – main results: (top) the normalized ranges of rotation of ten subjects when wearing the neck brace in each direction and (bottom) average ranges of rotation in three planar motions. The natural ranges are labeled between two solid blue lines, the ranges allowed by the brace (BR) are labeled between two solid red lines, and the measurable ranges (MR) are labeled between two dashed black lines. MR refers to the range where the error of measurement is within a 3° margin as compared to the ground truth.

This experiment quantified the quality of measurement of this robotic brace. As more accurate sensors (encoders) and stronger mechanical components have been implemented in the current neck brace, the measurement accuracy is believed to be higher. Nonetheless, the results from this study provided a floor of measurement accuracy of this neck brace. Additionally, the experiment demonstrated that this brace is highly wearable and can be used by individuals of different sizes.

3.2 Assistance Mode

Two key challenges in developing the neck brace are providing adequate physical support throughout the motion, and accurately translating user intent into motion. These two aspects were evaluated through a pair of human experiments.

Experiment I: Assisting Head-Neck Motion Using the Robotic Brace

Eight healthy subjects (gender: 1 female and 7 males, age: 26.5 ± 3.5 yr, height: 181.1 ± 5.6 cm, and weight: 79.4 ± 15.1 kg) participated in the first experiment[6]. A joystick was used as the input device to control the neck brace.

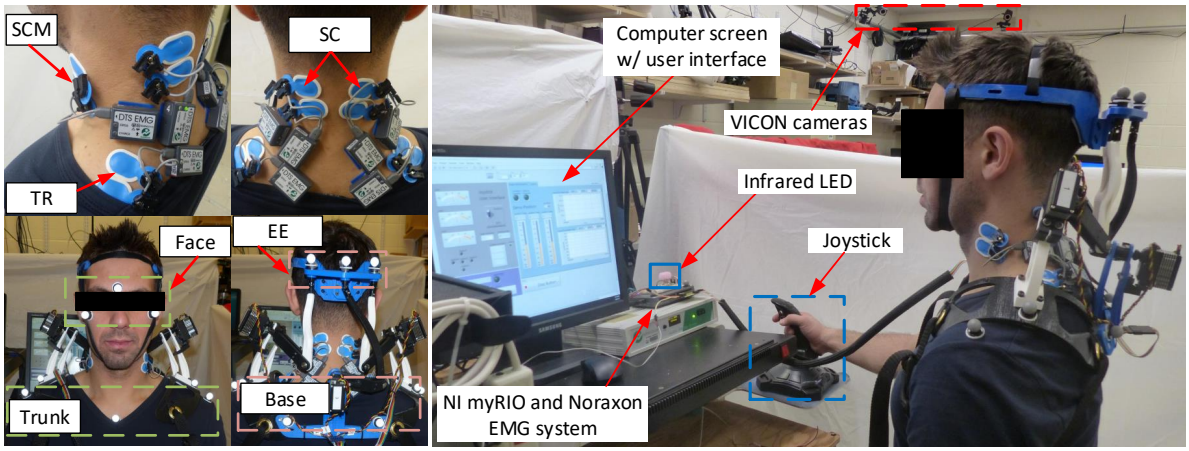

Figure 3.2: Validating the neck brace to assist head-neck motion with healthy subjects using a joystick – experiment setup: (left) infrared marker and EMG electrode placements and (right) a subject using the joystick to control the neck brace during the experiment.

[6]An earlier version of the neck brace was used in this experiment where three off-the-shelf servomotors were used. The brace cannot be operated in 'transparent' mode with these motors due to their high gear ratios.

The study was aimed to compare the muscle activation of these healthy subjects in assisted and unassisted situations when moving the head-neck. Since this version of the neck brace did not allow transparent head movement, the unassisted head-neck motion was conducted by each subject without the neck brace attached. As a result, the head kinematics was measured by the MoCap system with infrared markers attached to both the subject and the neck brace. Surface electromyography (EMG) was recorded (TeleMyo DTS, Noraxon, Arizona, USA) from six neck muscles: sternocleidomastoid (SCM), splenius capitis (SC), and trapezius (TR) on both sides of the body. The muscle signals, the cameras, and the neck brace were synchronized (Figure 3.2).

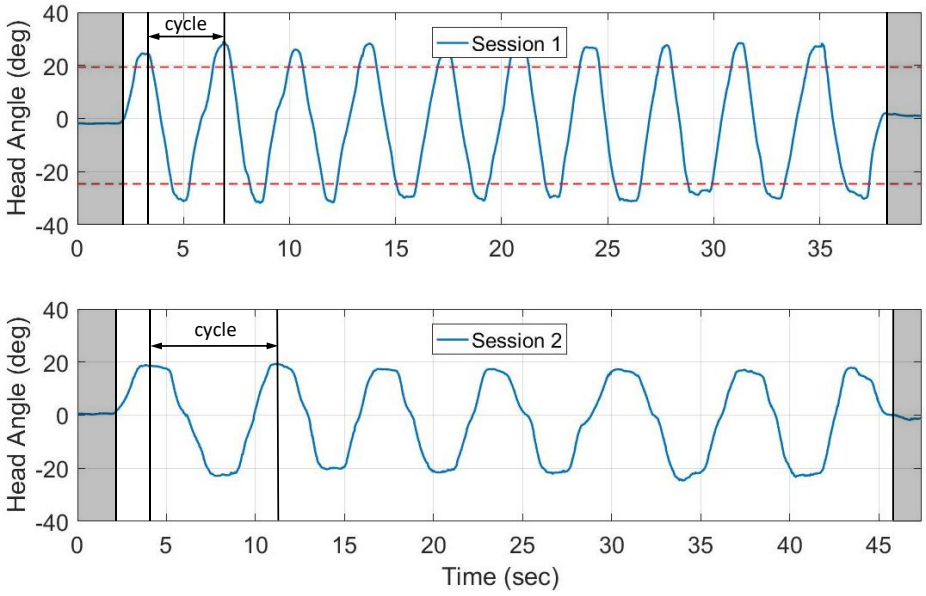

Figure 3.3: Validating the neck brace to assist head-neck motion with healthy subjects using a joy-stick – data segmentation: head angle trajectories of a representative subject during lateral bending in (top) Sessions I and (bottom) Session II. The shaded portion of the data at the beginning and end were cropped because the subject was static at neutral. The data were segmented into cycles defined between two vertical black lines. Two horizontal red dashed lines in the top figure indicate the ROM of the subject achieved with the brace in Session II. The data outside this range in Session I were not used in result comparisons.

The experiment had two sessions (Sessions I: without brace; Session II: with brace). The subjects were instructed to perform a series of head motions at their comfortable speeds in three anatomical planes, including sagittal plane flexion/extension, coronal plane lateral bending, and transverse plane axial rotation, and a general rolling in space. A static trial was recorded prior to

the starts of both sessions to register the head angles and muscle activation of each subject relaxed at neutral. During a ten-minute break between sessions, the subjects were asked to practice using the joystick to control the neck brace. They were asked not to resist the movements from the brace.

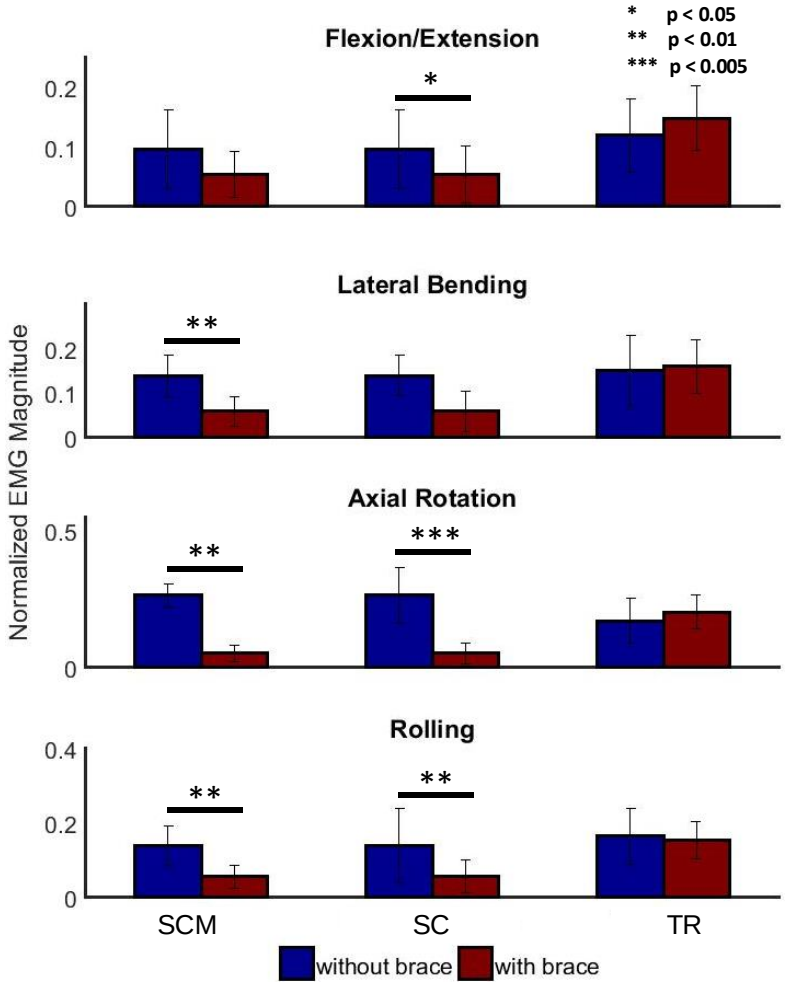

Figure 3.4: Validating the neck brace to assist head-neck motion with healthy subjects using a joystick – EMG results: Each bar represents the average EMG from a muscle group averaged from both sides of the body among all subjects.

The EMG signals were filtered and normalized with respect to the maximum value of each channel throughout the entire experiment. The mean value of a channel in a trial was then used for data comparison between conditions. Because the subjects could only move the head within the workspace of the neck brace in Session II, the head angles spanned less compared to those in

Session I where the subjects moved their head in full ranges. To address this issue, only the EMG produced during the same ranges of motion in both sessions were compared (Figure 3.3).

The group results (Figure 3.4) show overall reductions in activation of SCM (flexor) and SC (extensor) among subjects during movements with the neck brace. This suggests that the neck brace assisted the movements of the subjects by reducing their muscle inputs. The activation in TR slightly increased, however, possibly due to the involvement of the right upper limb using the joystick. When using the neck brace to move the head, the speed is much slower than moving the head without the brace although the speed allowed by the neck brace is close to the natural movement. This suggests that commanding a head movement through a hand-held joystick may not be intuitive for a subject without extensive practice.

Experiment II: Validating the Eye-Control Interface

As introduced in Chapter 2, an eye-controlled interface was developed to provide a more intuitive control for the robotic neck brace. This method was inspired by a natural head-eye movement pattern when reacting to a visual cue in the FOV. If this eye control interface was designed properly, natural eye movements would command the brace to move the head towards a goal position.

A human experiment was carried out with nine healthy individuals (gender: 3 females and 6 males, age: 28.0 ± 3.1 yr, height: 175.0 ± 7.7 cm, and weight: 82.7 ± 14.2 kg) to validate this control interface. The study was conducted while seated. The subject was asked to keep the back on a vertical backrest (Figure 3.5) to ensure the distance between the trunk and the visual display. The subject completed the same task in two conditions where the radii of the neutral zone were different (0.12 *vs* 0.15[7]). The order of the conditions was randomized.

An array of six targets was displayed on a computer screen (Figure 3.5). Prior to the start, the device was attached and secured to the subject. After the eye-tracker was calibrated, the experiment started with the target 'N' illuminated. At this moment, the head was aligned with this target in a self-reported upright neutral posture. Then, the targets were activated in sequence, triggered by the eye movement of the subject. Once the subject successfully kept the head at a target, i.e., the gaze

[7]These are normalized values with respect to the world image.

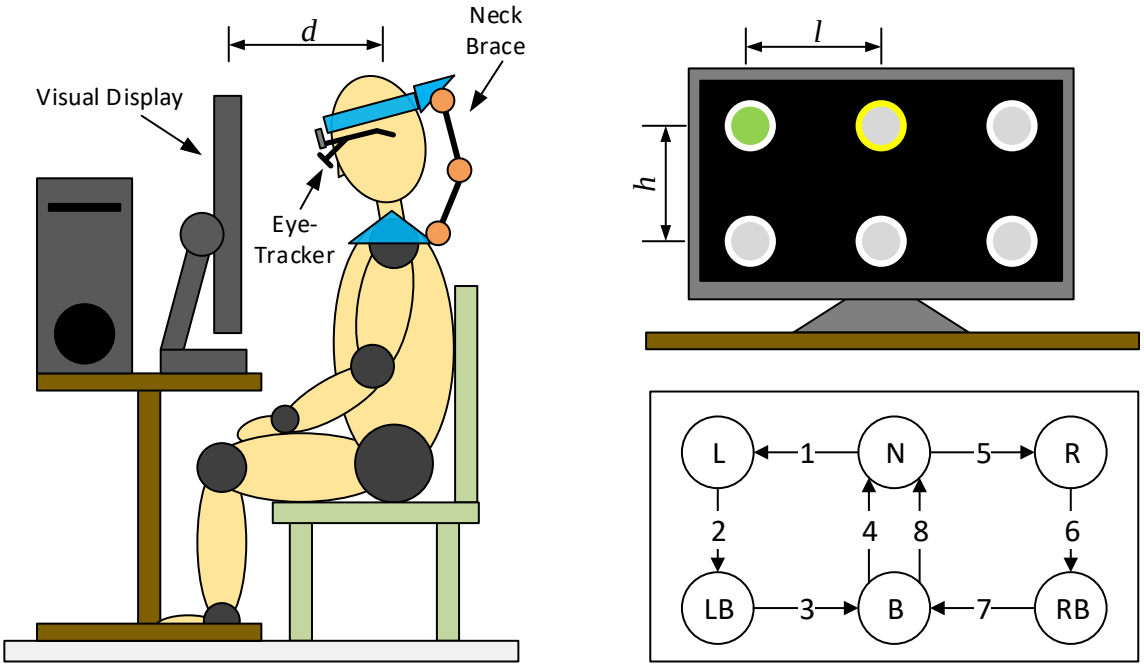

Figure 3.5: Validating the eye-control interface with healthy subjects – Setup: (left) illustration of a user sitting in front of the visual display at a distance d (45 cm) during the experiment, (top right) details of the visual display from a user perspective where the targets are separated with a width l (18.75 cm) and a height h (15.0 cm), and (bottom right) sequence of the targets consisting of eight moves following the numbered arrows.

stayed inside the neutral zone, for 2 seconds, the next target would be activated and the current target would be turned off. The sequence of the targets was designed to include all directional moves, e.g., from 'Left' to 'Down', from 'Down' to 'Right', etc. In an ideal scenario, one rotation of the head is needed in each step without coupled movement. A practice trial was given to each subject to understand the control of the device and the task of the experiment. Each subject then completed the task three times in each condition and the average was used for data analysis.

As shown in Figure 3.6, a representative subject moved the head when there was a directional command given by the gaze input. Most steps were single-command moves. In these steps, the head rotations showed almost linear changes with respect to time, with the slope indicating the predefined step size ($0.4°$/command). There were exceptions. For example, in steps 3 and 7, multiple gaze commands were given, meaning that the subject performed multiple head rotations

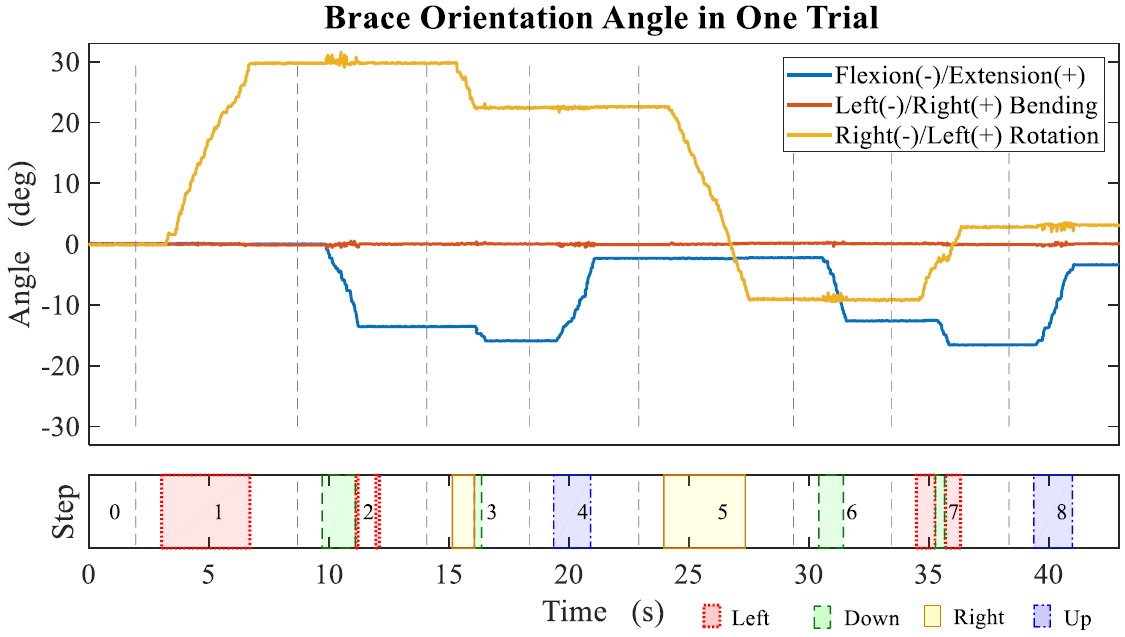

Figure 3.6: Validating the eye-control interface with healthy subjects – representative data of a subject in a trial: The radius of neutral zone was set to be 0.15. The top chart shows the three angles of the head rotation. The shaded areas at the bottom indicate the commands by the user's eye movement. The white areas are when the gaze was located inside the neutral zone.

to achieve these targets. Another observation is that the bending angle remained zero throughout the trial. This validated the interface to allow only two rotations. It also shows that the times used to move the head among steps were different depending on the distances between targets.

The raw data in each trial were segmented into steps based on the time stamp when each target was lighted up. The location of the screen target in each step with respect to the neutral zone of the world image was examined. A post-processing routine was conducted to locate an active screen target by extracting green features in the image[8]. A step was labeled as a 'successful step' if the final location of a target was at least partially within the neutral zone of the world image. In a 'successful' step, the head is aligned to a desired target, resulting the gaze point to be inside the neutral zone.

In total, 216 data points were obtained (three trials of eight steps for nine subjects) in each

[8]YCbCr color space was used for this purpose. It was followed by erosion and dilation to eliminate noise.

condition. The results show that with a neutral zone radius of 0.12, 206 targets (95.2%) were at least partially inside the neutral zone and 136 (63.0%) of them had their centers located in this zone. With a slightly larger neutral zone (0.15), 211 targets (97.7%) were partially inside the neutral zone and 158 (73.2%) of them had the centers in the zone. These suggest that the brace correctly interpreted the eye commands of the subjects and consistently moved the head towards the targets. Slightly different sizes of the zone had little impact on this reliability of the brace control.

The instruction given to the subjects was to follow the targets with the eyes. If the brace moves the head, then try not to resist but to follow it. This prevented the subjects from knowing how exactly the system worked and therefore eliminated any behavioral bias. To determine a 'successful' step, an independent routine of image processing was performed. This obtained the ground truth and ensured the correctness of the evaluation. The speed of the brace was fixed to be relatively low. Current and motion thresholds were also set in software to limit any sudden or large movement from the brace. An emergency switch was also at hand of the experimenter monitoring the experiment. These measures ensured safety.

3.3 Cartesian Force Controller

The ability of producing a desired force at a configuration was validated through a tabletop testing (Chapter 2). In this section, an experiment is presented to evaluate the force controller when interacting with human subjects. Ten healthy young adults (gender: 3 females and 7 males, age: 28.9 ± 3.9 yr, height: 178.1 ± 7.5 cm, and weight: 80.3 ± 14.7 kg) participated in this experiment.

Two modalities were subsequently evaluated: force perturbation and a cone-shaped force field (Figure 2.7). Subjects were seated in front of a visual display while wearing the neck brace. Muscle activities were recorded using surface EMG at four sites (SCM and SC on both sides of the body). A six-axis force/torque transducer was installed between the headband and the end-effector to record the force between the brace and the head[9]. A visual display (Figure 2.3 (B)) was used to provide visual feedback to the subjects. Non-parametric (Kruskal-Wallis) test was used for analyzing group

[9]This force/torque sensor was not used in the control.

data and the statistical significance was set at $p < 0.05$.

Experiment I: Force perturbation with different visual feedback

In the first experiment, force perturbation was tested. After a baseline trial where the subject sat upright with eyes closed for 60 seconds, three perturbation trials followed. The differences among these three trials were the visual information received by the subject: (i) eyes closed (EC), (ii) eyes open with no visual feedback (EO), and (iii) receiving a visual feedback from a 2-dimensional monitor display (VF)[10]. Each perturbation trial was 90 seconds long. An impulsive force of 10 N (Figure 3.7 (left)) was applied to the head of the subject every 10 seconds randomly in one of the eight directions, as shown in Figure 3.8. Therefore, anticipation and pre-planning were not expected from the subject.

When a perturbation occurred (Figure 3.9), the force created a sudden movement to the head so that it deviated from the neutral position. Then, the head was returned to a new 'neutral' which was perceived by the subject (with eyes closed). The neutral became slightly different each time

[10]In this case, the target (blue circle) is centered at the origin, and the red dot represents the projection of a reference point in the moving frame onto the transverse plane of the inertial frame.

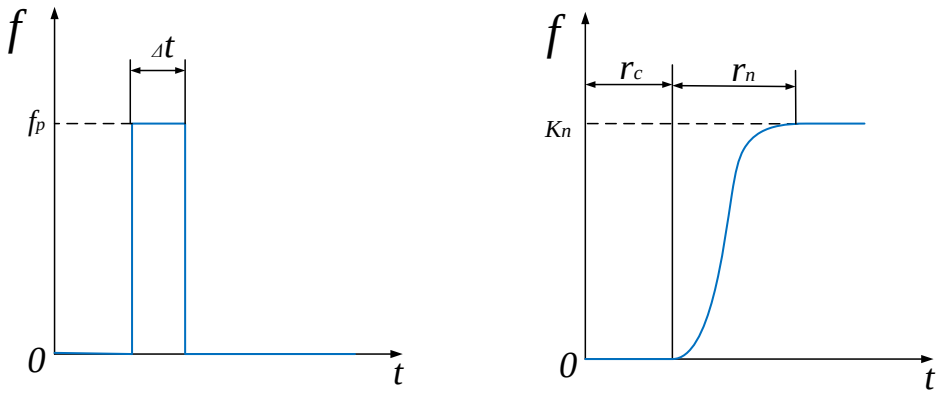

Figure 3.7: Validating force control with health subjects – forcing functions: (left) impulse function for force perturbation and (right) forcing function (Equation 2.2) of a cone-shaped Cartesian force field. $f_p = 10$ N, $\delta t = 0.3$ s, $K_n = 10$ N, and $r_n = 60$ mm. The reference point P is located at the origin of the F/T sensor. $r_c = 24$, 18, and 12 mm in *large*, *medium*, and *small* trials, respectively.

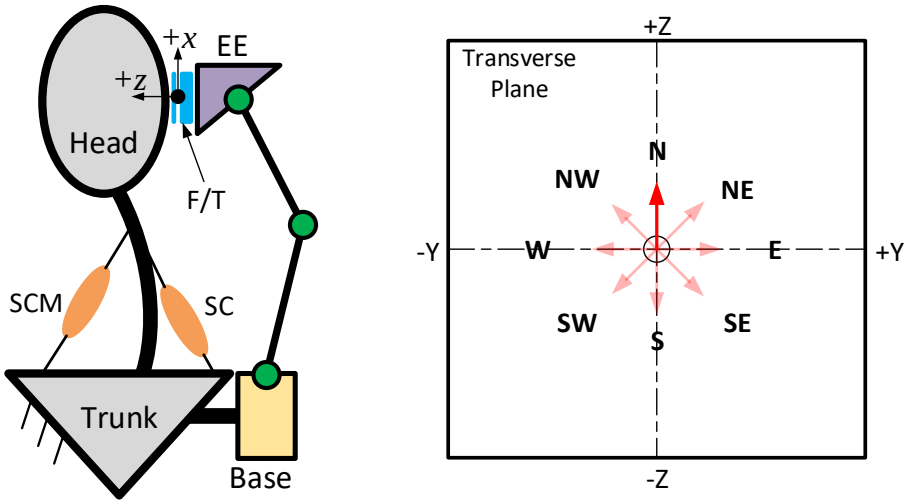

Figure 3.8: Validating force control with health subjects – schematics of perturbation session: (left) a model of head-neck at neutral configuration with neck brace attached, viewed in the sagittal plane and (right) force perturbation viewed on the transverse plane. A force/torque sensor (Mini 45, ATI Industrial Automation, Apex, NC, USA) is attached between the end-effector and head with shown coordinate system. The forces are applied at the origin of the force/torque sensor in eight different directions in a random order. In the present example, the force (highlighted) is applied in 'N' direction which pushes the head forward.

after a perturbation. Due to the movement of the head, the forces recorded from the F/T sensor were less than the nominal value (10 N)[11].

The EMG data of both SCM (flexor) and SC (extensor) peaked as each perturbation occurred. This means that the person reacted to each perturbation also on the muscular level where the neck was stiffed to soften the drastic change in head orientation. The muscles were also activated when returning to the neutral configuration of the head. It also shows that the force perturbations occurred at the correct times, evidenced by the time stamps the spikes occurred in these graphs (Figure 3.9).

The subjects needed to return the head back to neutral after each perturbation. Because the visual condition was different, this behavior may change among trials. To test this, the maximum component of the change of head angles ($\Delta\psi_{\max}$) before a perturbation and after the subject returned to neutral from it was computed for each subject in each trial. This variable indicates the amount of angular deviation between neutral configurations caused by a perturbation. The absolute mean of

[11] Other factors could have also contributed to the loss such as the accuracy of the controller, soft headband, etc.

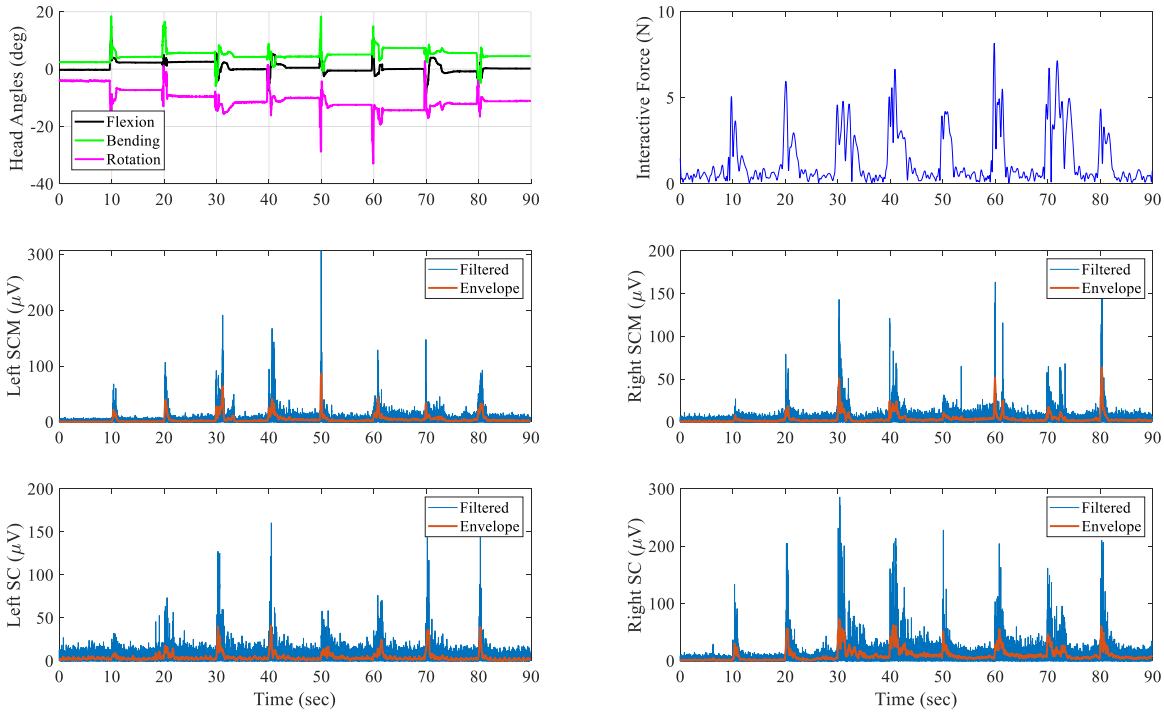

Figure 3.9: Validating force control with health subjects – representative data from a subject during force perturbation with eyes closed. Head angles are plotted using space three 1-2-3 sequence. The force data is low-pass filtered at 30 Hz. EMG signals (blue) are processed following the steps of (i) detrending, (ii) band-pass filtered at 10 and 450 Hz, and (iii) rectification. EMG envelopes (red) are obtained using moving RMS with a window size of 150 samples.

this variable of all eight perturbations in a trial, $\overline{|\Delta\psi_{\max}|}$, was used to quantify the average precision of a subject recovering from force perturbations in a visual condition.

The result reveals that $\overline{|\Delta\psi_{\max}|}$ did not change ($p = 0.96$) with different visual conditions. When removing the angle component rotating about the vertical axis from $\overline{|\Delta\psi_{\max}|}$ calculation, however, $\overline{|\Delta\psi_{\max}|}$ reduced when more visual information was given (EC: $2.2° \pm 0.9°$, EO: $1.8° \pm 0.8°$, VF: $1.4° \pm 0.9°$). Additionally, $\overline{|\Delta\psi_{\max}|}$ was significantly higher ($p < 0.05$) when eyes were closed than receiving visual feedback. These results suggest that the on-screen visual feedback helped the subjects to return the Cartesian position of the reference point (red dot) but did not help correct the deviation in rotation about the vertical axis.

The average of the maximum muscle EMG from all four channels before and after each per-

turbation, $\overline{\epsilon_{\text{max}}}$ was used to quantify the muscular reaction of the subject. The mean of $\overline{\epsilon_{\text{max}}}$ during eight perturbations was then used to quantify the overall muscular input of the subject in a trial. This variable was found to be significantly higher ($p < 0.05$) in perturbation trials than the baseline trial[12]. This result suggests that the force perturbations caused the subjects to produce muscle forces to stabilize the head-neck. However, no statistical difference was found in this variable among perturbation trials ($p = 0.20$) which indicates that visual feedback does not influence the reaction to the perturbations at the muscular level.

Overall, this experiment demonstrated the ability of providing force perturbation in different directions to human subjects using the neck brace.

Experiment II: Targeting with a cone-shaped Cartesian force field

In the second experiment, the cone-shaped force field was evaluated. Each subject was asked to complete the same task four times with different cone sizes of the force field[13]. The size of the cone, in which the head moves freely, gradually shrinks as the trials continue. These four trials are labeled as *transparent*, *large*, *medium*, and *small*, respectively, to reflect the size of the cone.

The task was the following: a target (blue circle) was firstly shown randomly in one of the four directions (N, S, E, W). The subject needed to move the head, represented by the red dot, to the target. Once the red dot was inside the blue circle, the LED changed color from red to green. After keeping the red dot inside the target for 2 seconds, the blue circle would be automatically updated to a location in one of the remaining three directions. The subject then needed to move the head back to neutral first prior to moving towards the new target. The subject repeated this for all four targets to complete the task. The profile of the force field remained the same across subjects. With a smaller cone, it was hypothesized that the task becomes more difficult as the subject needs to exert more forces in the neck muscles, thereby spending more time to reach the targets.

As shown in Figure 3.10, in order to reach a target outside the cone, this subject had to push

[12]Since there was no perturbation in this trial, the mean value of the maximum from all EMG channels was used.

[13]In the first trial, the subjects completed task with the neck brace in 'transparent' mode. The size of the cone can be considered as infinitely large.

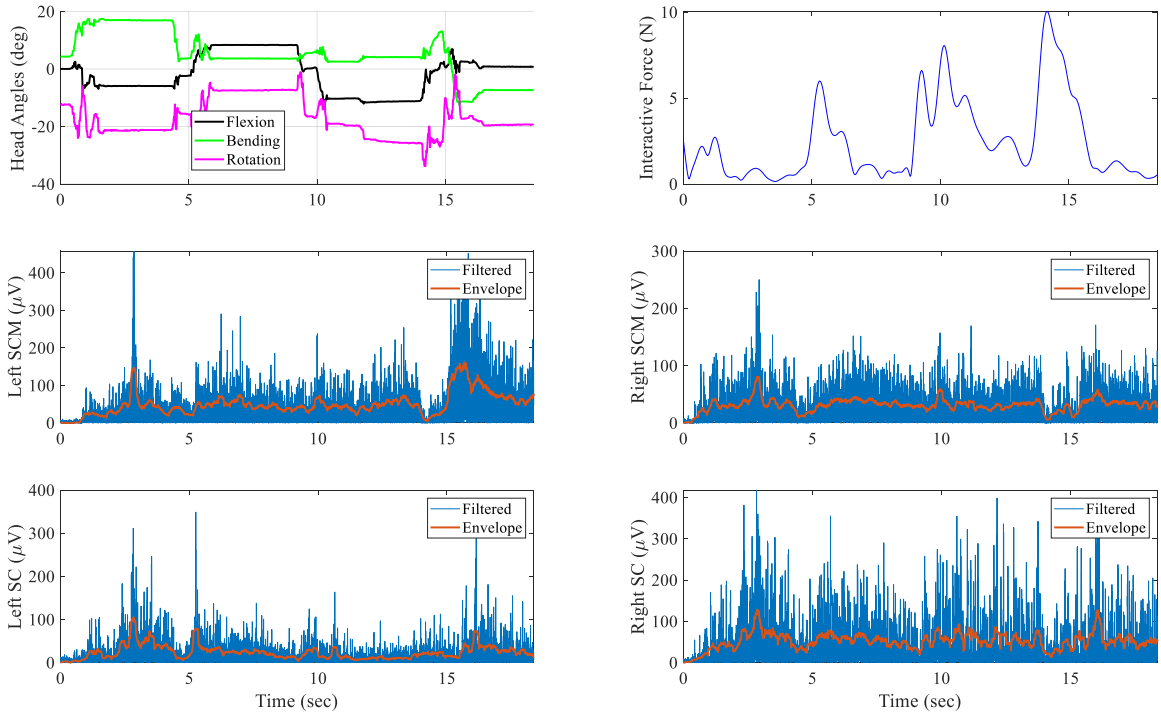

Figure 3.10: Validating force control with health subjects – representative data from a subject during targeting with the force field (*medium*). The sequence of the targets in this specific trial was: E (right bending) - S (extension) - N (flexion) - W (left bending). The recording ended when the subject successfully reached to and maintained possession for 2 seconds in the last target.

against the force field as expected, resulting in large muscle EMG and recorded force values. The mean EMG value of all four muscles during a trial was used to indicate the overall muscle input from the subject. The group result shows a positive trend of this EMG variable when the cone size becomes smaller (Figure 3.11). This EMG variable in trials *medium* and *small* are significantly higher than *transparent* ($p < 0.05$). These suggests that a smaller cone increased the amount of muscular inputs from the subjects.

On the other hand, the overall time was not found to be significantly different among trials ($p > 0.05$), as shown in Figure 3.11. It shows, however, that the time did not vary much during the *transparent* trial but varied more when the force field was present. The overall time trended upwards from *transparent* to *large*, but decreased on average in *medium* and *small*. This might have been because the healthy subjects were able to adapt to the task rather quickly. Despite applying

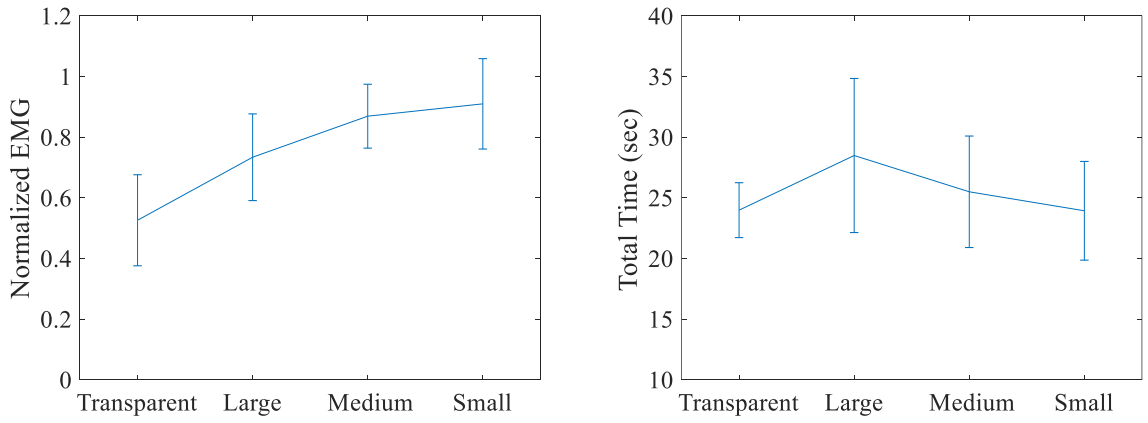

Figure 3.11: Validating force control with health subjects – group results during targeting with a cone-shaped force field: (left) the average EMG by the subjects where the average EMG is normalized with respect to the largest value among trials for each subject and (right) the total time used by the subjects to complete the task.

more muscle forces, they were able to complete the task even faster.

Patients with cerebral palsy (CP) may present poor head control in severe cases. Physical therapies using the principle of motor learning have been shown to be effective in restoring coordinated limb movements to accomplish functional tasks in CP. However, there has been a paucity in research of training head control due to a lack of viable tools. The presented Cartesian force controller of the neck brace can potentially be used in such a scenario to help stabilize a patient's head as needed while interacting with a therapist. The cone size of the force field can also be used to assess the head stability as training progresses.

3.4 Joint Torque Controller

As introduced in Chapter 2, this controller modulates the interactive force applied to the user's head at the joint level and moves the head to match a desired orientation. In this section, a human study is presented to test this controller where it was used to train ten healthy subjects (Gender: 4 female and 6 male, Age: 25.9 ± 3.8 yr, Height: 173.0 ± 8.8 cm, Weight: 74.5 ± 16.6 kg) to learn a head trajectory: a pure lateral bending of the head-neck[14]. From previous observations, a pure bending

[14]The trajectory was a sinusoidal function with an amplitude of $20°$ and a frequency of 0.25 Hz.

motion of the head was found to be difficult as it naturally couples with axial rotation. This choice of target motion creates challenges to even healthy subjects.

The subject was asked to complete a same training protocol on two separate days but with different conditions (Figure 3.12). In the first condition (*visual*), the subject was only given a visual feedback (Figure 2.3 (A)). In the second condition (*force*), the subject was also provided with a force feedback from the brace using this joint torque controller in conjunction with the visual feedback. These subjects were randomly divided into two groups, with the order of the conditions switched between them.

A baseline (BL) trial was conducted before the start of training in each condition to evaluate the pre-training performance of the subject. After five training (TR 1-5) trials separated by short breaks (SB) of 15 seconds, three post trials (PS 1-3) followed to evaluate the post-training performance of the subject. Long breaks (LB) of one minute were given between the post trials. The BL and PS trials were designed similar except that the BL was 30-second long while each PS was one minute long. The last 20 seconds of BL and the middle 20 seconds of each PS were recorded for data analysis. Visual feedback was given in these trials, and the brace was turned into the 'transparent' mode so that the subject can track the trajectory freely with the head. Each TR lasted one minute long, with the middle 20 seconds recorded for analysis.

If this controller was to be effective, the subjects were expected to perform the task more accurately with force feedback. The accuracy was quantified by the spatial and temporal errors of the head during tracking. The *absolute mean error* in each direction was defined as the absolute mean of the difference between the target and actual head angles in a trial. The *time delay* was quantified by the phase difference corresponding to the principal frequency between the target and actual motions. Two-way ANOVA was used to explore the influence of the conditions (*visual* and *force*) and all nine trials (BL, TR 1-5, and PS 1-3) to each outcome variable (*absolute mean error* and *time delay*). The statistical significance was set at $p < 0.05$.

Both outcome variables were not significantly ($p > 0.05$) different in both conditions during baseline trials which confirms that the performances of the subjects were statistically the same prior

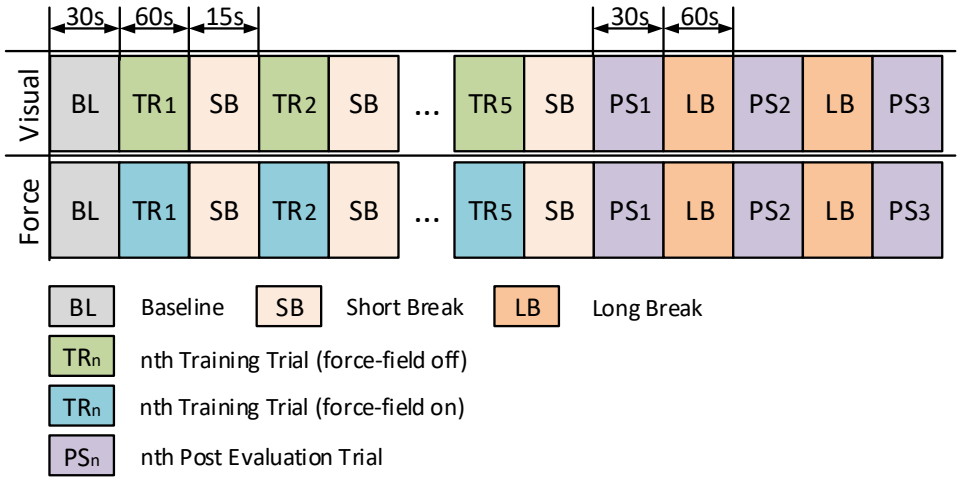

Figure 3.12: Validating joint torque control with health subjects – training protocol. It consists of three sessions, i.e., baseline, training (five trials), and post evaluation (three trials), in two conditions, i.e., *visual* and *force*. In the *visual* condition, only visual feedback is given while both visual and force feedback are given in the *force* condition. All subjects completed both conditions on two different days with a randomly assigned order.

to training. While the flexion and bending components of the *absolute mean error* did not show any difference in both conditions, the rotation component was significantly less during training sessions with the force feedback ($p < 0.05$), as shown in Figure 3.13. This suggests that the undesired coupling in rotation was suppressed due to the force feedback in training. However, this reduction in rotation did not retain as these rotation errors were similar ($p > 0.05$) in three post-training trials in both conditions. On the other hand, the *time delays* were significantly larger ($p < 0.05$) in training trials with force feedback. It is possible that the subjects paid extra attention to the force applied by the brace and therefore slowed their head movements. This delay became similar to the *visual* condition when the force feedback was removed during post-training.

The pilot study demonstrated that the neck brace can facilitate training of coordinated head-neck movements using the joint torque controller. The experiment was designed to compare in-training and post-training performance in both conditions where each condition was a short single-session training. The results suggested that the force feedback from the brace helped a subject improve the spatial performance during training, although this improvement was not retained after the feedback

was removed. The combination of force and visual feedback may require extra training time for a subject to adapt, as evidenced by the temporal delay during training with this regime.

3.5 Passive Support

The spring-loaded brace was designed to (1) apply support to the head at a chosen configuration by tuning the free-angles of the torsional springs and (2) allow small ranges of movements around this equilibrium configuration.

A human validation with ten healthy subjects (gender: 3 female and 7 male, age: 27.1 ± 3.2 yr, height: 176.1 ± 7.6 cm, weight:77.9 ± 15.1 kg) was designed. Each subject completed the experiment while seated with the brace attached. The experiment had two sessions: The springs were not tightened to the brace in the first session (S1) while were tightened in the second one (S2) when the subject was at the neutral configuration. The subject was asked to reach extreme angles allowed by the brace in each direction, i.e., flexion, extension, left/right lateral bending, and left/right axial rotations, after keeping the head upright for 30 seconds.

The head angles were computed using the measurements from the potentiometers mounted on the second revolute joints (Chapter 2). Muscle activities were recorded at SCM, SC, and TR on

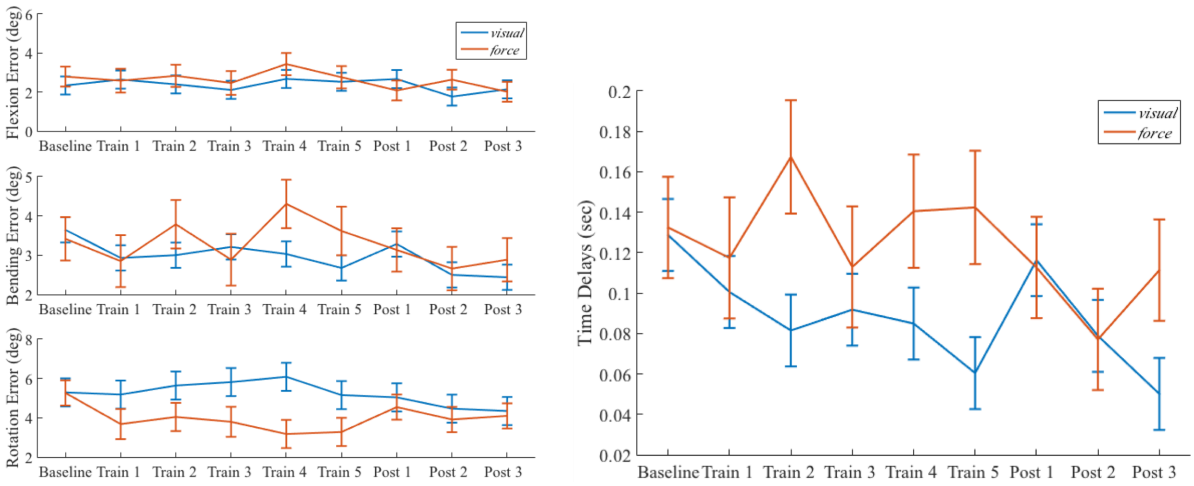

Figure 3.13: Validating joint torque control with health subjects – group results: (left) *absolute mean errors* and (right) *time delays* in each trial in *visual* and *force* conditions.

both sides of the body. The force/moment applied to the head from the brace were recorded by a six-axis force/torque sensor mounted between the end-effector and the headband.

Table 3.2: Validating the spring-loaded brace with health subjects – absolute mean of the group [average (standard deviation)]

ROM(°)			
	Sagittal Plane	Coronal Plane	Transverse Plane
S1	40.9 (9.4)	46.0 (14.0)	76.7 (11.4)
S2	28.0 (7.5)	35.1 (7.2)	67.5 (11.4)
Normalized EMG Magnitude			
	SCM	SC	TR
S1	0.08 (0.04)	0.15 (0.06)	0.209 (0.05)
S2	0.09 (0.04)	0.15 (0.05)	0.220 (0.06)
Force Data (N)			
	Fx	Fy	Fz
S1	3.4 (1.5)	1.5 (0.6)	5.3 (1.5)
S2	5.9 (2.4)	2.5 (0.9)	8.6 (2.4)

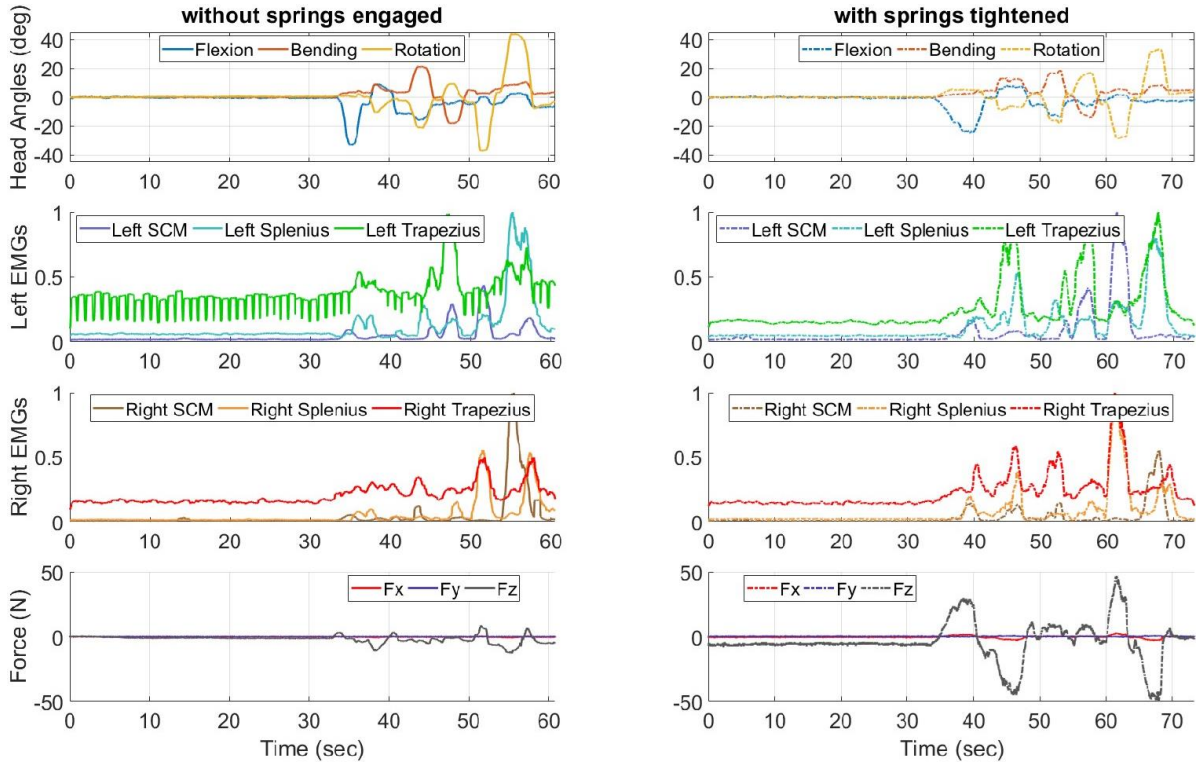

Figure 3.14: Validating the spring-loaded brace with health subjects – representative data of a subject during *range of motion* task.

As shown in Figure 3.14, the subject experienced larger forces from the brace and moved in smaller ranges when the springs were tightened. These suggest that the subject had to push against the spring torques to move the head in each direction. These observations were consistent when examining the group data of this task (Table 3.2): the forces transmitted to the head were larger and the ranges of motion were smaller when the springs were tightened to the brace ($p < 0.05$). This result validates the tightening mechanism of the spring actuator. The level of muscle activation were found to be similar ($p > 0.05$) during this task between both sessions. This suggests that the subjects attempted the task with similar efforts, making the results of ranges of motion and recorded forces comparable between sessions.

Chapter 4

Using the Head-neck as an Input to Command Orientations

4.1 Overview

The motion of the head-neck is similar to the one of the hand-wrist in that both joints allow large ranges of rotation. Human beings excel at using their hand-wrist to rotate a grasped object in space. This ability allows a person to use tools such as a hand-held joystick to operate machines. However, this ability may be missing for individuals with hand-wrist impairment or amputation. Therefore, they may benefit from using their head-neck as an alternative to complete the same orientation

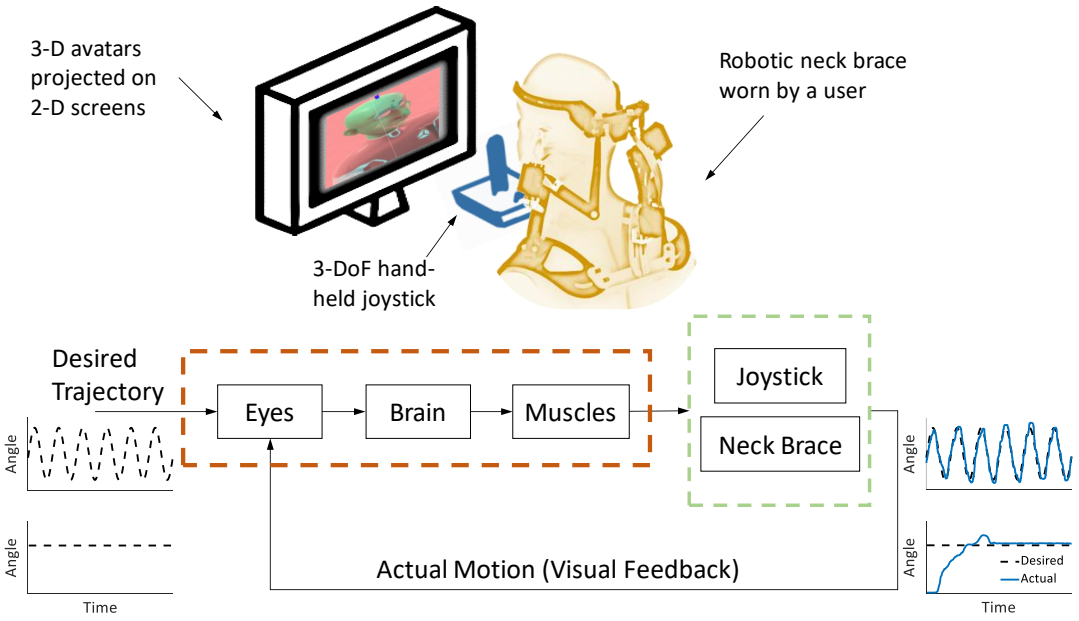

Figure 4.1: System design of using the robotic neck brace as a motion joystick. A visual interface on a computer screen is shown to a participant. Both the target and actual trajectories of the head of a human-like avatar were displayed. The participant needs to track dynamic motions of the avatar's head using either the head-neck or the hand-wrist. The orientation of the head is measured by the robotic neck brace and of the hand by a hand-held joystick. Sinusoidal and step functions are chosen as the target motions to study continuous tracking and discrete orientation targeting.

tasks. Additionally, when performing complex tasks such as intense video gaming or machine operations, a controller enabled by the head-neck may provide even an able-bodied person much needed help. Therefore, a scientific question is posted in this study - Can the head-neck be used to command orientations just as good as those by the hand-wrist?

The performance of using the head-neck to control the orientation of a virtual object was investigated. This performance was compared to the one using the hand-wrist. The neck brace and a 3 DOF hand-held joystick were used to provide control input for the head-neck and the hand-wrist, respectively. Human subjects were tasked with tracking and targeting using both head-neck and hand-wrist (Figure 4.1). These tasks were intended to be general, including tracking continuous angle trajectories and achieving discrete target orientations. The spatial and temporal errors of these subjects during the tasks were measured. The hypothesis was that the performance of using the head-neck and the hand-wrist show no difference, i.e., neither in spatial nor temporal, during different orientation tasks among these subjects.

4.2 Methods

The system consists of a visual display (Figure 2.3 (A)), a 3-DOF joystick (Extreme 3D Pro, Logitech Inc., Newark, CA, USA), and the robotic neck brace, as shown in Figure 4.2. The color of the bar indicator above the head of UA[1] renders the angular error between the target and the actual motions. This color turns to yellow when the angular error is less than 8° and green when the error is less than 3°. Otherwise, the color stays as red. Therefore, a user can rely on the color along with other facial features of the avatars to align the UA to a target orientation. These color thresholds are chosen so that the level of difficulty was reasonable for a healthy participant. The camera view of the visual display is set to be at default, i.e., the front view of the mirrored avatar images are shown. The angle of the joystick is mapped one-to-one to the angle of the head of UA in each direction without any scaling factors.

[1]UA, as opposed to TA (Target Avatar), is the phantom-like avatar showing the subject performance. Please refer to Chapter 2 for more details.

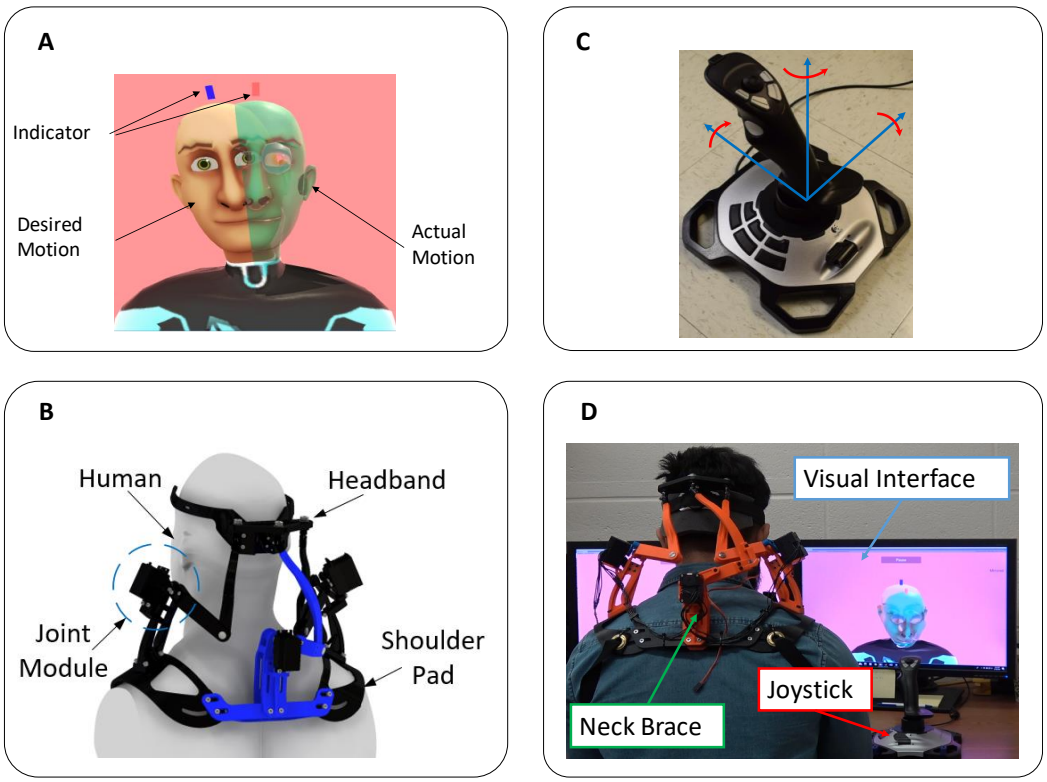

Figure 4.2: Overview of the system: (A) front view of the visual interface, (B) schematics of the neck brace, (C) a hand-held joystick which permits three rotations about its three axes, and (D) integration of the devices and visual interface during the human experiment.

Fourteen healthy adults were recruited as subjects (gender: 3 female and 11 male, age: 28.0 ± 3.1 yr, height: 177.0 ± 7.8 cm, and weight: 77.0 ± 15.0 kg). This experiment was approved by the IRB at Columbia University. An informed consent was signed by each participant and obtained by an investigator prior to the start of the experiment. These subjects were asked to complete the same tasks using both the joystick and the neck brace in accordance to visual instructions. The subjects were randomly divided into two groups. The order of using the two devices was reversed between the groups.

Two tasks were designed. In the first task, each subject was required to follow a predetermined avatar head trajectory in each of the anatomical planes, i.e., the sagittal, coronal, and transverse planes. Sinusoidal functions with predefined frequencies and amplitudes were used for each of these trajectories (Table 4.1). Each motion trial was one-minute long, and the subjects were asked

to repeat it for three times. In the second task, each subject was asked to achieve a desired head posture of the avatar in the shortest possible time. They started each trial with the head at upright neutral and also repeated each target for three times.

Table 4.1: Target avatar motions during tracking and targeting tasks

Tracking	
Flexion/Extension	$\theta_x^d = 25^\circ \sin(0.4\pi t) - 15^\circ$
Lateral Bending	$\theta_y^d = 20^\circ \sin(0.4\pi t)$
Axial Rotation	$\theta_z^d = 35^\circ \sin(0.4\pi t)$
Targeting	
25° Flexion	$\theta_x^d = -25^\circ$
20° Bending to Right	$\theta_y^d = 20^\circ$
30° Rotation to Left	$\theta_z^d = 30^\circ$

The independent variables in this study are: *condition*, *motion*, and *order*. The *condition* indicates which input device was used, i.e., the joystick or the neck brace. The *motion* specifies a motion trial, i.e., flexion/extension, lateral bending, and axial rotation in tracking tasks and flexion, bending, and rotation in targeting tasks. The *order* suggests the group a subject belonged to, i.e., joystick first or neck brace first. Each sample was averaged from the three attempts in each trial.

Three outcome measures were derived from the raw data: (i) *mean absolute error* and (ii) *time delay* during tracking and (iii) *settling time* during targeting. The tracking accuracy was quantified by the mean of the absolute error between the target and actual orientation in three dimensions during tracking tasks. The angles were computed using space three 1-2-3 representation. The error of each component angle was computed by subtracting the actual angle from the desired one at each time instance (Figure 4.3). The mean of the absolute error during the a trial was then used to quantify the overall tracking accuracy. The *mean absolute error* was further classified into two categories when considering a desired motion: *primary error* and *secondary errors*. The *primary error* specifies the absolute mean of the tracking error in the desired plane while the *secondary errors* quantifies the absolute mean of the nonzero angles in the other two planes.

When tracking a desired motion, the spatial errors alone may not fully quantify the performance. For instance, a participant may be able to track the sinusoidal motion but with a temporal error,

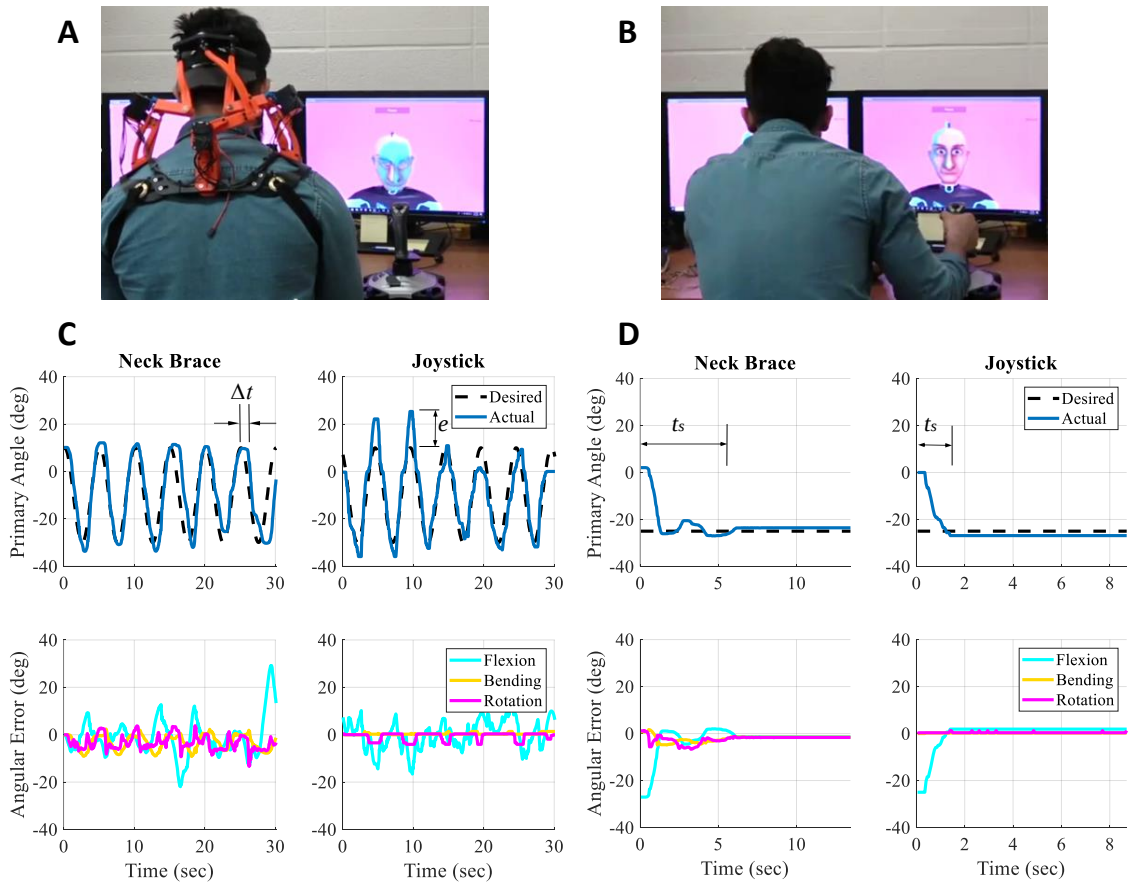

Figure 4.3: Representative data from a participant: (A) a participant performing tasks using the head-neck, (B) the same participant performing tasks using the hand-wrist, (C) tracking performance of the participant using head-neck and hand-wrist during a trial in flexion/extension, and (D) targeting performance of the participant using head-neck and hand-wrist during a trial in flexion. 'Primary angle' is defined as the angle in the commanded plane of motion.

which would result in larger tracking error at a given time. The *time delay* was therefore computed using a frequency approach [38] to quantify the temporal performance of a subject.

The *settling time* was defined as the time taken by the participant to reach and stabilize at the target posture during targeting tasks, when the absolute error and its time derivative are within predefined error boundaries. Figure 4.3 shows the settling times for a representative participant in the head-neck and hand-wrist conditions, respectively.

Shapiro-Wilk test was used to determine the normality in samples. Paired t-test and Wilcoxon

test were used to examine whether an outcome is significantly different between *conditions*, i.e., joystick and neck brace. Analysis of Variance (ANOVA) was used to investigate the effects of independent variables on the outcome measures. Data analyses were performed in MATLAB (The MathWorks Inc., Natick, MA, USA). The statistical significance was set at $p < 0.05$.

4.3 Results

The group results are shown in Figure 4.4. The *primary error* using the head-neck motion was found to be higher ($p < 0.01$) in flexion/extension and axial rotation than using the hand-wrist. The *secondary errors* in these two movements were also higher ($p < 0.001$) when the head-neck

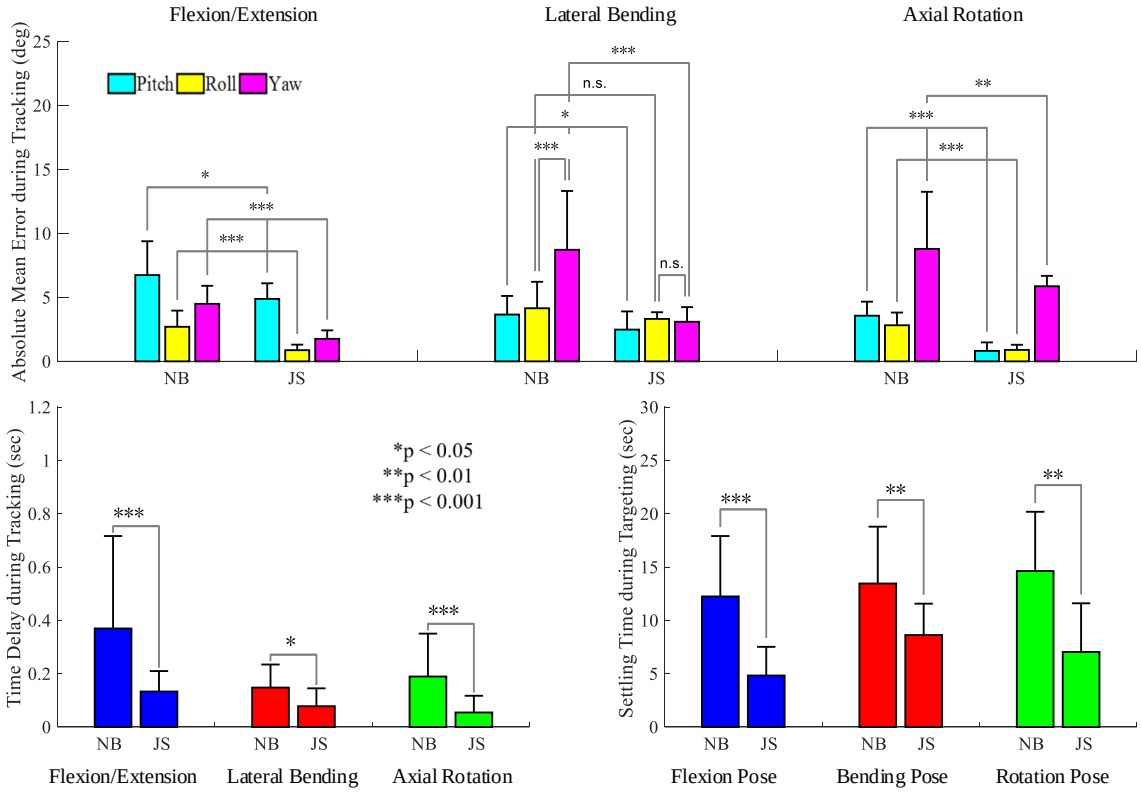

Figure 4.4: Group results: (top) tracking errors, (bottom left) time delays, and (bottom right) settling times of using the head-neck (NB) and the hand-wrist (JS) in different tasks. The height of each bar represents the group mean of the average performance of all participants in three attempts for each task. The whiskers represent the group standard deviations in the average performance of all participants.

was used. No statistical difference ($p = 0.255$) in *primary error* was found between using the head-neck and the hand-wrist in lateral bending. During lateral bending, however, the error in rotation angle (*secondary error*) was found to be higher ($p < 0.001$) when the head-neck was used. Paired t-test further showed that the error in rotation angle was significantly larger ($p < 0.001$) than the *primary error* when the head-neck was used during lateral bending. The order of using the head-neck ($p = 0.198$) and hand-wrist ($p = 0.142$) did not have a significant impact on neither the *primary error* nor the *secondary errors*. The magnitudes of the *primary error* and *secondary errors* were also not different ($p > 0.05$) over three attempts in each motion with either the head-neck or the hand-wrist.

The *time delay* was found to be influenced ($p < 0.05$) by the *conditions*. Similar to the tracking accuracy, the *time delay* was higher ($p < 0.05$) when the head-neck was used. The *time delay* in flexion/extension was also higher ($p < 0.01$) than in lateral bending and axial rotation when the head-neck was used. There was no significant influence of the *order* in which the experiments were done on the *time delay*. The participants did not ($p > 0.05$) reduce the *time delay* over the three attempts in each session.

The *settling time* was affected ($p < 0.05$) by both the *conditions* (i.e., head-neck vs. hand-wrist) and the desired targets (i.e., flexion, bending and rotation). Given a target, the *settling time* was much larger ($p < 0.05$) in the head-neck. There was no difference ($p > 0.05$), however, when comparing the *settling time* among different targets given a particular condition. The order did not impact ($p > 0.05$) the results in *settling time*. The results were also found to be similar ($p > 0.05$) among three attempts in each session.

4.4 Discussion

This study provides a quantitative comparison of the performance when the head-neck or the hand-wrist is used as a motion joystick to perform general orientation tasks with visual feedback. While that the head-neck was found to be less accurate and slower when compared to the hand-wrist in these tasks, it is not unexpected considering from the evolutionary and biological perspectives.

With the ability of humans to walk bipedally, it freed their upper extremities to become skillful in other higher-level tasks, such as grasping, maneuvering, and throwing an object to a target. As a result, the human beings could use their hands and grasp tools to hunt for food and defend themselves from predators. Over the years of evolution, the brain has refined and evolved its circuitry in the control of the hands [39, 40]. The homuncular map of the brain naturally shows a much larger area devoted to the upper extremities in order to facilitate the dexterous and fine motions executed by the hands. In contrast, the head houses vision and vestibular systems. The inertia of the eyeballs is much smaller compared to that of the head. As a result, the head has evolved as a unit that enlarges the range of human vision and the eyes respond to quickly track moving targets. Hence, in fine and fast visuomotor tasks, the head-neck plays a secondary role compared to the eyes [41–43].

However, in modern days, hand-held controllers, including gaming controllers and different joysticks, are being extensively used in video games and to perform virtual tasks of increasing complexity. Head-neck has the potential to be used as an alternative or an additional novel joystick to enhance human performance. Due to its anatomical structure, the head-neck movement is a viable option for orientation control. Even though the performance of the head-neck is not superior to the hand-wrist, the present study shows the feasibility of its use as an alternative controller for reorientation in visuomotor tasks. All participants in the study were able to quickly learn and complete the tasks without prior training.

Vision plays a key role in orientation tasks using the hand. The orientation of the hand can be corrected when within the FOV [41]. In contrast, with the head-neck, the sensory feedback relies mainly on the vestibular system or proprioception, i.e., stretch receptors in the muscles within the cervical joints [44–46]. The orientation of the head-neck cannot be seen by the eyes. In order to compare the orientation performance of the head-neck and the hand-wrist in visuomotor task, this missing visual information the head-neck was provided to the study participants through an avatar interface. However, this may still be considered as a new task to the participants that they may need practices to learn how to incorporate this additional information into their action. Additionally, as

the joystick placed within sight, participants may have used their eyes to adjust the orientation of the joystick in hand. As a result, the reaction time is more sluggish and angular errors are larger during target tracking when using the head-neck compared to using the joystick.

With the head-neck, the participants followed the target motions in the sagittal (flexion/extension) and transverse planes (axial rotation) well in comparison to the coronal plane (lateral bending). Nodding in agreement (flexion/extension of the head) and shaking the head during disagreement (axial rotation) are common social cues during communication. However, lateral bending of the head is not performed commonly and is not a well-practiced task. Therefore, one expects to have more errors while performing such a task. In fact, coupled rotation is commonly observed during lateral bending of the head-neck [47, 48]. This may have been the cause of large angular errors in rotation during tasks in the coronal plane.

When performing flexion/extension and axial rotation using the head-neck, the eyes were moved away from the center of the screens, vertically or horizontally, respectively. In order to look at the avatars, the eyes needed to move in a direction opposite to the head motion. This phenomenon is also labeled as vestibulo-ocular reflex (VOR). Although the VOR is considered to be one of the fastest reflexes in the human body, it usually lags behind the head motion roughly by 10 milliseconds [49]. The participants had to continuously adjust their field of view during the head motion [50] and this may have caused larger temporal delays during flexion/extension and axial rotation when using the head-neck.

Although daily orientation tasks usually involve spatial rotations, movements in single anatomical planes were used in this experiment. With this choice, isolated performance in each direction can be studied and compared between the head-neck and the hand-wrist. The avatars were presented as mirrored on the screen so that their facial features, such as the nose and eyes, of the avatars can be used by the participants for alignment in addition to the color indicator. These made the tasks intuitive so that the participants could comprehend well the movement goals and perform these. The amplitudes were selected such that the motions were within the workspace of both the neck brace and the joystick. The frequency (0.2 Hz) of the dynamic motions was relatively slow so

that the participants could easily follow the target cues. The participants performed 3-dimensional motions while the visual information was provided on a 2-dimensional screen. This makes it challenging to perceive the depth. In the future, the studies could be performed in a more immersive virtual environment to study how the visual immersion affects the results.

This study demonstrated that the healthy participants could use their head-neck as an orientation joystick to perform visuomotor tasks, but with less accuracy and larger time delays compared to using the hand-wrist with a conventional joystick. These results could potentially help design tasks and special controllers in rehabilitation and intense gaming that are tailored for these attributes of the head-neck control. The participants completed the tasks with their head-neck without extensive practices. This suggests that the performance of using the head-neck as a joystick may be improved through assistance or training, as the brain has the ability to learn [51, 52].

Chapter 5

Characterizing and Assisting Head-Neck Movements in ALS

5.1 Overview

Amyotrophic lateral sclerosis (ALS) is an adult-onset neurodegenerative disease characterized by progressive loss of upper and lower motor neurons [53–55]. The disease leads to limb and bulbar paralysis and respiratory failure. Patients with ALS show variability in their clinical course with duration ranging from several months to more than 10 years, although the majority of the patients die within a few years after symptom onset. At present, the disease is clinically diagnosed based on an array of symptoms and laboratory testing while excluding other definable diseases.

Dropped head is one of the features of the disease due to progressive loss of neck muscle strength [14, 17, 20, 23]. Eventually, the patients lose mobility of the head completely, settling in chin-on-chest posture with complications in speech, breathing, and swallowing. Patients with neck weakness often use braces to keep the head-neck in a neutral configuration, e.g., Miami J or a Head Master [14, 17]. The neck braces progressively become uncomfortable to wear and constrict breathing, swallowing and speech [23, 24]. There is a paucity of literature on new neck braces for this user group to facilitate activities of daily living.

Recent studies have shown that weakness of neck muscles is a significant prognostic marker [56, 57] for milestones such as loss of speech, loss of swallowing, loss of upper limb function, difficulty in turning on the bed, loss of walking, and ultimately the death [53, 54, 58, 59]. In addition to moving and supporting the head-neck, some of the neck muscles, such as Sternocleidomastoid (SCM), also play an important role in respiratory functions. The neck muscles and respiratory muscles are innervated by motor neurons in the cervical cord at levels C3 through C5. SCM is innervated by the spinal accessory nerve - cranial nerve XI. This postulates why the weakness of

the neck muscles is correlated with weakness of respiratory muscles.

While studies of neck movements in ALS are limited, a recent study concluded that the head motion of ALS patients is more jerky compared to healthy controls [47]. In this study, head-neck movements of ALS patients with minor strength loss in the neck muscles were investigated in conjunction with concurrent recordings of surface electromyography (EMG). The data from these patients were compared to the ones from a group of age-matched healthy controls. Patients with ALS were found to have different head movement and muscle activation patterns during single plane motions of the head. The findings suggest that the nature of head-neck movements may have been altered even when the ALS patients still have relatively large range of motion and strength in the neck.

One of the goals of designing a robotic brace was to assist ALS patients with head drop. As an extension of this characterization study, the assistance of the neck brace was evaluated with three ALS patients with head drop. The data echoed the ones obtained from healthy subjects (Chapter 3): the neck brace showed strong promises in lifting and moving the head of these patients. As a result, the subjects gained better control of the head movements and larger range of neck rotation when assisted by the robotic brace.

5.2 Methods

Eleven ALS patients (Table 5.1), diagnosed and treated at the Eleanor and Lou Gehrig MDA/ALS Research Center, Columbia University, and ten age-matched healthy controls (Age: 54.3 ± 10.6 yr, Height: 173.4 ± 10.1 cm, and Weight: 78.6 ± 11.6 kg) consented and participated in this experiment. The diagnoses were based on El Escorial ALS Diagnostic Criteria [60, 61], clinical judgment [62, 63], and supported by lab testing [63]. This study was approved by the Institutional Review Board (IRB) of Columbia University.

The patients enrolled in this study were examined and referred by a treating physician. All subjects had the ability to keep the head upright and return it back to neutral without external support. The strength of the neck extensor and flexor muscles were evaluated by a clinician and

Table 5.1: Characteristics of enrolled ALS patients

ID	Gender	Age (yr)	Height (cm)	Weight (kg)	FVC (%)	ALSFRS-r
1	F	76	150	50	75	37
2	F	69	173	82	21	23
3	F	57	167	69	75	31
4	M	77	178	66	61	38
5	M	64	170	82	109	42
6	M	61	182	82	91	42
7	M	60	170	74	108	36
8	M	51	180	75	65	26
9	M	49	175	83	47	n/a
10	M	33	180	83	60	36
11	M	67	165	80	68	42

*Note - For subject 9, the ALSFRS-r score was not available.

the minimum score among the subjects was 4 (on a 0-5 scale, with 5 being normal). Healthy controls were recruited to match the age of the patients. The control subjects did not have a history of neck injury. The age ($p = 0.192$), height ($p = 0.887$), weight ($p = 0.306$), and sex ($p = 0.730$, chi-square $= 0.120$) were not significantly different between the two groups.

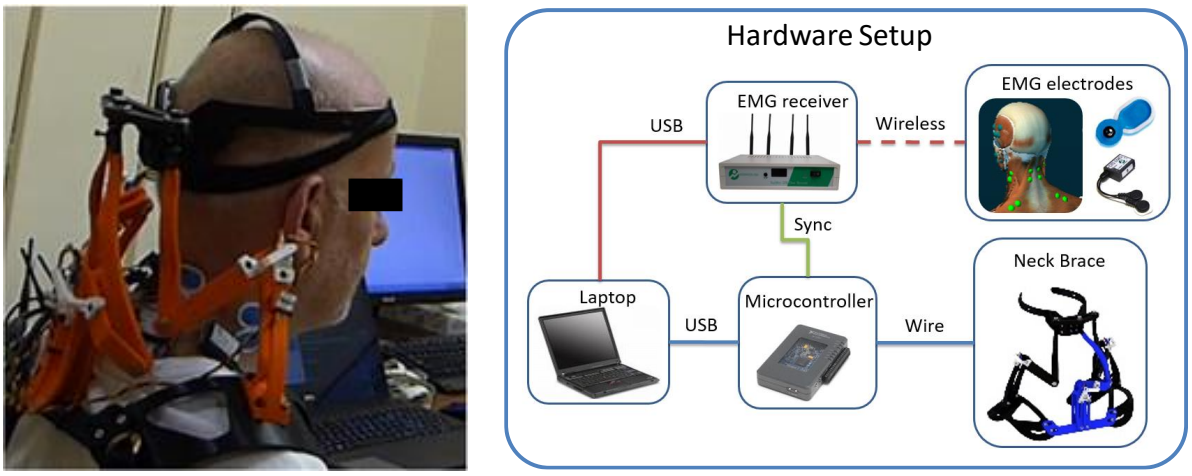

Figure 5.1: A participant and the system overview: (left) a participant with ALS wearing the neck brace and (right) system overview. The head angles of the participant are measured by the robotic neck brace. Muscle activation of the major surface neck muscles, SCM and SC, are measured using a wireless EMG system. The EMG measurements are synchronized with the movement of the neck brace via a trigger input from the microcontroller. The data from the two systems are recorded on a laptop and a graphical user interface displays the recorded data.

All procedures and data handling followed the approved protocol. All participants remained seated throughout the experiment. The skin around the neck and shoulder areas were cleaned with alcohol pads. A pair of electrodes was then attached along the fibers of each SCM and splenius capitis (SC) muscle. A transmitter unit for each channel was wired to the electrode and taped on the body. The neck brace was then firmly attached to the shoulders and the end-effector of the brace was tied to the forehead (Figure 5.1). Padding was added to the head and the shoulders to increase comfort and avoid sliding. A static trial was recorded where each participant was asked to relax and self-support the head in upright neutral position for five seconds. This static trial recorded the head angles and baseline muscle activation at the neutral configuration. The entire setup time for the experiment was around five to ten minutes, depending on the brace fit to the subject.

Each participant was then asked to perform three single-plane motions that included flexion-extension in the sagittal plane, lateral bending in the coronal plane, and axial rotation in the transverse plane. Each motion was performed in a cycle and was repeated five times at self-selected speeds. The subjects were asked to move as far as they could or what the brace allows. At the end of the experiment, each patient was asked to evaluate their experience with the neck brace during movements. A comfort scale was designed (Table 5.2). Each patient was asked to select a number between 0 (painful) and 8 (unnoticeable).

Table 5.2: Scale used in subjective evaluation

8	Unnoticeable	
7	Occasionally Noticeable	Psychologically Discomfort
6	Constantly Noticeable	
5	Occasionally Annoying	
4	Constantly Annoying	
3	Itchy Irritant	Physical Discomfort
2	Concerning Pressure	
1	Hurts	
0	Painful	

For ALS patients, ALS Functional Rating Scale-Revised (ALSFRS-r) and Forced Vital Capacity (FVC) were also measured to correlate outcomes measured from the brace and EMG recordings. ALSFRS-r is an estimate of the patient's functional impairment and objectively assesses response

to a treatment or progression of the disease. FVC is an index of respiratory function that is often used to indicate potential respiratory compromise in ALS.

The neck brace was sampled at 100 Hz and the EMG system at 1.5 kHz. An electronic trigger was used to synchronize the data from both systems. As an example, shown in Figure 5.2, the head angles were low-pass filtered (4th order Butterworth) at 6 Hz to reduce noise. The processing of the EMG signal from each channel followed these steps: (1) remove the DC offset, (2) band-pass filter ($10 - 450$ Hz), (3) rectify, (4) envelope using an RMS window approach, and (5) normalize each channel using the largest value recorded in that channel during experiment with the participant.

The middle three cycles during a motion were averaged and used for computing the outcomes. The cycles were segmented based on the primary angle of motion and normalized with respect to time. Teague-Kaiser Energy Operation was used for EMG onset detection following the steps in [64]. These onset times of EMG, along with timing of head motions, were used in data analysis to investigate the muscle coordination differences between the healthy and ALS groups.

The normality of the samples was tested using one-sample Kolmogorov-Smirnov test. Due to small sample size, measurement variables in the two groups, i.e., ALS and control, were not normally distributed. Wilcoxon rank-sum test was hence used to compare the variables between the two groups. Spearman rank correlation was used to examine the relationship between the variables and the clinical evaluation scores, i.e., ALSFRS-r and FVC. Data analysis was performed in Matlab (The MathWorks Inc., Natick, MA, USA) and the statistical significance was set at $p < 0.05$.

5.3 Results

Representative Results from a Healthy Control

This section summarizes the results of head-neck motion, along with EMGs from left and right SCM and SC muscles, in a single anatomical plane. This motion establishes the physiology to compare abnormal motions observed in ALS patients. We use the muscle activity to develop an analogy where each of the four muscles represents a rope between the shoulders and the head. We interpret the start, peak, and end of the muscle activity as a pattern for corresponding force pull

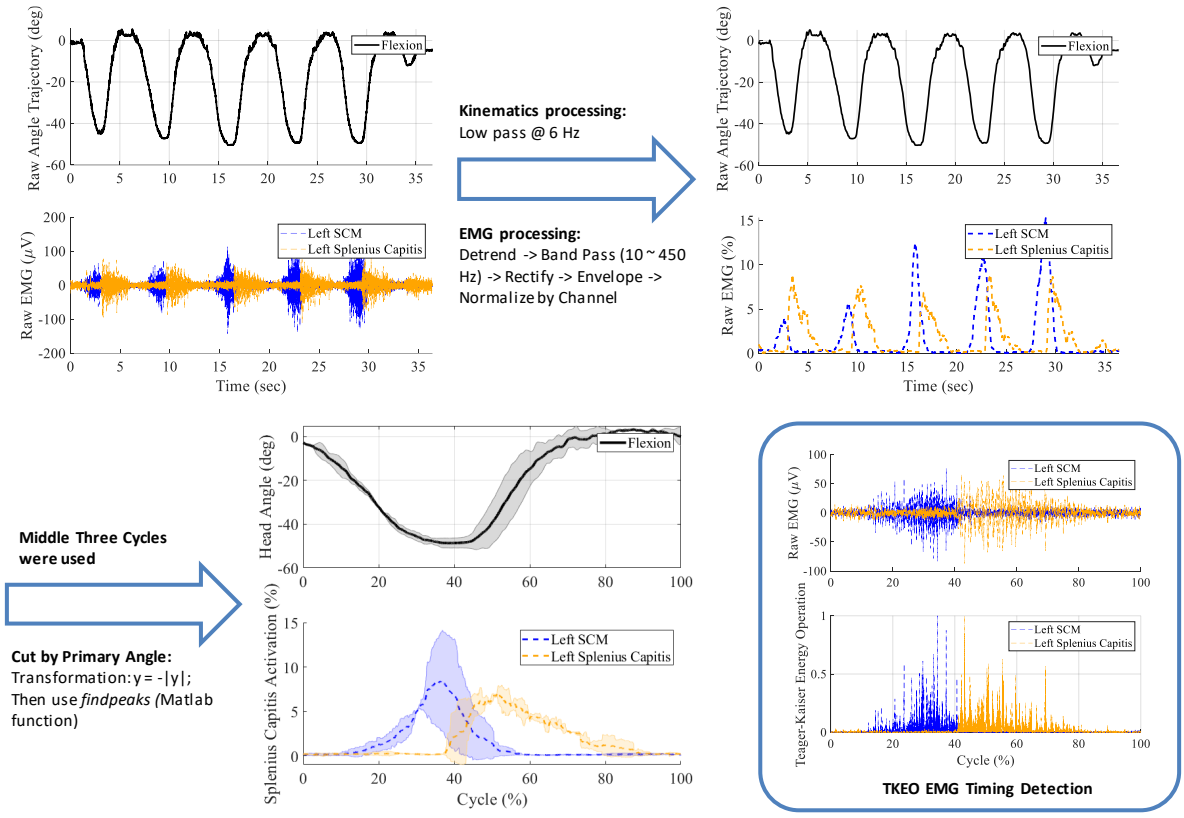

Figure 5.2: Data processing procedure of characterizing head-neck movements. The raw data of a subject during a session were filtered and smoothed. The middle three cycles were segmented and averaged based on the primary head angle. The EMG onset times were computed using Teague-Kaiser Energy Operation.

by the rope. While head-drop is an abnormality during flexion-extension, motions such as axial rotations and bending are simpler to understand and their physiology are described first.

The salient features of axial neck rotations are shown in Figure 5.3: (i) During right axial rotation of the head-neck, the left SCM and right SC are active together, (ii) During left axial rotation, the right SCM and left SC are active together, (iii) The temporal patterns of activity of the left SCM/right SC muscles and right SCM/left SC muscles are similar and the muscle peaks precede axial rotation motion peak. Effectively, the axial rotation can be visualized as being caused by a contralateral pair of ropes attached between the shoulders and head. The lateral bending of the head-neck similarly is caused by an ipsilateral pair of ropes attached between the shoulders and the head (Figure 5.4).

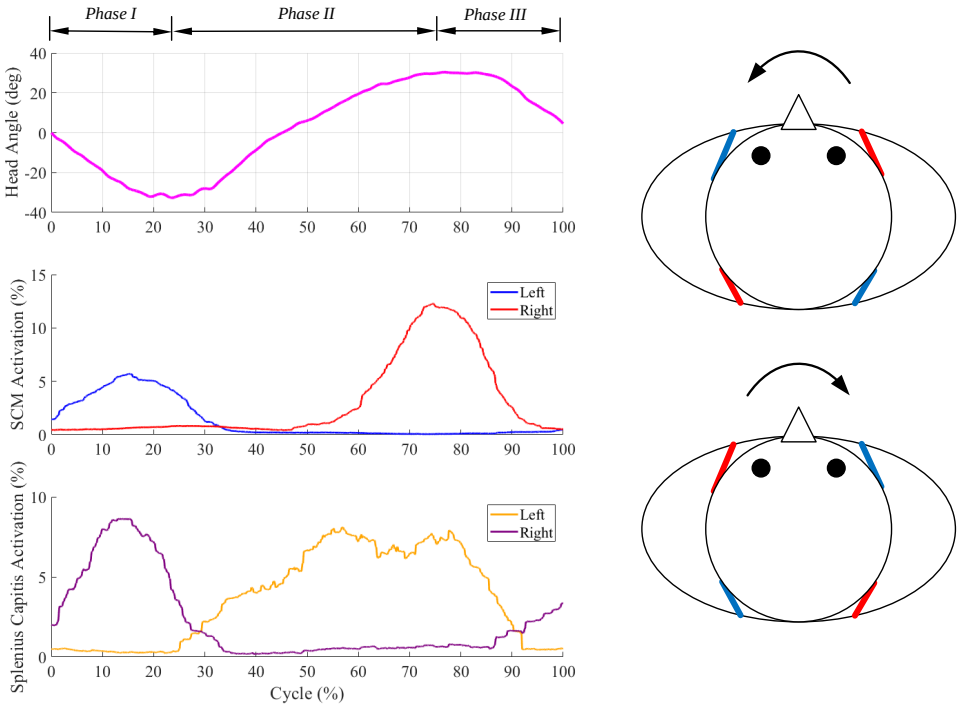

Figure 5.3: Axial rotation of a control subject: motion (primary head angle) and EMG patterns of neck muscles of a healthy subject during a movement cycle. Axial rotation is caused by a contralateral pair of muscles. For example, the simultaneous actuation of left SCM rope and right SC rope results in right axial rotation. The arrows indicate the directions of motion, blue (inactive) and red (active) lines indicate the activation of corresponding muscles during motion.

Gravity plays an important role in flexion-extension compared to lateral bending and axial rotation. As seen in Figure 5.5, flexion-extension is coordinated by a pair of ropes at the front or back attached between the shoulders and head. As the head starts to fall forward under gravity, the ropes at the back apply forces to prevent the head from falling forward uncontrollably. During extension from fully flexed position of the head, ropes at the back pull to restore the head to the neutral position.

Group Results

In contrast with healthy subjects, as detailed in Table 5.3 and Table 5.4, the head-neck movements in ALS patients showed salient differences. These could suggest that the ability to activate a pair of muscles to execute single-plane motions, in contrast to healthy subjects, has been compromised

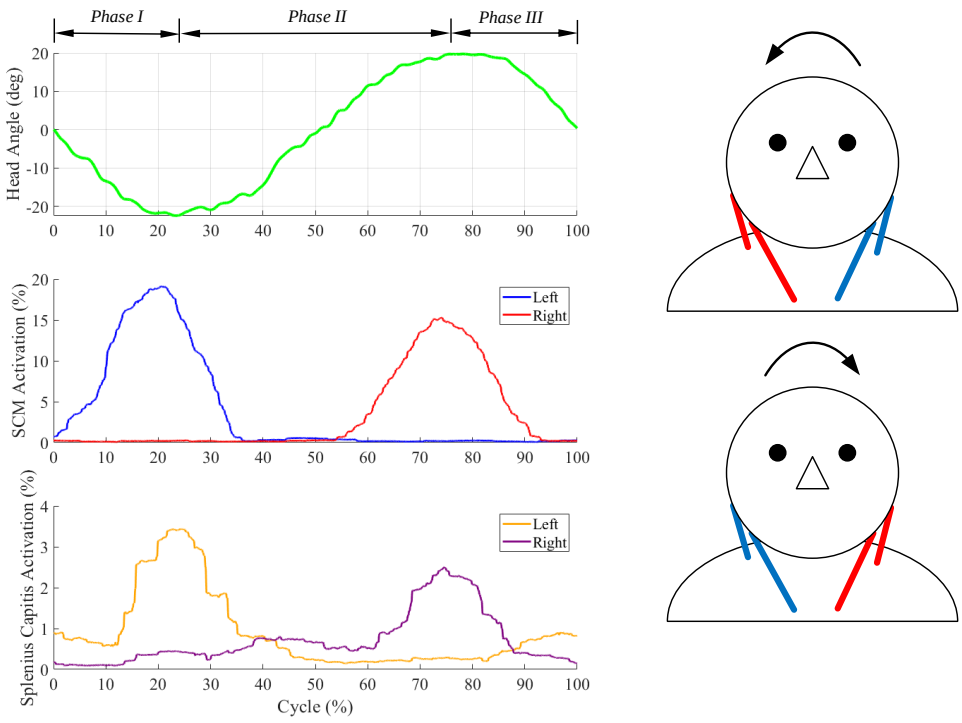

Figure 5.4: Lateral bending of a control subject: motion (primary head angle) and EMG patterns of neck muscles of a healthy subject during a movement cycle. Lateral bending is caused by an ipsilateral pair of muscles. For example, the simultaneous actuation of left SCM rope and left SC rope results in left lateral bending. The arrows indicate the directions of motion, blue (inactive) and red (active) lines indicate the activation of corresponding muscles during motion.

in the patient group.

During axial rotation in Phase II, where subjects moved from axially rotated one extreme position to the other, right SCM was found to have a longer duration of activation in ALS subjects (p = 0.013). Additionally, this variable seems to have a correlation with the clinical scores, i.e., ALSFRS-r (r = -0.62, n = 10, p = 0.08) and FVC (r = -0.56, n = 11, p = 0.09). With a lower clinical score, it is possible that a patient has a shorter activation in SCM during Phase II in axial rotation. However, no statistical significance was found.

During lateral bending in Phase II, where subjects moved from laterally bent one extreme position to the other, right SC was found to have a longer duration of activation in ALS subjects ($p = 0.012$). During flexion-extension, the length of Phase I, where the subjects flexed their head

Table 5.3: Onset time and duration of activation of each muscle as a fraction of the cycle during movements in three anatomical planes of ALS and control group

Axial Rotation								
	Onset Time				Duration of Muscle Activation			
	lSCM	rSCM	lSC	rSC	lSCM	rSCM	lSC	rSC
Controls	0.114 (0.13)	0.585 (0.08)	0.265 (0.21)	0.046 (0.12)	0.312 (0.29)	0.256 (0.08)	0.646 (0.27)	0.479 (0.30)
ALS	0.101 (0.17)	0.413 (0.27)	0.216 (0.24)	0.030 (0.08)	0.493 (0.33)	0.419 (0.28)	0.723 (0.29)	0.717 (0.33)
Lateral Bending								
	Onset Time				Duration of Muscle Activation			
	lSCM	rSCM	lSC	rSC	lSCM	rSCM	lSC	rSC
Controls	0.083 (0.12)	0.474 (0.23)	0.033 (0.08)	0.234 (0.25)	0.504 (0.32)	0.424 (0.28)	0.779 (0.29)	0.627 (0.33)
ALS	0.047 (0.06)	0.409 (0.25)	0.035 (0.07)	0.125 (0.21)	0.363 (0.22)	0.426 (0.27)	0.828 (0.30)	0.828 (0.27)
Flexion-Extension								
	Onset Time				Duration of Muscle Activation			
	lSCM	rSCM	lSC	rSC	lSCM	rSCM	lSC	rSC
Controls	0.086 (0.11)	0.131 (0.15)	0.264 (0.19)	0.298 (0.19)	0.506 (0.29)	0.472 (0.36)	0.612 (0.24)	0.580 (0.24)
ALS	0.085 (0.14)	0.121 (0.21)	0.097 (0.15)	0.121 (0.16)	0.510 (0.32)	0.596 (0.32)	0.792 (0.31)	0.811 (0.23)

Table 5.4: Head angles during movements in three anatomical planes of ALS and control group

Axial Rotation			
	Phase I	Phase II	Phase III
Control	0.245 (0.07)	0.526 (0.08)	0.229 (0.09)
ALS	0.231 (0.07)	0.539 (0.10)	0.230 (0.05)
Lateral Bending			
	Phase I	Phase II	Phase III
Control	0.290 (0.07)	0.501 (0.08)	0.209 (0.05)
ALS	0.264 (0.09)	0.516 (0.08)	0.220 (0.06)
Flexion-Extension			
	Phase I	Phase II	Phase III
Control	0.345 (0.08)	0.481 (0.09)	0.174 (0.07)
ALS	0.282 (0.08)	0.510 (0.08)	0.208 (0.08)

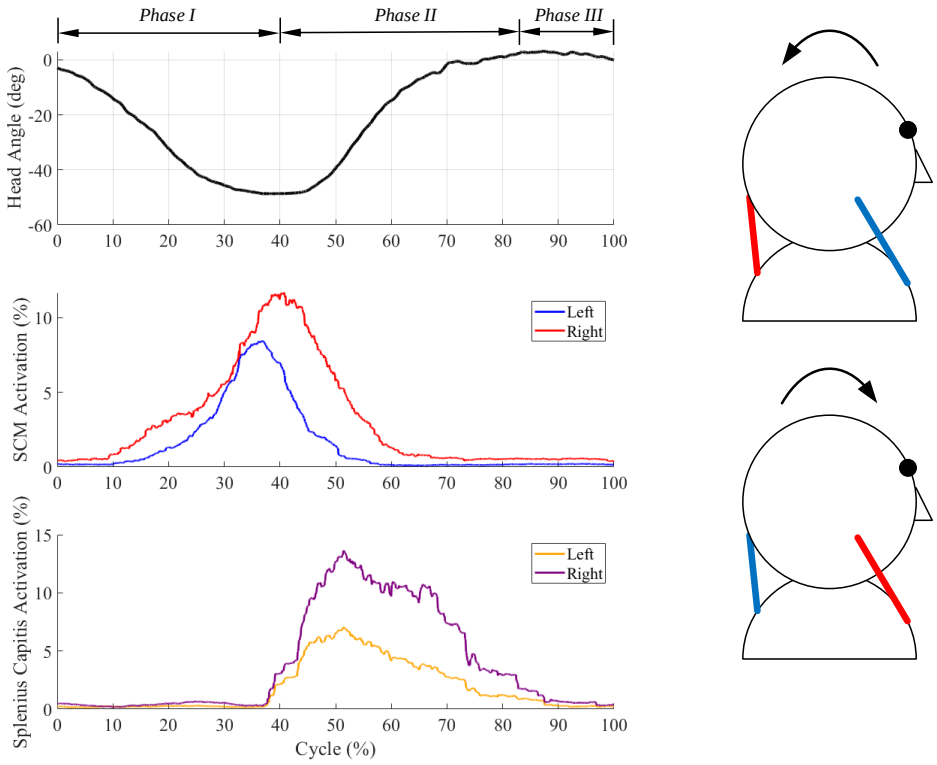

Figure 5.5: Flexion/extension of a control subject: motion (primary head angle) and EMG patterns of neck muscles of a healthy subject during a movement cycle. Flexion-extension is caused by simultaneous actuation of the front/back pair of muscles. For example, the actuation of front SCM ropes results in flexion and the actuation of back SC ropes results in extension. The arrows indicate the directions of motion, blue (inactive) and red (active) lines indicate the activation of corresponding muscles during motion.

under gravity from the neutral to the maximum, was found to be longer in ALS than the control group (p = 0.001). The onset times of SC of these patients, however, suggested that their neck extensor muscles tend to activate much earlier ($p < 0.001$).

In the control group, we found strong correlations between temporal variables of neck muscle activation and head angles, as illustrated using scatter plots in Figure 6. Results of Spearman correlation indicated that there was a positive association between the average EMG onset times of all four neck muscles and the time of maximum flexion during single plane flexion-extension motion ($r = 0.903$, $n = 10$, $p = 0.0009$). A positive correlation was also found between the average EMG onset time of the contralateral SCM muscle and the time of maximum rotation during

single plane axial rotation ($r = 0.891, n = 10, p = 0.0014$). This suggests that the head movements are coordinated by certain muscles consistently in the healthy controls. However, such relationships were not found in the patient group ($p > 0.05$).

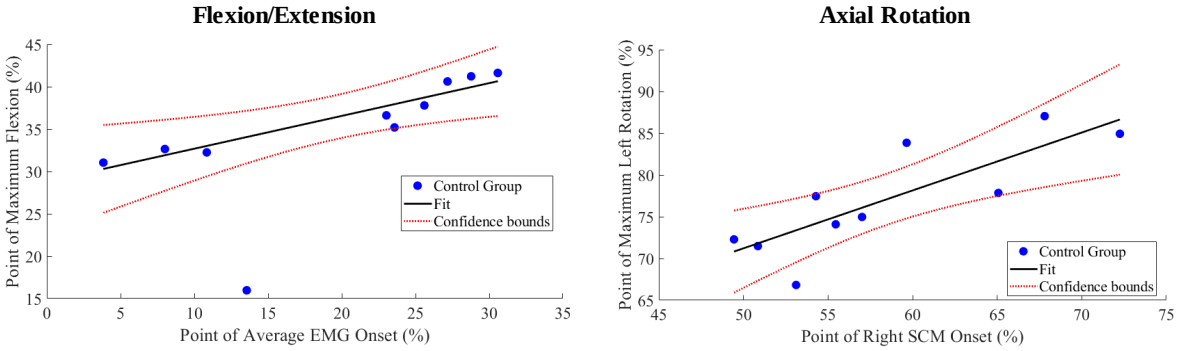

Figure 5.6: Correlating muscle EMG onsets with motion peaks in the group of healthy subjects: (left) scatter plot of the time of maximum flexion against the average onset times of all four SCM and SC during a cycle and (right) scatter plot of the time of maximum left rotation against the average onset time of the right SCM muscles during the cycle. Each dot represents a subject and the straight line represents the least-square fit of the data.

5.4 Discussion

We observed the kinematics and surface EMG of the head-neck during simple single-plane motions. An important goal of this paper was to identify features that may be valuable clinically. The brace was evaluated by ALS subjects as highly wearable and comfortable (average self-evaluation score of 7.18 ± 0.8 out of a maximum of 8). A 'four-rope' analogy was derived to explain the head movement activated by four neck muscles. The pairs of SCM and SC on the two sides of the neck form four ropes connecting the head and the shoulders. A pair in these four ropes pull synergistically to generate a specific movement. This muscle-motion pattern was found to be clear and consistent in healthy controls but were absent in ALS patient group.

During single-plane flexion-extension, under the gravity, ALS patients showed a shorter duration to reach the maximum flexion starting from the neutral, whereas their neck extensor muscles activated much sooner during flexion phase. This is likely to protect the head from falling and thus

co-contracted with flexor muscles during flexion motion. This strategy may have been adopted to increase cervical joint stiffness during the flexion motion. The head weighs about 5 kg and the gravity plays an important role during flexion-extension motion and may have biased the control of muscles in patients.

The duration of muscle activity to go from one extreme to the other, i.e., SC in lateral bending and SCM in axial rotation, were found to be longer in patient group. This may result in excessive fatigue in those who have head drop in early stages and could justify the use of neck braces.

The brace measurements in ALS patients were highly correlated with the clinically measured scores, such as the ALSFRS-r and the FVC used in clinic. Hence, this procedure can be adopted in a clinic to complement self-reporting. The activation duration of SCM plays a role in respiration and this was correlated with the ALSFRS-r and FVC in ALS patients during axial rotation.

The movement of the head is achieved not only by surface muscles, such as SCM and SC used in this study, but also by deeper muscles. However, obtaining signals from those muscles requires invasive methods. The presented procedure was intended to be non-invasive and easy to conduct so that it can be potentially adapted in a clinic. The data show that differences in head-neck coordination can still be extracted in ALS patients using surface neck muscles.

Temporal variables of neck EMG were compared between the patient and the control group. These variables, in conjunction with the timing of the head angles, reveal the muscle-movement patterns. Additionally, temporal information is more reliable when comparing surface EMG among different subjects as there usually are slight differences in sensor placements and skin preparation.

The sample size of this study was small and the group characteristic of the patients was heterogeneous. Additionally, the brace used in this experiment had only one size, and fitted subjects within a range of anatomical sizes. However, this study demonstrated the feasibility of using this robotic brace for ALS patients. The brace could allow relatively large ranges of motion of the head and was comfortable to wear. These made it possible to use the robotic neck brace in assisting movement of the head in ALS patients with more severe neck muscle weakness.

5.5 Extension: Assisting head-neck movements in ALS

As an extension of this study, the robotic neck brace was evaluated by three ALS patients with clinically reported neck muscle weakness. The primary goal of this evaluation was to demonstrate that the brace can provide sufficient support during controlled movements, thereby increasing the range of motion of the head and reducing the muscle input of the patient. This evaluation by patients with neck muscle weakness gives direct insights in terms of the efficacy of using the robotic neck brace to assist dynamic head motion in impaired populations.

The experiment was designed to have two sessions with the same tasks. The tasks were tracking a continuous head trajectories (Table 5.5), displayed using the avatar visual interface (Figure 2.3 (A)), in each of the anatomical planes. The subjects needed to follow these trajectories five times continuously. The data recorded during the middle three cycles were used for data analysis.

Table 5.5: Target avatar head trajectories in evaluation with ALS patients

Flexion/Extension	$\theta_x^d = 15^\circ \sin(0.2\pi t) - 10^\circ$
Lateral Bending	$\theta_y^d = 20^\circ \sin(0.2\pi t)$
Axial Rotation	$\theta_z^d = 25^\circ \sin(0.2\pi t)$

The subjects were seated with the neck brace attached. The brace was operated in the 'transparent' mode in the first session (Baseline) while in the 'assistance' mode in the second session. The control input for the 'assistance' mode was provided through a keyboard by an experimenter[1]. During the Baseline session, another experimenter put the hands around the subject's head to avoid any involuntary head fall due to weakness of the subject. In the event where the subject struggled to return the head back against gravity, this experimenter would push the head gently to help the subject continue the task. The number of such a support was also documented as a reference.

Head trajectories were measured through the neck brace and muscle activation was recorded using surface EMG at four sites (SCM and SC on both sides). There were three outcomes derived from the head kinematics and the EMG of the muscles, including *RMS error*, integrated EMG

[1]Considering the possible upper extremity weakness in ALS, the control input was given by an experimenter. Since the desired head-neck motion was displayed on the computer screen, the subject could therefore anticipate the movement command from the experimenter, making it a safe choice.

Table 5.6: Outcomes of the first subject (male, age: 55 yr, height: 195 cm, weight: 91 kg)

		RMS Error (°)		iEMG ($\mu V \cdot min$)				ROM (°)	# of Supports
		In-Plane	Out-of-Plane	lSCM	rSCM	lSC	rSC		
F/E	Baseline	15	10	209	163	164	245	n/a	6
	Assist	4	0	173	106	131	212	35	0
LB	Baseline	13	13	191	246	121	205	2	0
	Assist	2	0	140	159	72	174	37	0
AR	Baseline	20	14	168	320	127	218	3	0
	Assist	5	1	148	180	119	181	59	0

Table 5.7: Outcomes of the second subject (male, age: 33 yr, height: 185 cm, weight: 116 kg)

		RMS Error (°)		iEMG ($\mu V \cdot min$)				ROM (°)	# of Supports
		In-Plane	Out-of-Plane	lSCM	rSCM	lSC	rSC		
F/E	Baseline	7	3	286	199	477	551	30	0
	Assist	2	0	207	187	390	487	33	0
LB	Baseline	4	11	292	239	485	542	35	0
	Assist	2	0	195	158	345	398	38	0
AR	Baseline	7	7	363	310	460	507	63	0
	Assist	4	0	147	156	343	409	56	0

Table 5.8: Outcomes of the third subject (female, age: 55 yr, height: 172 cm, weight: 65 kg)

		RMS (°)		iEMG ($\mu V \times min$)				ROM (°)	# of Supports
		In-Plane	Out-of-Plane	lSCM	rSCM	lSC	rSC		
F/E	Baseline	4	5	166	86	195	206	42	0
	Assist	2	0	77	73	125	133	35	0
LB	Baseline	3	4	288	308	147	181	44	0
	Assist	2	0	121	244	92	108	38	0
AR	Baseline	10	4	214	452	146	220	67	0
	Assist	3	0	111	78	81	108	55	0

(*iEMG*), and range of motion (*ROM*) during each motion trial. The *RMS error* was decomposed into two categories, *in-plane* and *out-of-plane*, where the *in-plane* referred to the primary angle corresponding to the target motion while the *out-of-plane* was the maximum error in the other two planes. The *iEMG* was computed by integrating the EMG (detrended, filtered, and rectified) in microvolt (μV) from each channel over the recorded period of time (half a minute) during a motion. The *ROM* was calculated by the difference between the maximum and minimum value of the primary angle during a motion.

Tables 5.6, 5.7, and 5.8 summarize the outcomes from each patient. The first patient was weaker in terms of the neck muscle strength compared to the other two patients, as evidenced by the ranges of motion in the baseline session. This subject was not able to track the desired movements, resulting very little voluntary movement of the head [2]. In this case, the neck brace significantly increased the range of motion of the head with slight lower muscle input on his own. The second and the third subjects had only mild weakness in the neck muscles. They presented good ranges of motion and tracking accuracy during the baseline trials. When assisted by the brace, where they were verbally encouraged to relax their heads, the total muscle EMG reduced. This means that the neck brace made the tasks easier for them as the head was primarily moved by the neck brace.

One limitation of this experiment was that the experimenter controlled the brace through the keyboard when it was used to assist the subjects. Therefore, the lower *in-plane* tracking errors when assisted by the neck brace could be attributed to the good finger control of the experimenter. Nonetheless, the ability of translating a user's input command into accurate head movements was still reflected from these results. This suggests that it is very likely that the subjects could have achieved similar performance if they had commanded the brace on their own. The neck brace was only evaluated by a small number of subjects with various level of weakness in neck muscles. More patients need to be enrolled to draw definitive conclusions on its efficacy in assisting head motion.

[2]The *ROM* in flexion/extension cannot be extracted because the subject could not continue the task without external hand support from the experimenter.

Conclusion

A robotic neck brace was developed in this dissertation. This brace was originally motivated to enable head-neck movements for patients with head drop. It was then developed into a versatile robotic platform aimed to meet various needs in research and clinical community. This robot has been validated through a series of experiments with healthy human subjects. This dissertation also presented two scientific studies, where this wearable robot was used to study the head-neck movements. To the best of our knowledge, it is the first wearable robot of its kind to assist, train, and study head-neck movements in the literature.

Novelty in robot design

The neuromusculoskeletal system has perfected human movements during daily activities. Due to diseases, injuries, and aging, the ability to perform natural movements of an individual may be compromised. Exoskeletal robots are possible solutions. These machines often use linkages[3] to connect body segments in parallel to the anatomical joint of interest, e.g., ankle, wrist, knee, etc. The linkages are jointed[4] so that the motion of the effector can be computed mathematically and empowered by common actuators such as electromagnetic motors. However, the motion characteristics of these machines often slightly deviate from the intended natural movements.

This mismatch between the human and machine movements leads to the *axes misalignment* and *hyperstaticity* problems which have been well documented in the literature [65–67]. Popular treatments include using single contact point between the effector and the human body [12, 68,

[3]There has been a rising number of designs using soft materials instead of traditional linkage mechanisms. Though promising, it is still facing numerous challenges such as difficult to characterize, power, and control.

[4]From a synthesis point of view, any mechanical joint can be regarded as combinations of simple revolute (rotational) and/or prismatic (translational) joints with special axes alignments.

69], adopting flexible attachments such as cuffs [5, 70]), and inducing passive mechanical joints explicitly [65, 71, 72] or implicitly [73, 74] to compensate for the misalignment. However, only adding compliance (cuffs) at the attachment point could not reduce the shear force, which may lead the robot to on the skin or causing discomfort [66]. Adding passive joints, on the other hand, increases the complexity and bulkiness of the robot.

The design of the robotic neck brace implemented a new approach where a lower mobility parallel mechanism[5] with deliberately introduced parasitic (coupled) motion was used[6]. The chosen mechanism was modified from the 3-RRS wrist where the end-effector moves on a spherical surface without any translation. The parasitic motion[7] was then parameterized and optimized to fit the translation of the effector to the empirical human data. Additionally, soft attachments were also used in the physical model to increase comfort while wearing. Without increasing the physical complexity of the robot, the *axes misalignment* and *hyperstaticity* problems can be better managed using this approach than only using compliant cuffs.

The design choice of perturbing the 3-RRS spherical mechanism also made it easier to realize into a physical neck brace. In order for the spherical mechanism to avoid translation, the axes from different RRS chains must intersect at a single point (spherical center of the effector). If this constraint is violated, the motion computation may not produce viable solutions. However, this constraint is very difficult to meet in a physical model due to inevitable assembly errors and deflections of mechanical components during operations.

This design approach could potentially be applied to future wearable robot, especially considering the motion similarities, i.e., predominantly rotations with small translations, between the neck and other human joints such as hips and shoulders.

---

[5] A parallel mechanism which allows less than six degrees of freedom is called a lower mobility parallel mechanism.

[6] Typically, parasitic motions are avoided for designing a parallel mechanism in that these are usually undesired coupled motions and induce control and analysis challenges [75].

[7] The parasitic motion of the neck brace was chosen to be the translation of the end-effetor.

A solution for head drop

The prescription of a neck brace to a patient with head drop is primarily due to its ability of supporting the head-neck. By using such a static brace, the heaviness of the head can be alleviated and the patient may have a better upright view. However, most of current neck braces are not designed for head drop. They are primarily used to fixate a person's head-neck after a traumatic head or neck injury with suspected cervical fracture. The brace disallows the head from moving and thus prevents the spinal cord from being injured by such a fracture. These neck braces are not recommended for long-term use due to discomfort. Additionally, because the brace is fitted between the chin and chest, it blocks the airway and creates challenges for patients with neck muscle weakness to breath, speak, and swallow. From a patient perspective, restoring normal head-neck movement, not supporting the head at a fixed configuration, is the real and unmet need.

The presented robotic neck brace provides a possible solution to empower normal head-neck movements in patients with head drop. The robotic brace is lightweight and portable, allowing three rotations of the head in a wide range (70% of natural range of motion). It attaches to the user's forehead and shoulders without pressing on the chest and enclosing the neck so that the patient can breath and speak with ease. The mechanical linkages connecting these attachments are located at the back to ensure a full front view for the user. This design choice also limits the range of neck extension which prevents undesired hyper-extension of the cervical spine.

The user can control intended head-neck movements through several input devices, including joysticks, keyboards, and eye-trackers. The intent of the user is interpreted by designed control logic to obtain the desired head motion. The inverse kinematics model is then used to compute the motor commands to control the movement of the brace. Of the three input devices, the joysticks and keyboards require a user to command the head movement through certain hand maneuvers while the eye-tracking interface mimics one of the head-eye behaviors in human. When responding to a visual stimulus within the field of view, the eyes move towards the stimulus first and then the head follows and stops at the target. All these three interfaces have been validated by human studies with healthy individuals.

One question about this robotic brace, when it is used by a head drop patient, was whether the physical model of the brace can supply the movement of the head. A pilot study was conducted where three ALS patients with neck muscle weakness were recruited. The results have shown that the brace, when powered by motors, enables larger range of motion of the head. Additionally, the level of muscle activation was reduced, suggesting a smaller effort needed by the patients themselves. A future study with more patients would help draw definitive conclusions about the efficacy of the neck brace in head drop.

A robot for training and studying the head-neck movements

During a movement training, a therapist interacts with a patient to (re)learn a functional task. This interaction often requires the therapist to apply forces to the patient at certain movement phases. For example, when training a stroke patient to walk on a treadmill with better foot clearance off the ground, a therapist may lift the ankle on the affected side of the patient during swing phase of a gait cycle. The amount of interactive forces is also updated with the progression of the therapy. In this example, the therapist may apply less forces when the stroke patient improves the ankle trajectory. In this way, the patient can be challenged constantly and encouraged to improve more.

Robotic training using force control mimics this interaction dynamics between the therapist and the patient. This type of control modulates the forces applied to the patient based on the task performance, e.g., tracking errors of a trajectory. This training concept has been widely used to improve gait and balance, arm reaching, and trunk stability. However, there has been a paucity in research using a robot to train movement of head-neck because of lack of a validated platform. The robotic neck brace developed in this thesis provides a tool to perform such researches. Multiple force controllers have been developed to apply perturbation, to track movement trajectories with assist as needed, and to reach targets with gradually increased resistance.

In some neurological diseases, such as severe cases in cerebral palsy (GMFCS[8] IV-V), the full body movement of the patient, including the head-neck, is undermined. Such a patient must rely

[8]Gross motor function classification system

on a wheelchair with headrests to ambulate and interact with the environment. Targeted therapy[9] cannot be applied to the torso or limbs until the movement function in the head-neck has been improved. This is because the patient is not capable of lifting the head up and making eye contact, thereby limiting the effectiveness of interaction with the therapists. Therefore, the robotic neck brace can potentially be used in such a scenario to facilitate training of head-neck. The robot can also provide quantifiable assessments of training outcomes.

In this thesis, two studies were introduced where the robotic neck brace was used to explore scientific questions. The first question was whether the head-neck can perform orientation tasks as good as the hand-wrist given that the movement characteristics of the two are very similar. Answering this question can create new tasks tailored for head-neck to achieve, thereby increasing productivity or assisting patients with hand-wrist impairment. An experiment was conducted where healthy subjects were tasked with orienting virtual objects using both their head-neck and hand-wrist. The neck brace was used to record the movements of the head-neck and display these to the subjects through a visual interface. The results have shown that the head-neck can perform orientation tasks, albeit less accurate and slower compared to the performance by the hand-wrist.

The second study was to investigate the movement patterns in ALS patients with early signs of neck muscle weakness. Recent research has suggested that the neck muscle strength is correlated to the progression of the disease because the innervation of the neck muscles shares the same region as the respiratory muscles in the spinal cord. In the present study, a group of ALS patients with mild neck weakness were recruited to perform head-neck movements. Their head movements were measured by the robotic brace while the activation of the neck muscles was recorded through surface EMG. Their performances were compared with an age-matched healthy control group. A clear muscle-movement pattern can be observed in the control data where a pair of muscles work in synergy to activate a target head-neck motion in an anatomical plane. However, this pattern was absent when examining the data from ALS patients. In movements against gravity, such as

[9] A type of physical training which targets a segment of the body. For example, it has been shown to improve the sitting stability in children with cerebral palsy [76, 77].

flexion, some patients showed a co-contraction pattern in flexor and extensor muscles which stiffs the neck and prevents the head from falling. The study concluded that ALS patients with early neck muscle weakness may have already developed different activation strategies to conduct the same head movements. The muscle-movement data of these patients also correlate to their clinical score such as ALSFRS-r and FVC(%), suggesting the assessment method can be adopted in clinic.

What is ahead

This thesis introduced the first robotic neck brace for assisting, training, and studying the head-neck movements. Studies have been performed to demonstrate the potential use of this brace for different applications. Although most of these studies were conducted with healthy individuals, they provided critical design insights and baseline datasets for future studies with impaired populations.

It is hoped that the methodology of the robot development can inspire future wearable robot designs, that the robotic neck brace can help patients with head-drop, thereby improving their quality of life, and that this device can provide a research tool to explore scientific questions related to the movement of the head-neck.

Bibliography

[1] Sunil Agrawal. *The Encyclopedia of Medical Robotics*. WORLD SCIENTIFIC, 2018. DOI: 10.1142/10770-vol4. eprint: https://www.worldscientific.com/doi/pdf/10.1142/10770-vol4. URL: https://www.worldscientific.com/doi/abs/10.1142/10770-vol4.

[2] Lisa Lighthall Haubert et al. "A comparison of shoulder joint forces during ambulation with crutches versus a walker in persons with incomplete spinal cord injury." In: *Archives of physical medicine and rehabilitation* 87.1 (2006), pp. 63–70.

[3] KMM Van Riel et al. "Four-wheeled walker related injuries in older adults in the Netherlands." In: *Injury prevention* 20.1 (2014), pp. 11–15.

[4] WK Lam et al. "Biomechanical and electromyographic evaluation of ankle foot orthosis and dynamic ankle foot orthosis in spastic cerebral palsy." In: *Gait & posture* 22.3 (2005), pp. 189–197.

[5] Sašo Jezernik et al. "Robotic orthosis lokomat: A rehabilitation and research tool." In: *Neuromodulation: Technology at the neural interface* 6.2 (2003), pp. 108–115.

[6] Sai K Banala et al. "Robot assisted gait training with active leg exoskeleton (ALEX)." In: *2008 2nd IEEE RAS & EMBS International Conference on Biomedical Robotics and Biomechatronics*. IEEE. 2008, pp. 653–658.

[7] Alberto Esquenazi et al. "The ReWalk powered exoskeleton to restore ambulatory function to individuals with thoracic-level motor-complete spinal cord injury." In: *American journal of physical medicine & rehabilitation* 91.11 (2012), pp. 911–921.

[8] Aaron M Dollar and Hugh Herr. "Lower extremity exoskeletons and active orthoses: challenges and state-of-the-art." In: *IEEE Transactions on robotics* 24.1 (2008), pp. 144–158.

[9] Joaquin A Blaya and Hugh Herr. "Adaptive control of a variable-impedance ankle-foot orthosis to assist drop-foot gait." In: *IEEE Transactions on neural systems and rehabilitation engineering* 12.1 (2004), pp. 24–31.

[10] Cassie Meeker et al. “EMG pattern classification to control a hand orthosis for functional grasp assistance after stroke.” In: *2017 international conference on rehabilitation robotics (ICORR)*. IEEE. 2017, pp. 1203–1210.

[11] Samuel Au, Max Berniker, and Hugh Herr. “Powered ankle-foot prosthesis to assist level-ground and stair-descent gaits.” In: *Neural Networks* 21.4 (2008), pp. 654–666.

[12] Michael F Eilenberg, Hartmut Geyer, and Hugh Herr. “Control of a powered ankle–foot prosthesis based on a neuromuscular model.” In: *IEEE transactions on neural systems and rehabilitation engineering* 18.2 (2010), pp. 164–173.

[13] Frank Sup, Amit Bohara, and Michael Goldfarb. “Design and control of a powered transfemoral prosthesis.” In: *The International journal of robotics research* 27.2 (2008), pp. 263–273.

[14] M Gourie-Devi, A Nalini, and S Sandhya. “Early or late appearance of “dropped head syndrome” in amyotrophic lateral sclerosis.” In: *Journal of Neurology, Neurosurgery & Psychiatry* 74.5 (2003), pp. 683–686.

[15] Steven M Albert et al. “Prospective study of palliative care in ALS: choice, timing, outcomes.” In: *Journal of the neurological sciences* 169.1-2 (1999), pp. 108–113.

[16] Kenichi Kashihara, Manabu Ohno, and Susumu Tomita. “Dropped head syndrome in Parkinson’s disease.” In: *Movement disorders: official journal of the Movement Disorder Society* 21.8 (2006), pp. 1213–1216.

[17] Timothy G Petheram et al. “Dropped head syndrome: a case series and literature review.” In: *Spine* 33.1 (2008), pp. 47–51.

[18] JS Katz et al. “Isolated neck extensor myopathy: a common cause of dropped head syndrome.” In: *Neurology* 46.4 (1996), pp. 917–921.

[19] WGH Oerlemans and M De Visser. “Dropped head syndrome and bent spine syndrome: two separate clinical entities or different manifestations of axial myopathy?” In: *Journal of Neurology, Neurosurgery & Psychiatry* 65.2 (1998), pp. 258–259.

[20] Richard A Smith and Forbes H Norris. “Symptomatic care of patients with amyotrophic lateral sclerosis.” In: *Jama* 234.7 (1975), pp. 715–717.

[21] Marilyn Trail et al. “Wheelchair use by patients with amyotrophic lateral sclerosis: A survey of user characteristics and selection preferences.” In: *Archives of Physical Medicine and Rehabilitation* 82.1 (2001), pp. 98–102.

[22] Heath Reed et al. “Head-Up; An interdisciplinary, participatory and co-design process informing the development of a novel head and neck support for people living with progres-

sive neck muscle weakness." In: *Journal of medical engineering & technology* 39.7 (2015), pp. 404–410.

[23] Silvia Pancani et al. "Assessment of the Sheffield Support Snood, an innovative cervical orthosis designed for people affected by neck muscle weakness." In: *Clinical Biomechanics* 32 (2016), pp. 201–206.

[24] Pamela Glazener. "Pilot study to determine the effectiveness of a new neck brace design for patients with amyotrophic lateral sclerosis." In: *Journal of Nursing Education and Practice* 4.6 (2014), p. 1.

[25] Graeham Douglas et al. *Motorized Headrest for People with Neck Muscle Weakness | RESNA Student Design Competition*. `https://sites.psu.edu/resnasdc/2010/05/13/motorized-headrest-for-people-with-neck-muscle-weakness-the-university-of-british-columbia/`. (Accessed on 04/20/2019). 2010.

[26] Dongsu Wu, Lin Wang, and Peng Li. "A 6-DOF exoskeleton for head and neck motion assist with parallel manipulator and sEMG based control." In: *2016 International Conference on Control, Decision and Information Technologies (CoDIT)*. IEEE. 2016, pp. 341–344.

[27] Haohan Zhang and Sunil K Agrawal. "Kinematic design of a dynamic brace for measurement of head/neck motion." In: *IEEE Robotics and Automation Letters* 2.3 (2017), pp. 1428–1435.

[28] Haohan Zhang, Keenan Albee, and Sunil K Agrawal. "A spring-loaded compliant neck brace with adjustable supports." In: *Mechanism and Machine Theory* 125 (2018), pp. 34–44.

[29] Haohan Zhang and Sunil K Agrawal. "An active neck brace controlled by a joystick to assist head motion." In: *IEEE Robotics and Automation Letters* 3.1 (2018), pp. 37–43.

[30] Haohan Zhang, Biing-Chwen Chang, and Sunil Agrawal. "Using a Robotic Neck Brace for Movement Training of the Head-Neck." In: *IEEE Robotics and Automation Letters* (2019).

[31] H Zhang et al. "A robotic neck brace to characterize head-neck motion and muscle electromyography in subjects with amyotrophic lateral sclerosis." In: *Annals of clinical and translational neurology* (2019).

[32] Haohan Zhang et al. "Using the Motion of the Head-Neck as a Joystick for Orientation Control." In: *IEEE Transactions on Neural Systems and Rehabilitation Engineering* (2019).

[33] Xianwen Kong and Clément M Gosselin. "Type synthesis of three-degree-of-freedom spherical parallel manipulators." In: *The International Journal of Robotics Research* 23.3 (2004), pp. 237–245.

[34] Raffaele Di Gregorio et al. “The 3-RRS wrist: a new, simple and non-overconstrained spherical parallel manipulator.” In: *Transactions-American Society of Mechanical Engineers Journal of Mechanical Design* 126 (2004), pp. 850–855.

[35] Narayan Yoganandan et al. “Physical properties of the human head: mass, center of gravity and moment of inertia.” In: *Journal of biomechanics* 42.9 (2009), pp. 1177–1192.

[36] RF Chandler et al. *Investigation of inertial properties of the human body*. Tech. rep. Air Force Aerospace Medical Research Lab Wright-Patterson AFB OH, 1975.

[37] Federica Aprigliano et al. “Effects of repeated waist-pull perturbations on gait stability in subjects with cerebellar ataxia.” In: *Journal of neuroengineering and rehabilitation* 16.1 (2019), p. 50.

[38] Milos Sedlacek and Michal Krumpholc. “Digital measurement of phase difference-a comparative study of DSP algorithms.” In: *Metrology and Measurement Systems* 12.4 (2005), pp. 427–448.

[39] Frank R Wilson. *The hand: How its use shapes the brain, language, and human culture*. Vintage, 1999.

[40] John Napier, John Russell Napier, and Russell H Tuttle. *Hands*. Vol. 9. Princeton University Press, 1993.

[41] Jeff Pelz, Mary Hayhoe, and Russ Loeber. “The coordination of eye, head, and hand movements in a natural task.” In: *Experimental brain research* 139.3 (2001), pp. 266–277.

[42] CHANTAL Bard, MICHEL Fleury, and JACQUES Paillard. “Different patterns in aiming accuracy for head-movers and non-head movers.” In: *The head-neck sensory motor system. Oxford University Press, New York* (1992), pp. 582–586.

[43] B Biguer, M Jeannerod, and C Prablanc. “The coordination of eye, head, and arm movements during reaching at a single visual target.” In: *Experimental brain research* 46.2 (1982), pp. 301–304.

[44] Bridget Armstrong, Peter McNair, and Denise Taylor. “Head and neck position sense.” In: *Sports medicine* 38.2 (2008), pp. 101–117.

[45] J De Vries et al. “Joint position sense error in people with neck pain: a systematic review.” In: *Manual therapy* 20.6 (2015), pp. 736–744.

[46] Kathleen E Cullen and Jefferson E Roy. “Signal processing in the vestibular system during active versus passive head movements.” In: *Journal of neurophysiology* 91.5 (2004), pp. 1919–1933.

[47] Silvia Pancani et al. “An objective functional characterisation of head movement impairment in individuals with neck muscle weakness due to amyotrophic lateral sclerosis.” In: *PloS one* 12.1 (2017), e0169019.

[48] Eva-Maj Malmström et al. “Primary and coupled cervical movements: the effect of age, gender, and body mass index. A 3-dimensional movement analysis of a population without symptoms of neck disorders.” In: *Spine* 31.2 (2006), E44–E50.

[49] ST Aw et al. “Three-dimensional vector analysis of the human vestibuloocular reflex in response to high-acceleration head rotations. II. Responses in subjects with unilateral vestibular loss and selective semicircular canal occlusion.” In: *Journal of neurophysiology* 76.6 (1996), pp. 4021–4030.

[50] Susana Martinez-Conde, Stephen L Macknik, and David H Hubel. “The role of fixational eye movements in visual perception.” In: *Nature reviews neuroscience* 5.3 (2004), p. 229.

[51] C Shawn Green and Daphne Bavelier. “Exercising your brain: a review of human brain plasticity and training-induced learning.” In: *Psychology and aging* 23.4 (2008), p. 692.

[52] Eran Dayan and Leonardo G Cohen. “Neuroplasticity subserving motor skill learning.” In: *Neuron* 72.3 (2011), pp. 443–454.

[53] Lewis P Rowland and Neil A Shneider. “Amyotrophic lateral sclerosis.” In: *New England Journal of Medicine* 344.22 (2001), pp. 1688–1700.

[54] Matthew C Kiernan et al. “Amyotrophic lateral sclerosis.” In: *The lancet* 377.9769 (2011), pp. 942–955.

[55] Robert H Brown and Ammar Al-Chalabi. “Amyotrophic lateral sclerosis.” In: *New England Journal of Medicine* 377.2 (2017), pp. 162–172.

[56] Susana Pinto and Mamede de Carvalho. “Motor responses of the sternocleidomastoid muscle in patients with amyotrophic lateral sclerosis.” In: *Muscle & Nerve: Official Journal of the American Association of Electrodiagnostic Medicine* 38.4 (2008), pp. 1312–1317.

[57] Ryoichi Nakamura et al. “Neck weakness is a potent prognostic factor in sporadic amyotrophic lateral sclerosis patients.” In: *J Neurol Neurosurg Psychiatry* 84.12 (2013), pp. 1365–1371.

[58] Aleksandar Radunović, Hiroshi Mitsumoto, and P Nigel Leigh. “Clinical care of patients with amyotrophic lateral sclerosis.” In: *The Lancet Neurology* 6.10 (2007), pp. 913–925.

[59] Hiroshi Mitsumoto et al. “Promoting excellence in end-of-life care in ALS.” In: *Amyotrophic Lateral Sclerosis* 6.3 (2005), pp. 145–154.

[60] Benjamin Rix Brooks et al. “El Escorial revisited: revised criteria for the diagnosis of amyotrophic lateral sclerosis.” In: *Amyotrophic lateral sclerosis and other motor neuron disorders* 1.5 (2000), pp. 293–299.

[61] Benjamin Rix Brooks. “El Escorial World Federation of Neurology criteria for the diagnosis of amyotrophic lateral sclerosis.” In: *Journal of the neurological sciences* 124 (1994), pp. 96–107.

[62] Bart Swinnen and Wim Robberecht. “The phenotypic variability of amyotrophic lateral sclerosis.” In: *Nature Reviews Neurology* 10.11 (2014), p. 661.

[63] W-K Kim et al. “Study of 962 patients indicates progressive muscular atrophy is a form of ALS.” In: *Neurology* 73.20 (2009), pp. 1686–1692.

[64] Xiaoyan Li, Ping Zhou, and Alexander S Aruin. “Teager–Kaiser energy operation of surface EMG improves muscle activity onset detection.” In: *Annals of biomedical engineering* 35.9 (2007), pp. 1532–1538.

[65] Arno HA Stienen et al. “Self-aligning exoskeleton axes through decoupling of joint rotations and translations.” In: *IEEE Transactions on Robotics* 25.3 (2009), pp. 628–633.

[66] Marco Cempini et al. “Self-alignment mechanisms for assistive wearable robots: A kinetostatic compatibility method.” In: *IEEE Transactions on Robotics* 29.1 (2012), pp. 236–250.

[67] Damiano Zanotto et al. “Knee joint misalignment in exoskeletons for the lower extremities: Effects on user’s gait.” In: *IEEE Transactions on Robotics* 31.4 (2015), pp. 978–987.

[68] Adam B Zoss, Hami Kazerooni, and Andrew Chu. “Biomechanical design of the Berkeley lower extremity exoskeleton (BLEEX).” In: *IEEE/ASME Transactions on mechatronics* 11.2 (2006), pp. 128–138.

[69] Sébastien Krut et al. “Moonwalker, a lower limb exoskeleton able to sustain bodyweight using a passive force balancer.” In: *2010 IEEE International Conference on Robotics and Automation*. IEEE. 2010, pp. 2215–2220.

[70] Paul Stegall. *Building Better Exoskeletons: Understanding How Design Affects Robot Assisted Gait Training*. Columbia University, 2016.

[71] S Roderick, Michael Liszka, and C Carignan. “Design of an arm exoskeleton with scapula motion for shoulder rehabilitation.” In: *ICAR’05. Proceedings., 12th International Conference on Advanced Robotics, 2005.* IEEE. 2005, pp. 524–531.

[72] Matjaz Mihelj, Tobias Nef, and Robert Riener. “ARMin II-7 DoF rehabilitation robot: mechanics and kinematics.” In: *Proceedings 2007 IEEE International Conference on Robotics and Automation*. IEEE. 2007, pp. 4120–4125.

[73] Xin Jin, Xiang Cui, and Sunil K Agrawal. “Design of a cable-driven active leg exoskeleton (c-alex) and gait training experiments with human subjects.” In: *2015 IEEE International Conference on Robotics and Automation (ICRA)*. IEEE. 2015, pp. 5578–5583.

[74] Vineet Vashista. “A cable-driven pelvic robot: Human gait adaptation and rehabilitation studies.” PhD thesis. Columbia University, 2015.

[75] Rongfu Lin, Weizhong Guo, and Feng Gao. “On parasitic motion of parallel mechanisms.” In: *ASME 2016 International Design Engineering Technical Conferences and Computers and Information in Engineering Conference*. American Society of Mechanical Engineers. 2016, V05BT07A077–V05BT07A077.

[76] Victor Santamaria et al. “The Impact of Segmental Trunk Support on Posture and Reaching in Children with Cerebral Palsy.” In: *Pediatric physical therapy: the official publication of the Section on Pediatrics of the American Physical Therapy Association* 28.3 (2016), p. 285.

[77] Penelope Butler et al. “Refinement, reliability and validity of the segmental assessment of trunk control (SATCo).” In: *Pediatric physical therapy: the official publication of the Section on Pediatrics of the American Physical Therapy Association* 22.3 (2010), p. 246.